

CERN-PH-EP-2014-118

Submitted to: JHEP

Measurement of differential production cross-sections for a Z boson in association with b -jets in 7 TeV proton-proton collisions with the ATLAS detector

The ATLAS Collaboration

Abstract

Measurements of differential production cross-sections of a Z boson in association with b -jets in pp collisions at $\sqrt{s} = 7$ TeV are reported. The data analysed correspond to an integrated luminosity of 4.6 fb^{-1} recorded with the ATLAS detector at the Large Hadron Collider. Particle-level cross-sections are determined for events with a Z boson decaying into an electron or muon pair, and containing b -jets. For events with at least one b -jet, the cross-section is presented as a function of the Z boson transverse momentum and rapidity, together with the inclusive b -jet cross-section as a function of b -jet transverse momentum, rapidity and angular separations between the b -jet and the Z boson. For events with at least two b -jets, the cross-section is determined as a function of the invariant mass and angular separation of the two highest transverse momentum b -jets, and as a function of the Z boson transverse momentum and rapidity. Results are compared to leading-order and next-to-leading-order perturbative QCD calculations.

Measurement of differential production cross-sections for a Z boson in association with b -jets in 7 TeV proton-proton collisions with the ATLAS detector

The ATLAS Collaboration

ABSTRACT: Measurements of differential production cross-sections of a Z boson in association with b -jets in pp collisions at $\sqrt{s} = 7$ TeV are reported. The data analysed correspond to an integrated luminosity of 4.6 fb^{-1} recorded with the ATLAS detector at the Large Hadron Collider. Particle-level cross-sections are determined for events with a Z boson decaying into an electron or muon pair, and containing b -jets. For events with at least one b -jet, the cross-section is presented as a function of the Z boson transverse momentum and rapidity, together with the inclusive b -jet cross-section as a function of b -jet transverse momentum, rapidity and angular separations between the b -jet and the Z boson. For events with at least two b -jets, the cross-section is determined as a function of the invariant mass and angular separation of the two highest transverse momentum b -jets, and as a function of the Z boson transverse momentum and rapidity. Results are compared to leading-order and next-to-leading-order perturbative QCD calculations.

Contents

1	Introduction	1
2	The ATLAS experiment	3
3	Simulated event samples	4
4	Event selection	5
5	Background estimation and reduction	7
6	Extraction of detector-level signal yields	9
7	Correction to particle-level	11
8	Systematic uncertainties	13
9	Theoretical predictions	18
10	Results	20
11	Conclusions	30
12	Acknowledgements	30

1 Introduction

The production of a Z boson (using Z as shorthand for Z/γ^*) decaying to electrons or muons provides a clear experimental signature at a hadron collider, which can be used as a probe of the underlying collision processes. Such events provide an opportunity for the study of associated heavy flavour production and dynamics, which can be experimentally identified by reconstructing displaced decay vertices associated with the relatively long lifetimes of b -hadrons. Predictions for heavy flavour production typically suffer from larger theoretical uncertainties than those for the more inclusive Z +jets processes, and measurements of Z boson production in association with b -jets can therefore provide important experimental constraints to improve the theoretical description of this process. The Z + b -jets signal is also an important background to ZH associated Higgs boson production with $H \rightarrow b\bar{b}$, as well as for potential signatures of physics beyond the Standard Model containing leptons and b -jets in the final state.

Two schemes are generally employed in perturbative QCD (pQCD) calculations containing heavy flavour quarks. One is the four-flavour number scheme (4FNS), which only

considers parton densities of gluons and of the first two quark generations in the proton. The other is the five-flavour number scheme (5FNS), which allows a b -quark density in the initial state and raises the prospect that measurements of heavy flavour production could constrain the b -quark parton density function (PDF) of the proton. In a calculation to all orders, the 4FNS and 5FNS methods must give identical results; however, at a given order differences can occur between the two. A recent discussion on the status of theoretical calculations and the advantages and disadvantages of the different flavour number schemes can be found in Ref. [1].

Next-to-leading-order (NLO) matrix element calculations have been available for associated $Z+b$ and $Z+b\bar{b}$ production at parton-level for a number of years [2–4]. The leading order (LO) Feynman diagrams shown in Figure 1 illustrate some of the contributing processes. Full particle-level predictions have existed at LO for some time, obtained by matching parton shower generators to LO multi-leg matrix elements in the 4FNS [5, 6], 5FNS [7], or both [8]. More recently, a full particle-level prediction for $Z+\geq 2$ b -jets at NLO in the 4FNS with matched parton shower has become available [9, 10]. The same framework can also be used to provide a full particle-level prediction for $Z+\geq 1$ b -jet at NLO in the 5FNS. In this article data are compared with several theoretical predictions following different approaches.

Differential measurements of $Z+b$ -jets production have been made in proton-antiproton collisions at $\sqrt{s}=1.96$ TeV by the CDF and D0 experiments [11, 12] as well as inclusively in $\sqrt{s}=7$ TeV proton-proton collisions at the LHC by the ATLAS and CMS experiments [13, 14]. The results presented in this paper significantly extend the scope of the previous ATLAS measurement, which used around 36 pb^{-1} of data recorded in 2010. The current analysis takes advantage of the full sample of $\sqrt{s}=7$ TeV proton-proton collisions recorded in 2011, corresponding to an integrated luminosity of 4.6 fb^{-1} , and uses improved methods for b -jet identification to cover a wider kinematic region. The larger data sample allows differential production cross-section measurements of a Z boson with b -jets at the LHC. These complement the recently reported results of associated production of a Z boson with two b -hadrons at $\sqrt{s}=7$ TeV by CMS [15].

A total of 12 differential cross-sections are presented here, covering a variety of Z boson and b -jet kinematics and angular variables sensitive to different aspects of the theoretical

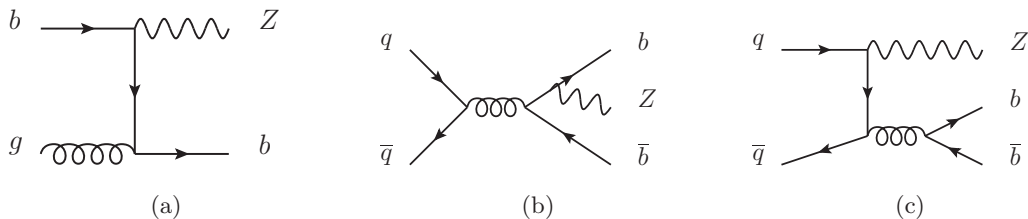


Figure 1. Leading order Feynman diagrams contributing to $Z+b$ -jets production. Process 1(a) is only present in a 5FNS calculation, while 1(b) and 1(c) are present in both the 4FNS and 5FNS calculations.

predictions, as listed in Table 1. All cross-sections include the Z boson branching fraction, $\text{Br}(Z \rightarrow \ell^+ \ell^-)$, where ℓ is a single lepton flavour, and are reported in a restricted fiducial region, defined using particle-level quantities, detailed in Section 7, which are chosen to minimise extrapolation from the corresponding measured detector-level quantities.

The results are grouped according to different selections which give four integrated cross-section definitions:

- $\sigma(Zb)$, the cross-section for events containing a Z boson and one or more b -jets in the fiducial region;
- $\sigma(Zb) \times N_{b\text{-jet}}$, the inclusive cross-section for all b -jets in the fiducial region in events with a Z boson;
- $\sigma^*(Zb) \times N_{b\text{-jet}}$, similar to $\sigma(Zb) \times N_{b\text{-jet}}$, with the additional requirement that the dilepton system has transverse momentum, $p_T > 20$ GeV, ensuring the $\phi(Z)$ coordinate¹ (which is taken from the direction of the dilepton system) is well defined and not limited by detector resolution. This is necessary for the differential measurements of $\Delta\phi(Z, b)$ and hence $\Delta R(Z, b)$ ².
- $\sigma(Zbb)$, the cross-section for events containing a Z boson and two or more b -jets in the fiducial region. When there are more than two b -jets, quantities are calculated using the two highest p_T b -jets in the event.

This paper will cover the experimental apparatus, simulation and event selection in Sections 2, 3 and 4, followed by the description of the methods used to determine backgrounds and extract the signal in Sections 5 and 6. Conversion of the measured data to differential cross-sections and the details of the systematic uncertainties are covered in Sections 7 and 8. A number of theoretical predictions, detailed in Section 9, are compared to the data in Section 10, before conclusions are drawn in Section 11.

2 The ATLAS experiment

The ATLAS experiment [16] is a multi-purpose particle detector with large solid angle coverage around one of the interaction regions of the LHC. It consists of an inner tracking detector surrounded by a superconducting solenoid providing a 2 T axial magnetic field, followed by electromagnetic and hadronic calorimeters and a muon spectrometer with three superconducting toroid magnets. The inner detector (ID) is made up of a high-granularity silicon pixel detector, a silicon microstrip tracker, and a straw-tube transition radiation tracker. These provide measurements of charged particles in the region $|\eta| < 2.5$. The calorimeter system covers $|\eta| < 4.9$ and utilises a variety of absorbing and

¹ATLAS uses a right-handed coordinate system, with the origin at the nominal interaction point, with the beam line defining the z axis, the x -axis pointing towards the centre of the LHC ring, and the y -axis vertically up. The azimuthal angle, ϕ , is defined in the transverse (x - y) plane, and the pseudo-rapidity is used instead of the polar angle: $\eta = -\ln \tan(\theta/2)$. Rapidity is defined in the usual way, $y = \ln[(E + p_z)/(E - p_z)]/2$.

²Two measures of angular separation are used: $\Delta\mathcal{R} = \sqrt{\Delta\phi^2 + \Delta\eta^2}$, and $\Delta R = \sqrt{\Delta\phi^2 + \Delta y^2}$.

Variable	Definition	Range	Integrated cross-section
$p_{\text{T}}(Z)$	Z boson transverse momentum	0–500 GeV	$\sigma(Zb)$
$ y(Z) $	Z boson absolute rapidity	0.0–2.5	$\sigma(Zb)$
$p_{\text{T}}(b)$	b -jet p_{T}	20–500 GeV	$\sigma(Zb) \times N_{b\text{-jet}}$
$ y(b) $	b -jet absolute rapidity	0.0–2.4	$\sigma(Zb) \times N_{b\text{-jet}}$
$y_{\text{boost}}(Z, b)$	$ (y(Z) + y(b)) /2.0$	0.0–2.5	$\sigma(Zb) \times N_{b\text{-jet}}$
$\Delta y(Z, b)$	$ y(Z) - y(b) $	0.0–5.0	$\sigma^*(Zb) \times N_{b\text{-jet}}$
$\Delta\phi(Z, b)$	$ \phi(Z) - \phi(b) $	0.0– π	$\sigma^*(Zb) \times N_{b\text{-jet}}$
$\Delta R(Z, b)$	$\sqrt{\Delta\phi(Z, b)^2 + \Delta y(Z, b)^2}$	0.0–6.0	$\sigma^*(Zb) \times N_{b\text{-jet}}$
$p_{\text{T}}(Z)$	Z boson transverse momentum	0–250 GeV	$\sigma(Zbb)$
$ y(Z) $	Z boson absolute rapidity	0.0–2.5	$\sigma(Zbb)$
$m(b, b)$	bb invariant mass	20–350 GeV	$\sigma(Zbb)$
$\Delta R(b, b)$	bb angular separation	0.4–5.0	$\sigma(Zbb)$

Table 1. Definitions of variables for which differential production cross-sections are measured and the ranges over which those measurements are performed. The integral of each differential cross-section yields one of the four integrated cross-sections defined in the text.

sampling technologies. For $|\eta| < 3.2$, the electromagnetic (EM) calorimeters are based on high-granularity lead/liquid-argon (LAr), while the $3.1 < |\eta| < 4.9$ forward region uses copper/LAr. Hadronic calorimetry is based on steel and scintillating tiles for $|\eta| < 1.7$, copper/LAr for $1.5 < |\eta| < 3.2$, and tungsten/LAr for $3.1 < |\eta| < 4.9$. The muon spectrometer (MS) comprises resistive plate and thin gap trigger chambers covering $|\eta| < 2.4$, and high-precision drift tubes and cathode strip tracking chambers, covering $|\eta| < 2.7$. ATLAS uses a three-level trigger system to select potentially interesting collisions. The Level-1 trigger is hardware based, and uses a subset of detector information to reduce the event rate to at most 75 kHz. Two software-based trigger levels follow, which reduce the event rate to about 300 Hz, for offline analysis.

3 Simulated event samples

The Monte Carlo (MC) simulations of proton-proton collisions and the expected response of the ATLAS detector to simulated particles are used in three ways in this analysis: first, to estimate signal and background contributions to the selected data sample; second, to determine correction factors for detector effects and acceptance when calculating particle-level cross-sections; and finally to estimate systematic uncertainties.

Inclusive $Z(\rightarrow \ell\ell)$ events, produced in associations with both light and heavy flavour jets, are simulated using ALPGEN 2.13 [5] interfaced to HERWIG 6.520 [17] to model the parton shower and hadronisation, and JIMMY 4.31 [18] to model the underlying event and multi-parton interactions (MPI). ALPGEN produces matrix elements with up to five partons using a LO multi-legged approach; these are matched to final state jets using the MLM method [19] to remove overlaps in phase-space between events containing jets produced in

the matrix element and jets produced in the parton shower. Samples are generated with the CTEQ6L1 [20] PDF set and the AUET2 tuning of parameters [21] for the description of the non-perturbative component of the generated events. In addition, overlaps between samples with heavy-flavour quarks originating from the matrix element and from the parton shower are removed. Events containing b -quarks are reweighted after hadronisation to reproduce b -hadron decay particle multiplicities predicted by the EVTGEN package [22], to correct mismodelling found in the decay tables of the HERWIG generator version used. Alternative $Z(\rightarrow \ell\ell)$ samples used for systematic cross-checks are generated with SHERPA 1.4.1 [7]. This generator is based on a multi-leg matrix element calculation using the CT10 [23] PDF set and matched to the parton shower using the CKKW prescription [24].

Backgrounds from $t\bar{t}$, single top quark production in the s -channel, $W + t$ production, and diboson processes are simulated using MC@NLO 4.01 [25] interfaced to HERWIG and JIMMY using the CT10 PDF set. Single top quark production in the t -channel is generated with ACERMC 3.7 [6] interfaced to PYTHIA 6.425 [26] using the CTEQ6L1 PDF set. Corrections to HERWIG b -hadron decay tables using EVTGEN are made for both $t\bar{t}$ and $ZZ(\rightarrow b\bar{b}\ell\ell)$ events which are the dominant backgrounds containing real b -jets. Samples of $W(\rightarrow \ell\nu)$ events are generated using ALPGEN interfaced to HERWIG and JIMMY in an identical configuration to that used for $Z(\rightarrow \ell\ell)$ +jets events described above. An alternative $t\bar{t}$ sample used for systematic cross-checks is generated with POWHEG [27] interfaced to PYTHIA using the CT10 PDF set.

The total cross-sections of the W , Z and $t\bar{t}$ simulated samples are normalised to NNLO predictions [28,29], while other backgrounds are normalised to NLO predictions [30,31]. All samples are overlaid with minimum bias interactions, generated with PYTHIA 6.425 using the CTEQ6L1 PDF set and AMBT2b tune [32], to simulate multiple interactions per bunch crossing (pile-up) such that the distribution of the average number of interactions observed in 2011 pp collision data, with mean value of 9.1, is accurately reproduced. Furthermore, the samples are weighted such that the z distribution of reconstructed pp interaction vertices matches the distribution observed in data. The ATLAS detector response is modelled using the GEANT4 toolkit [33,34], and event reconstruction similar to that used for data is performed.

4 Event selection

The data analysed were collected by the ATLAS detector in 2011 during stable pp collisions at $\sqrt{s}=7$ TeV when all components of the ATLAS detector were fully functioning. Dielectron candidate events were selected with a trigger requiring two electrons with $p_T > 12$ GeV. Dimuon candidate events were selected with a trigger requiring a single muon with $p_T > 18$ GeV. An integrated luminosity of 4.58 ± 0.08 fb $^{-1}$ [35] was taken with these triggers.

The primary interaction vertex (PV) is defined as the vertex with highest $\sum p_T^2$ of ID tracks with $p_T > 0.4$ GeV associated to it. Candidate events are required to have at least three such associated tracks.

Electron candidates are reconstructed by associating a cluster of energy deposits in the EM calorimeter to a well reconstructed ID track, and are required to have $E_T > 20$ GeV and $|\eta| < 2.47$, excluding the region $1.37 < |\eta| < 1.52$ where the transition between the barrel and endcap of the EM calorimeter occurs. Candidates are required to pass a ‘medium’ quality requirement based on analysis of various cluster properties and the associated ID track [36]. Muon candidates are reconstructed by associating well identified ID tracks to MS tracks [37]. Candidates are required to have $p_T > 20$ GeV and $|\eta| < 2.4$. Selections on the transverse energy (transverse momentum) of electron (muon) candidates are chosen to ensure the trigger is fully efficient.

To ensure that lepton candidates originate from the PV and to suppress those candidates originating from heavy flavour decays, ID tracks associated to lepton candidates are required to have an absolute longitudinal impact parameter with respect to the PV, $|z_0|$, less than 1 mm and absolute transverse impact parameter, $|d_0|$, no larger than ten (three) times its measured uncertainty for electron (muon) candidates. Muon candidates are additionally required to be isolated from local track activity by rejecting candidates where the summed transverse momenta of additional ID tracks within $\Delta\mathcal{R} = 0.2$ from the muon candidate is larger than 10% of the transverse momentum of the candidate itself. No additional isolation requirement is applied to electron candidates as the quality requirement and impact parameter selections already sufficiently reduce the contribution from jets misidentified as electrons in the calorimeter.

Selection efficiencies of lepton candidates as well as their energy resolution and momentum resolution are adjusted in simulation to match those observed in $Z \rightarrow \ell\ell$ events in data [36, 37]. The lepton energy scales and momentum scales are calibrated based on a comparison of the position of the Z boson mass peak in data and simulation. Events with exactly two lepton candidates of same flavour and opposite measured charge are kept for further analysis, provided the invariant mass of those leptons, $m_{\ell\ell}$, falls in the range $76 < m_{\ell\ell} < 106$ GeV.

Jets are reconstructed from topological energy clusters in the calorimeter [38] using the anti- k_t algorithm [39, 40] with radius parameter $R = 0.4$. The jet energy is calibrated as a function of p_T and η using MC simulation after correcting first for the energy offset due to pile-up activity in the calorimeter, and then redefining the origin of the jet to be the event PV. A residual in situ correction determined from Z +jet and γ +jet control samples is applied to jets in data to account for remaining differences in calorimeter response between data and simulation [41]. Jets from pile-up interactions are suppressed by requiring that ID tracks associated to the PV contribute at least 75% of the total scalar sum of transverse momenta from all ID tracks within $\Delta\mathcal{R} = 0.4$ from the jet centroid. Calibrated reconstructed jets are required to have $p_T > 20$ GeV, $|y| < 2.4$ and any jet within $\Delta\mathcal{R} = 0.5$ of a selected lepton candidate is removed.

Jets containing b -hadrons are identified using a neural network (NN) algorithm, MV1 [42]. The MV1 algorithm takes as inputs the results of lower-level likelihood and NN based b -tagging algorithms, which in turn take both secondary vertex kinematics and impact parameter information with respect to the PV as inputs, obtained from analysing ID tracks within $\Delta\mathcal{R} = 0.4$ from the jet centroid. The MV1 variable lies in the range $[0,1]$ with a

value closer to unity denoting a higher probability for the jet to be a b -jet. Reconstructed b -jet candidates are selected for the analysis when their MV1 output is greater than the value corresponding to a 75% average b -tagging efficiency in simulated $t\bar{t}$ events. In simulation, reconstructed jets are labelled as b -jets if they lie within $\Delta\mathcal{R} = 0.3$ from one or more weakly decaying b -hadrons with $p_T > 5$ GeV. Reconstructed jets not identified as b -jets are considered as c -jets if they lie within $\Delta\mathcal{R} = 0.3$ from any c -quark with $p_T > 5$ GeV. All other jets are classified as ‘light-jets’. Tagging efficiencies in simulation are scaled to match those measured in data for all flavours as a function of jet p_T (and η for light-jets) using weights derived from control samples enriched in jets of each flavour [42–44].

In each event, the missing transverse momentum, E_T^{miss} , is also used to reject backgrounds which typically contain high energy neutrinos, such as $t\bar{t}$. The E_T^{miss} is calculated by first forming the vector sum of all calibrated leptons and jets, along with any additional topological energy clusters not already associated to a reconstructed physics object. The magnitude of this sum in the transverse direction is a measure of the energy imbalance in the event, and is taken as the E_T^{miss} [45].

Events used for further analysis are separated into two categories: those with at least one tagged jet, referred to as 1-tag events; and those with at least two tagged jets, referred to as 2-tag events, which is a subset of the 1-tag sample.

5 Background estimation and reduction

Selected events in data contain the signal of interest as well as various background processes with either real or fake leptons and real or fake b -jets. By far the dominant contributions are Z +jets events where either a light-jet or c -jet has been misidentified as a b -jet. The amount of this background present in data is determined using fits to data as described in Section 6.

The next most important background arises from $t\bar{t}$ events where both W bosons decay to leptons. This background is estimated using simulated events normalised to the theoretically predicted cross-section. The $t\bar{t}$ background is suppressed by the requirements on $m_{\ell\ell}$, and its overall contribution to the event sample is small. However, it can be significant in some kinematic regions, particularly at higher jet p_T . To further reduce the $t\bar{t}$ contamination, events are required to have $E_T^{\text{miss}} < 70$ GeV. Figure 2 shows the E_T^{miss} distributions for signal and $t\bar{t}$ simulations in 1-tag and 2-tag events after combining the electron and muon channels. The 70 GeV selection rejects 44.8% (44.3%) of the $t\bar{t}$ background in 1-tag (2-tag) events while remaining over 99% efficient for signal events.

The total contribution to the final data sample from single top quark and diboson processes is estimated using samples of simulated events normalised to their theoretically predicted cross-sections. Other electroweak processes such as W +jets and $Z \rightarrow \tau\tau$ events are found to have a negligible contribution in the selected phase space.

Background contributions from multijet events are estimated using data-driven techniques separately in the electron and muon channels for both 1-tag and 2-tag events. Multijet-enriched control regions are used to derive the expected shape of this background in the $m_{\ell\ell}$ variable. These control regions drop the b -tagging requirement, and use an

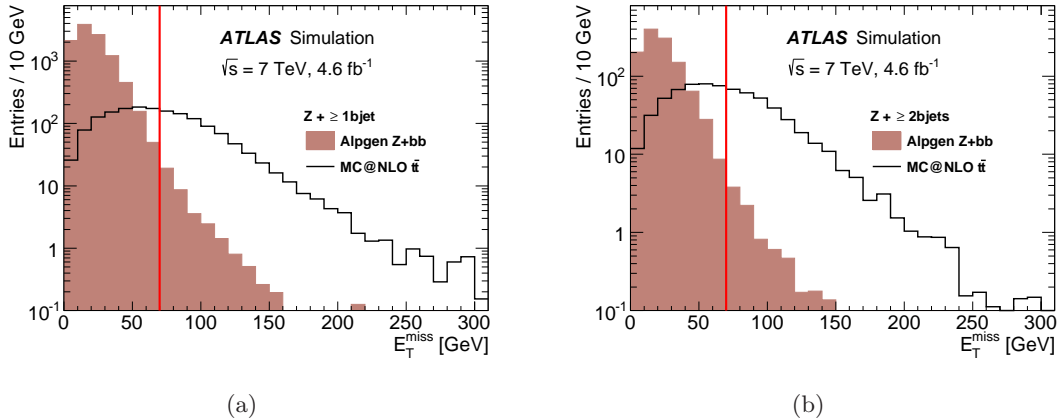


Figure 2. Comparison of simulated E_T^{miss} distributions for (a) 1-tag events and (b) 2-tag events after all other signal selection criteria are applied, normalised to the expected yields in the data sample. The shaded distributions are signal ALPGEN+HERWIG+JIMMY events, and the open distributions are selected $t\bar{t}$ events. The vertical line shows the selection applied to the analysis sample to reject $t\bar{t}$ events while keeping signal events.

extended range $50 < m_{\ell\ell} < 200$ GeV in order to maximise the available sample size. Studies found that no bias was introduced within the statistical uncertainties between the b -tagged and non- b -tagged samples. In the $Z(\rightarrow ee)+\text{jets}$ channel the multijet enriched control region is defined by following the full signal event selection with the exception of electron candidate impact parameter requirements, and requiring that one reconstructed electron candidate fails the ‘medium’ quality requirement. As requirements based on the shower shape and associated ID track are applied to both electrons at trigger-level in the default trigger, events for the control region are selected with a trigger which requires only a single electron with $E_T > 20$ GeV. This trigger was only available for about one third of the full 2011 data-taking period (1.7 fb^{-1} in total). In the $Z(\rightarrow \mu\mu)+\text{jets}$ channel the multijet-enriched control region is defined by following the full signal event selection with the exception of muon candidate impact parameter requirements, and inverting the isolation selection for both reconstructed muon candidates. In both channels, contributions from non-multijet sources in the control regions are taken from simulation, and subtracted from the data. The remaining distributions are used as shape templates for the dilepton invariant mass distribution of the multijet background.

Fits to $m_{\ell\ell}$ are then made after applying the full signal event selection, fixing the multijet shapes to those measured in the control regions. For 1-tag events the multijet contribution is determined to be $0.1 \pm 0.1\%$ in the electron channel and $0.02 \pm 0.07\%$ in the muon channel. The control regions are investigated as a function of all variables used to define the differential cross-sections measured here, and no significant variation in the multijet fraction is found; therefore, the measured multijet fractions are assumed to be constant in all differential analysis bins. For 2-tag events the multijet contributions are fitted to be zero, with an uncertainty of approximately 0.5%. This uncertainty is taken as a

systematic uncertainty to account for a possible residual multijet contribution, as discussed in Section 8.

6 Extraction of detector-level signal yields

The extractions of the integrated and differential detector-level signal yields for both the 1-tag and 2-tag selections are performed using maximum-likelihood fits to data based on flavour-sensitive distributions. The distribution used is constructed from the output of a neural network algorithm, JFCComb, which is one of the inputs to the MV1 b -tagging algorithm described in Section 4. JFCComb itself combines the information from two further algorithms, one of which aims to identify weak $b \rightarrow c$ cascade topologies using secondary vertices and displaced tracks reconstructed within a jet [46], and the other which calculates a likelihood based on the impact parameter significance with respect to the PV of pre-selected tracks within $\Delta\mathcal{R} = 0.4$ of the jet centroid [42, 47]. The JFCComb algorithm has three outputs in the range [0,1]: pb , pc , and pu , corresponding to the probability that a given jet is a b -jet, c -jet or light-jet, respectively. Combinations of these variables, namely $\text{CombNNc} = \ln(pb/pc)$ and $\text{CombNN} = \ln(pb/pu)$ provide good separation between jet flavours as shown in Figure 3 for all jets in the Z +jets MC simulation after the 1-tag event selection.

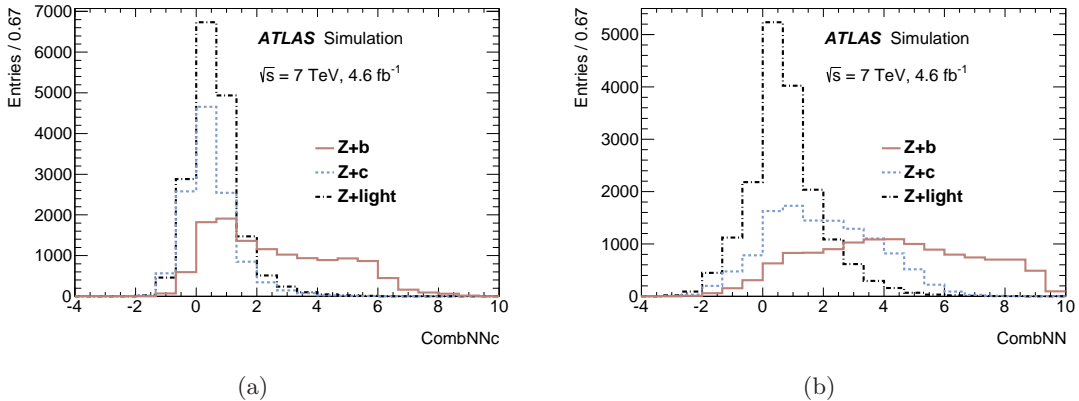


Figure 3. Distributions of (a) CombNNc and (b) CombNN for different jet flavours in simulated Z +jets events for all selected tagged jets, in events with at least one tagged jet. The $Z \rightarrow ee$ and $Z \rightarrow \mu\mu$ channels are combined and simulated data are normalised such that the predicted number of jets in 4.6 fb^{-1} are shown.

In the 1-tag event selection, fits are made to the CombNNc distribution as it is found to give the best statistical separation between b -jets and non- b -jets. Templates are derived from MC simulation for all non-multijet contributions. For the multijet background, templates are derived from the respective control regions in each lepton channel after reintroducing the b -tagging requirement as in the baseline selection. As shown in Figure 3(a), the c -jet and light-jet CombNNc shapes are very similar. They are therefore combined into a single non- b -jet template before the fit, using the predicted c -to-light jet ratio from sim-

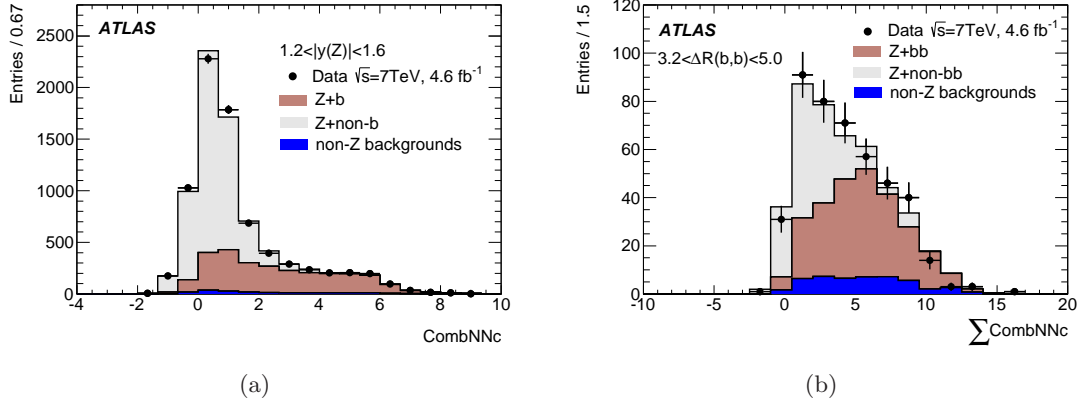


Figure 4. Example fits to the distribution of (a) CombNNc at jet-level for 1-tag events with $1.2 < |y(Z)| < 1.6$, and (b) $\sum(\text{CombNNc})$ at event-level for 2-tag events with $3.2 < \Delta R(b, b) < 5.0$.

ulation. Fits to data allow the b - and non- b -jet Z +jets yields to float, while backgrounds from sources other than Z +jets are combined into a single template whose normalisation is determined from the sum of their predicted contributions and fixed in the fit. Where a per b -jet yield is measured, all tagged jets are used in the fit; where a per-event yield is measured, only the highest p_T tagged jet in an event is used in the fit. The electron and muon channel templates in data are combined before the fit to maximise the statistical precision. For measurements of differential cross-sections, these fits are performed independently in each bin, and Figure 4(a) shows an example fit to the CombNNc distribution in one differential bin, which is typical of the results obtained. Table 2 summarises all signal and background contributions compared to data for the integrated 1-tag selections at detector-level after the jet-flavour fits. Also shown in Table 2 are the ALPGEN+HERWIG+JIMMY 1-tag predictions, where it can be seen that they significantly underestimate the fitted b -jet yields.

In the 2-tag event selection fits are made to $\sum(\text{CombNNc})$, where the sum is over the two highest p_T tagged jets in an event. There are six possible flavour combinations of b -jets, c -jets, and light-jets in the Z +jets MC simulation. The highest statistical precision on the signal bb -yield is obtained when the other five flavour combinations are combined into a single non- bb template. However, the shapes of the non- bb templates are not degenerate, as the presence of a single b -jet in the b +light or $b+c$ cases results in a higher value of $\sum(\text{CombNNc})$ compared to light+light, light+ c and $c+c$ cases. Therefore, the overall number of these single- b events is important in determining the shape of the non- bb template. As discussed above, and can be seen in Table 2, the ALPGEN+HERWIG+JIMMY simulation is observed to underestimate the b -jet yield in data, and it follows that the number of b +light and $b+c$ events cannot be taken directly from the simulation when forming the non- bb template, but must be measured. To determine the appropriate scaling for the templates containing a single b -jet, a fit is performed to CombNN in an alternative sample containing a reconstructed Z boson with at least two jets, of which exactly one is

tagged. The b -jet, c -jet and light-jet Z +jets yields are allowed to float in the fit, while all non- Z +jets backgrounds are combined into a single template whose normalisation is determined from the sum of their predicted contributions and fixed in the fit; the multijet yields and shapes in this sample are extracted in a fashion analogous to that used for the 1-tag events. Even after scaling up the total Z cross-section to the NNLO prediction as described in Section 3, the predicted b -jet yield must be increased by an additional factor of 1.35 ± 0.03 to match the fitted data yield, where the quoted uncertainty is the statistical component of the fit to data. Scale factors for c -jet and light-jet yields are found to be consistent with unity. Based on this result, templates containing one b -jet are weighted by a factor 1.35 compared to the predicted cross-section, while templates with no b -jets are included using the default predicted cross-section. This factor of 1.35 is taken as constant across all distributions as, normalisation aside, the default simulation is found to give a good description of the kinematics of the single b -jet sample. This scale factor is slightly different from the $Z + \geq 1$ b -jet scale factors in Table 2, due to the different jet requirements. A systematic uncertainty on the scale factor is obtained by varying these requirements, as described in Section 8.

Signal fits to data float the Z +jets bb and non- bb yields while combining all other backgrounds into a single template whose normalisation is determined from the sum of their predicted contributions and fixed in the fit. As with 1-tag events, the electron and muon channels are combined before fitting to data to maximise the statistical precision. Figure 4(b) shows an example fit of $\sum(\text{CombNNc})$ in one differential bin, and Table 2 summarises all signal and background contributions compared to data for the integrated 2-tag selection at detector-level after the jet-flavour fit.

All fits are checked with ensemble tests using the simulated samples, including checks for any bias in the fit results compared to the true number of b -jets in the simulation. Negligible biases in the fit responses are observed.

Analysis selection	Data yield	Fitted Components		Fixed Components	
		$Z + b(b)$ -jets [ALPGEN+HJ]	$Z + (\text{other})$ jets	$t\bar{t}$	other
$\sigma(Zb) \times N_{b\text{-jet}}$	49701	18010 ± 210 [12470]	29780 ± 230	1330	590
$\sigma^*(Zb) \times N_{b\text{-jet}}$	41243	15640 ± 190 [10460]	23840 ± 210	1230	540
$\sigma(Zb)$	47138	16610 ± 200 [11410]	29090 ± 220	930	520
$\sigma(Zbb)$	2494	1170 ± 60 [950]	860 ± 50	395	60

Table 2. Detector-level yields for each analysis selection. Statistical uncertainties from the fits to data are shown for the signal and Z +jets backgrounds. The $t\bar{t}$ and other (diboson, single top quark and multijet) background normalisations are also shown. The signal yields predicted by ALPGEN+HERWIG+JIMMY (ALPGEN+HJ) are shown in square brackets for reference.

7 Correction to particle-level

Signal yields fitted at detector-level are corrected for reconstruction efficiencies and detector resolution effects using simulation. This unfolding procedure determines fiducial particle-

level yields in data, which when divided by the measured integrated luminosity determine cross-sections. Particle-level objects are selected with requirements chosen to be close to the corresponding requirements for reconstructed signal candidate detector-level objects, in order to minimise unfolding corrections. Final state electrons and muons are ‘dressed’, such that the four-momentum of collinear photons within $\Delta\mathcal{R} = 0.1$ from those leptons are added to their four-momentum. These dressed leptons are then required to have $p_T > 20$ GeV and $|\eta| < 2.5$. The two leptons with highest p_T , same flavour and opposite charge are used to reconstruct the Z boson, with the invariant mass of the pair required to lie in the range $76 < m_{\ell\ell} < 106$ GeV. Jets of particles, excluding leptons used to reconstruct the Z boson and any photons used in dressing them, but including leptons and neutrinos from heavy flavour decays, are reconstructed with the anti- k_t algorithm with radius parameter $R = 0.4$. As with simulated reconstructed jets, particle-level jets are defined as b -jets if they lie within $\Delta\mathcal{R} = 0.3$ from one or more weakly decaying b -hadrons with $p_T > 5$ GeV. Selected jets are required to have $p_T > 20$ GeV and $|y| < 2.4$. Jets within $\Delta\mathcal{R} = 0.5$ of a lepton used to reconstruct the Z boson are discarded.

The classification of simulated signal events is based on the presence of detector-level and particle-level objects, and matching criteria between the two are defined. The matching criteria require that detector-level and particle-level event selections are passed and that each detector-level b -jet lies within $\Delta\mathcal{R} = 0.4$ from a particle-level b -jet. For event-level (jet-level) differential measurements, matched events (b -jets) are used to populate detector response matrices for the distribution in question. These matrices characterise the bin migrations between detector-level and particle-level quantities and are used to unfold the fitted signal yields at detector-level into signal yields at particle-level.

Before unfolding, a multiplicative matching correction derived from simulation is applied to the fitted signal yields, to account for cases where the detector-level signal failed the matching criteria. This correction is 6–9% for the integrated selections, although it becomes as large as 20% in the lowest bin of b -jet p_T in the 1-tag analysis due to migration from particle-level b -jets below the 20 GeV p_T threshold. In order to avoid bias in the differential cross-section measurement of b -jet p_T , detector-level b -jets are considered as matched if they are associated to particle-level b -jets with $p_T > 10$ GeV. For other variables the migration outside of acceptance is found to introduce negligible bias and hence the particle-level b -jet selection is only relaxed in the unfolding of b -jet p_T . For 2-tag events, where simulation sample size for matched events is a limiting factor, the b -tagging efficiency correction is included as part of the matching correction. This allows all detector-level b -jets, tagged or otherwise, to be used in the response matrices.

In the 1-tag analysis, corrected fitted yields and response matrices are used as input to an iterative Bayesian technique [48] to extract the particle-level signal yields. Three further iterations on the initial response matrix are required to remove bias from previous iterations as determined from MC simulation ensemble tests of the statistical robustness of the unfolding procedure. The binning of differential distributions is chosen to always be significantly wider than the detector resolution in that quantity, which is only a relevant factor for b -jet p_T . Related to this resolution effect, and to again mitigate the biases mentioned above, the response matrix for b -jet p_T is also populated with particle jets with

$p_T > 10$ GeV, and the portion of the resulting particle-level distribution below 20 GeV is removed. In the 2-tag differential distributions, fewer events are selected and binnings are chosen to optimise statistical precision while maintaining as many bins as possible. This coarse binning results in little bin-to-bin migration, and a negligible difference is observed between the result of the iterative procedure used for 1-tag events and that obtained by simply applying fiducial matching and efficiency corrections³ individually for each bin. As a consequence, the latter, more straightforward, technique is used to extract differential yields in 2-tag events.

Since the electron and muon Z boson decay channels are combined to increase the precision of the signal fits to data, the corrections and response matrices described above must unfold both channels simultaneously to obtain combined particle-level yields. To validate this approach, an identical analysis of each individual lepton channel is performed. Their sum after unfolding is checked for consistency with the default combined unfolded result and excellent agreement is observed in both the 1-tag and 2-tag cases. Furthermore, the results obtained from the individual lepton channels agree reasonably well, being compatible within 1.7σ or less, considering only the sum in quadrature of the statistical and uncorrelated systematic uncertainties.

8 Systematic uncertainties

Several sources of systematic uncertainty are considered. These can impact either the fit, through modification of template shapes and background normalisations; the unfolding, through modification of correction factors and response matrix; or both the fit and unfolding in a correlated manner. Each independent source of uncertainty is varied successively up, and then down by one standard deviation, and in each case the full analysis chain is repeated. The relative change in the result with respect to the default analysis is then assigned as the up or down uncertainty due to that source. The following sources are considered and the resulting uncertainties on the measured 1-tag and 2-tag cross-sections are summarised in Table 3.

Tagging efficiency and mistag rates. Calibration factors are applied to the jet b -tagging efficiency in simulation to match that measured in data for each flavour. These have associated systematic uncertainties as a function of jet p_T (and η for light-jets). For b -jets, the uncertainties derived from calibration analyses are divided into 10 sub-components corresponding to the eigenvectors which diagonalise the associated covariance matrix; each sub-component is then varied independently by $\pm 1\sigma$ and the systematic uncertainties from each are added in quadrature. Typically two of the sub-components dominate the uncertainty, with one at around 4.5% at low b -jet p_T , and the other rising to around 13% at high b -jet p_T . Across other distributions, both remain between 2-3%. For c -jets and light-jets, the mistag correction factors from each respective calibration analysis are varied by $\pm 1\sigma$ and propagated through the analysis chain to obtain the corresponding systematic

³The efficiency correction refers to the multiplicative factor obtained from the ratio of the total number of fiducial particle-level events to the number which is also reconstructed at the detector-level and matched appropriately.

uncertainties. These contribute significantly smaller uncertainties, peaking at around 1% at high b -jet rapidity and low p_T . All uncertainties related to b -jets approximately double in size when requiring two tagged jets for the $Z + \geq 2$ b -jets distributions.

Jet energy scale. Systematic uncertainties on the difference between the jet energy scale (JES) in data and simulation are derived using a variety of studies based on in situ measurements and simulation [41]. These uncertainties are decomposed into 16 independent components, including those arising from the influence of close-by low-energy jets, the correction for pile-up activity and differences in detector response to light-quark jets, gluon jets and heavy flavour jets. Each component is propagated through the analysis chain independently by simultaneously varying the signal and background simulation jet response by $\pm 1\sigma$. The impact of the total JES uncertainty on the final cross-sections is typically around 2-5%, rising with p_T and rapidity, with uncertainty on the b -jet response uncertainty being an important contribution.

Jet energy resolution. Jet energy resolution (JER) is studied in dijet data and compared to simulation [49]. Simulated signal and background samples are then modified by applying a Gaussian smearing of the resolution function according to the maximum degradation allowed by the JER measurement from data to evaluate the associated systematic variation. This is taken as a symmetrised uncertainty on the measured results, and is typically less than 1%.

b -jet template shapes. The uncertainty on the shape of b -jet templates used in fits to data is a dominant contribution to the overall systematic uncertainty for this analysis. The shape is cross-checked in a $t\bar{t}$ -enriched control region which requires a single well identified and isolated lepton in association with at least four reconstructed jets passing the same kinematic cuts as signal jets, of which exactly two are tagged with the MV1 algorithm described in Section 4. This selects a sample of $t\bar{t}$ events in which over 90% of the tagged jets are expected to be true b -jets. Contributions from W +jets and single top quark events in this control region are estimated from simulation; contributions from other electroweak processes and multijet backgrounds are found to be negligible. A residual underestimate of the total number of events predicted by simulation is found to be less than 10%, and is corrected for by scaling up the $t\bar{t}$ contribution to match the data normalisation. Figure 5 shows the CombNNc distributions for different jet flavours, and the ratio of data to default simulation for all tagged jets in this control region; the corrections of the HERWIG b -hadron decays to the EVTGEN prediction described in Section 3 are applied. It can be seen that the simulation provides a reasonable description of the data; the residual differences of up to 5% are used to derive a b -jet template reweighting function shown by the dashed line in Figure 5. Investigation of the control-region data in bins of tagged jet p_T and rapidity finds that the deviations between data and simulation have no strong dependence on tagged jet kinematics; this is despite the CombNNc distribution shape itself having a strong dependence on tagged jet p_T . The reweighting function is used to directly reweight CombNNc b -jet distributions in the signal Z +jets simulation and the fits to data are repeated. The relative differences with respect to the default results are typically less than 5%, and this difference is taken as a systematic uncertainty due to b -jet template shape, which is then symmetrised around the nominal value to give an up-

and down-uncertainty. It is possible that the b -jet template reweighting function derived reflects some mismodelling of the non- b -jets component in Figure 5. To this end the systematic uncertainty is also evaluated by only reweighting b -jet templates for values of CombNNc larger than 2.0. The result is a smaller overall uncertainty; however, as the fraction of b -jets is still larger than the fraction of non- b -jets for CombNNc less than 2.0 in Figure 5, the more conservative value obtained from reweighting the full b -jet template is taken as the uncertainty. As a further cross-check, the fits are repeated using b -jet templates obtained from the SHERPA Z +jets sample; deviations observed are all within the uncertainties already derived from the $t\bar{t}$ -enriched control-region method, so no further uncertainty is assigned.

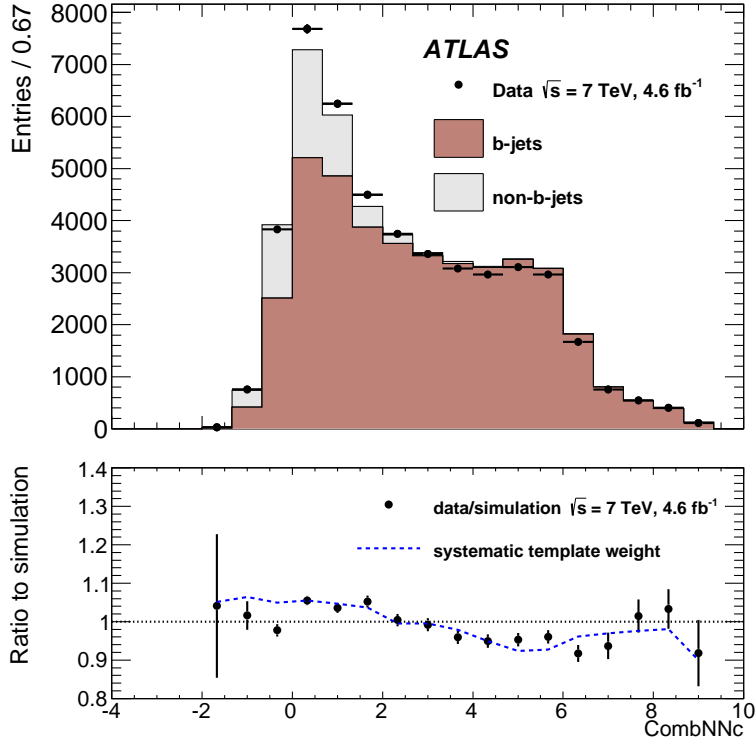


Figure 5. The tagged-jet CombNNc distribution in the $t\bar{t}$ enriched control region described in the text, with the simulation split by jet flavour (top), and the ratio of data to default simulation (filled circles, bottom). The dashed line shows the b -jet template reweighting function derived from the difference between data and simulation in this control region.

Non- b -jet template shapes. Mismodelling of template shapes derived from Z +jets simulation for c -jets and light-jets can also cause a systematic shift in the results of fits to data. The corresponding uncertainties are estimated by substituting the default templates with templates derived from the SHERPA Z +jets simulation, which uses a different parton shower and hadronisation model. The difference between the default fit response and the response obtained with the alternative templates is taken as the systematic uncertainty, which is typically less than 1%.

Further tests are made by repeating the entire analysis using an MV1 operating point

which rejects significantly more c - and light-jet background (but with a lower signal efficiency), reducing the sensitivity to any potential mismodelling of these templates. The results are entirely consistent with those obtained using the default value, so no further uncertainty is assigned.

Finally, the template shapes may be influenced by a mismodelling of the light- and c -jet kinematics, and by the light-/ c -jet ratio in the simulation when building the non- b template. The data are fitted using CombNN rather than CombNNc (defined in Section 6), which provides a better discrimination between light- and c -jets, and all three templates (light-, c - and b -jet) are allowed to float. Across all distributions, the fitted light- and c -jet normalisations are consistent with the prediction of the default simulation within the statistical uncertainties (typically 2-4%), indicating the kinematic modelling of these contributions, and their ratio, is correct. Therefore no further systematic uncertainty is assigned.

Template scale factor. The $b+c$ and b +light jet templates in 2-tag events are scaled up by a factor of 1.35, as described in Section 6, based on fits to data with two or more jets, of which exactly one is tagged. A fit to integrated 1-tag data yields a factor of 1.48; the default scale factor of 1.35 is varied up and down by 0.13 to cover this difference, resulting in a change in the final cross-sections of around 2%, which is assigned as a symmetric up and down systematic uncertainty. The c - and light-jet fractions in these templates are also independently varied up and down by 0.13, significantly larger than the fit uncertainties and differences in the two control regions used to derive the b -jet scale factor, but chosen to be based on the b -jet result to provide a conservative bound on mismodelling of the c -jet fraction. This results in a further systematic uncertainty of around 1%.

Multiple parton interactions. Associated $Z+b$ -jets production from MPI where the Z and b -jets are produced in separate hard scatters within a single pp interaction (double parton interactions) is included in the analysis signal definition. Fits to data and unfolding to particle-level use the MPI fraction predicted by JIMMY in Z +jets simulation to determine its relative contribution to the signal processes. The contribution is largest at lower b -jet p_T ; any misestimate of this fraction can alter the CombNNc shapes, which are p_T -dependent, and can also alter the efficiency correction and the bin-by-bin migration in p_T -dependent variables. The default double parton interaction fractions as a function of b -jet p_T and rapidity are cross-checked by combining ATLAS measurements of the Z boson production cross-section [50], the differential inclusive b -jet cross-section [51] and pp effective cross-section [52] using the phenomenological model described in reference [52]. The prediction from JIMMY is found to be consistent with this data-based cross-check to within 50%, hence the predicted fraction is varied by this amount to determine an associated systematic uncertainty. The uncertainty is typically around 2% on the measured cross-sections.

Gluon splitting. The dominant mechanism to produce two b -hadrons in one jet is the $g \rightarrow b\bar{b}$ process. An inaccurate estimate of the rate of two b -hadron decay vertices within $\Delta\mathcal{R} = 0.4$ from the jet centroid can affect the accuracy of the CombNNc template shapes, by impacting distributions which are inputs to the NN. Furthermore, as gluon splitting becomes more important for high p_T jets, a mismodelling of its rate can impact the

efficiency correction and bin migrations in variables correlated with b -jet p_T . No well defined data control region has been identified to constrain this process; therefore the sample of simulated events with reconstructed and particle-level jets matched to two b -hadrons is first enhanced by a factor of 2, then completely removed, with the full analysis being repeated in both cases. This variation is larger than the difference observed between predictions from the default signal ALPGEN+HERWIG+JIMMY and SHERPA Z +jets simulations and is therefore considered to give a conservative upper limit on the magnitude of this uncertainty, and is found to be less than 2%.

Background normalisation. The contributions of $t\bar{t}$, single top quark and diboson backgrounds are taken from theoretical predictions. To account for theoretical uncertainties in these predictions the normalisation of each component is varied independently by $\pm 10\%$, which covers both cross-section and acceptance uncertainties. For 1-tag events the multijet background is varied within its fitted uncertainty. For 2-tag events, fits for the multijet backgrounds yielded a normalisation close to zero, and the uncertainty from those fits is taken as an upper bound for possible multijet contamination, translating into an uncertainty of 0.5% on the bb yield.

Background modelling. A cross-check of $t\bar{t}$ -background modelling is made by substituting the default MC simulation with an alternative sample simulated with POWHEG and repeating the data fits. For 1-tag events no significant difference is found, either inclusively or differentially. In 2-tag events a systematic deviation in excess of the existing template-shape uncertainty described above is observed. This difference is approximately 3%, which is taken as an additional systematic uncertainty due to $t\bar{t}$ modelling in the 2-tag sample.

Signal modelling. The corrections to particle-level cross-sections may include some residual dependence on the modelling of the kinematics in the simulation. To test for this, the particle-level b -jet p_T distribution in simulation is reweighted to the measured differential cross-section, and the full analysis repeated. A negligible effect is found. As the main kinematic distributions are generally well modelled by the simulation, no further uncertainties are assigned.

Simulation sample size. The impact of the finite simulation sample sizes in both the fit template shapes and unfolding procedure are evaluated through ensemble tests, repeating the analysis and randomly fluctuating bin entries of a given distribution in the simulation within their statistical uncertainty. The spread determined from these ensemble tests is around 1%, which is assigned as the systematic uncertainty.

Lepton efficiency, energy scale and resolution. The trigger and reconstruction efficiency, energy scale, and resolution of both reconstructed electron and muon candidates have been measured in $Z \rightarrow \ell\ell$ events and used to correct the simulation as described in Section 4. The uncertainties associated with the measurement of these quantities are propagated through the full analysis chain resulting in an uncertainty of around 1% on the final cross-sections.

Missing transverse momentum. The calculation of E_T^{miss} in each event is repeated for every systematic variation of reconstructed jet and lepton candidates as described above. An additional uncertainty arises from possible differences in data and simulation between

the component of E_T^{miss} from topological clusters not associated to reconstructed physics objects [45]. This additional component is propagated through the analysis as an independent uncertainty, and is typically well below 1%.

Luminosity. The luminosity scale is determined from a single calibration run taken in May 2011. The associated uncertainty is derived from the calibration analysis itself and from the study of its stability across the 2011 data taking period. A total uncertainty of 1.8% is assigned to the luminosity [35].

Source of uncertainty	$\sigma(Zb)$ [%]	$\sigma(Zbb)$ [%]
b -jet tagging efficiency	3.4	9.8
c -jet mistag rate	0.2	2.3
light-jet mistag rate	0.4	0.6
JES	2.9	4.7
JER	0.3	0.7
b -jet template shape	4.8	4.8
c -jet template shape	0.2	0.6
light-jet template shape	0.9	0.9
b -jet template scale factor	N/A	2.3
MPI	2.5	0.8
gluon splitting	1.2	1.5
background normalisation	1.1	3.6
$t\bar{t}$ modelling	0.0	2.9
MC sample size	1.0	1.4
lepton efficiency, scale and resolution	1.2	1.2
E_T^{miss}	0.1	0.6
luminosity	1.8	1.8
total	7.7	14.0

Table 3. Summary of the systematic uncertainties determined for the cross-section measurements of the $Z + \geq 1$ b -jet and $Z + \geq 2$ b -jets final states.

9 Theoretical predictions

Several theoretical predictions are compared to the measurements. Fixed-order pQCD parton-level predictions at NLO in the 5FNS are obtained from MCFM [53] for both the $Z + \geq 1$ b -jet and $Z + \geq 2$ b -jets final states. The calculation of $Z + \geq 1$ b -jet is made up of several sub-processes [2, 3] at $\mathcal{O}(\alpha_S^2)$, and the b -quark mass is ignored except in processes where one b -quark falls outside the acceptance or two b -quarks are merged in a single jet. For $Z + \geq 2$ b -jets production, the MCFM calculation uses a single process with both b -quarks in acceptance at $\mathcal{O}(\alpha_S^3)$ and the b -quark mass is ignored throughout. In all cases, the renormalisation and factorisation scales are set to $\sqrt{m(Z)^2 + p_T(Z)^2}$, and varied up and

down independently by a factor of two to assess the dependence on this scale choice. The MCFM predictions are performed using the CT10 [23], NNPDF2.3 [54] and MSTW2008 [55] PDF sets. The uncertainties associated with the PDF fits to experimental data are propagated appropriately for each PDF set. The dependence on the choice of $\alpha_S(m(Z))$ is assessed by using PDF sets with $\alpha_S(m(Z))$ shifted up and down by the 68% confidence level interval around the default value used in the PDF. For MSTW2008, fits using different b -quark masses are also available. The prediction from MCFM is at the parton-level, so must be corrected for the effects of QED final-state radiation (FSR), hadronisation, underlying event and MPI. The correction for QED FSR is obtained using PHOTOS, interfaced to the ALPGEN+HERWIG+JIMMY samples used in the data analysis, and evaluated by comparing the cross-sections obtained by applying the selection requirements to leptons before, and after FSR. The correction factors for hadronisation, underlying event and MPI are obtained for each differential cross-section from both PYTHIA and SHERPA, by taking the ratio of the predictions with these effects turned on and turned off. The versions used are PYTHIA 6.427, with the CTEQ5L PDF set and the Perugia 2011 tune, and SHERPA 1.4.1, with the CT10 PDF set. Differences between the correction factors obtained in PYTHIA and SHERPA, which are typically at the 1%-level, as well as the 50% uncertainty on MPI described in Section 8, are assigned as systematic uncertainties.

Full particle-level predictions with NLO matrix element calculations are also obtained using aMC@NLO [10], in both the 4FNS and 5FNS. In the 4FNS, the $Z + \geq 2$ b -jets process is calculated at $\mathcal{O}(\alpha_S^3)$, including the effects of the b -quark mass, and interfaced to the MSTW2008NLO_nf4 PDF set [55]. No kinematic cuts are applied to the b -jets in this calculation, therefore it is also used to derive a 4FNS prediction for the $Z + \geq 1$ b -jet final state. For the 5FNS prediction, the more inclusive $Z + \geq 1$ -jet process is calculated at $\mathcal{O}(\alpha_S^2)$ neglecting the b -quark mass and using the MSTW2008NLO PDF set. This is then used to derive a 5FNS prediction at $\mathcal{O}(\alpha_S^2)$ for $Z + \geq 1$ b -jet and $Z + \geq 2$ b -jets. The latter process is therefore LO only. In both cases, HERWIG++ is used to simulate the hadronisation, underlying event and MPI. Both predictions require a correction for a missing component of MPI, in which the Z boson and b -quarks are produced in separate scatters within the pp collision. This correction is estimated using the ALPGEN+HERWIG+JIMMY samples where the MPI contribution is included. Since the 4FNS and 5FNS use different matrix elements ($Z+bb$ and $Z+jet$ respectively), a different correction factor is derived in each case. In both the 4FNS and 5FNS predictions from aMC@NLO, the renormalisation and factorisation scales are set dynamically to the same definition used for the MCFM prediction. Since variations of the scales are the dominant sources of theory uncertainty, they have been evaluated for all aMC@NLO predictions using the same procedure as for MCFM. The overall scale uncertainty is found to have a comparable size in the 4FNS and 5FNS predictions, and to be consistent with the scale uncertainty for MCFM. However, the uncertainty is fully dominated by variations of the renormalisation scale in the 4FNS case, while for the 5FNS renormalisation and factorisation scale variations produce shifts which are similar in magnitude and opposite in direction, giving a total uncertainty dominated by the cases where one is shifted up and the other down (and vice versa). Uncertainties arising from the PDFs and the choice of α_S are obtained using MCFM.

Predictions are also obtained from SHERPA and ALPGEN+HERWIG+JIMMY, which combine tree-level matrix elements for multiple jet emissions with a parton shower, hadronisation and underlying event package. ALPGEN uses the 4FNS and has up to five partons in the matrix element, while SHERPA uses the 5FNS and has up to four partons in the matrix element.

10 Results

The cross-sections for $Z + \geq 1$ b -jet and $Z + \geq 2$ b -jets are shown in Figure 6, and Table 4. The MCFM predictions always agree with the data within the combined experimental and theoretical uncertainties. The prediction obtained with CT10 is lower, due primarily to the default choice of $\alpha_S(m(Z))$ in this PDF (0.118) compared to MSTW2008 and NNPDF2.3 (0.120 in each). The predictions do agree within the uncertainty on the choice of $\alpha_S(m(Z))$. For aMC@NLO, the 5FNS prediction describes $Z + \geq 1$ b -jet well, while the 4FNS underestimates the measured cross-section. This situation is reversed for the $Z + \geq 2$ b -jets case, where the 4FNS provides a good description, while the 5FNS underestimates the cross-section. However, as explained in Section 9, the 5FNS prediction from aMC@NLO is only LO for $Z + \geq 2$ b -jets, which may explain this underestimate. Considering only statistical uncertainties, both the 4FNS prediction from ALPGEN+HERWIG+JIMMY and the 5FNS prediction from SHERPA underestimate the data, with ALPGEN+HERWIG+JIMMY being consistently below SHERPA by around 30-40%.

	$\sigma(Zb)$ [fb]	$\sigma(Zb) \times N_{b\text{-jet}}$ [fb]	$\sigma^*(Zb) \times N_{b\text{-jet}}$ [fb]	$\sigma(Zbb)$ [fb]
Data	$4820 \pm 60^{+360}_{-380}$	$5390 \pm 60 \pm 480$	$4540 \pm 55 \pm 330$	$520 \pm 20^{+74}_{-72}$
MCFM \otimes MSTW2008	$5230 \pm 30^{+690}_{-710}$	$5460 \pm 40^{+740}_{-740}$	$4331 \pm 30^{+400}_{-480}$	$410 \pm 10^{+60}_{-60}$
MCFM \otimes CT10	$4850 \pm 30^{+580}_{-680}$	$5070 \pm 30^{+640}_{-710}$	$4030 \pm 30^{+350}_{-450}$	$386 \pm 5^{+55}_{-50}$
MCFM \otimes NNPDF23	$5420 \pm 20^{+670}_{-710}$	$5660 \pm 30^{+720}_{-740}$	$4490 \pm 30^{+380}_{-460}$	$420 \pm 10^{+70}_{-50}$
aMC@NLO 4FNS \otimes MSTW2008	$3390 \pm 20^{+580}_{-480}$	$3910 \pm 20^{+660}_{-560}$	$3290 \pm 20^{+580}_{-460}$	$485 \pm 7^{+80}_{-70}$
aMC@NLO 5FNS \otimes MSTW2008	$4680 \pm 40^{+550}_{-580}$	$5010 \pm 40^{+590}_{-620}$	$4220 \pm 40^{+460}_{-510}$	$314 \pm 9^{+30}_{-30}$
SHERPA \otimes CT10	3770 ± 10	4210 ± 10	3640 ± 10	422 ± 2
ALPGEN+HJ \otimes CTEQ6L1	2580 ± 10	2920 ± 10	2380 ± 10	317 ± 2

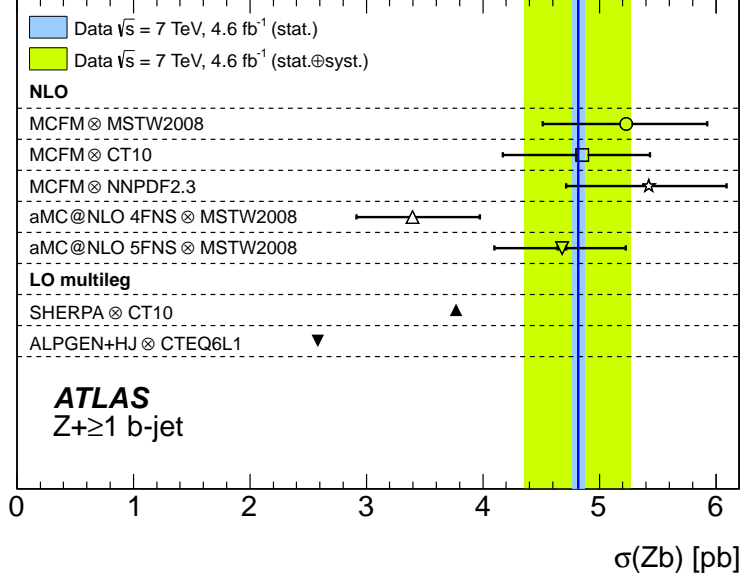
Table 4. The measurement and theory predictions for the integrated cross-sections and the integrated inclusive b -jet cross-sections. The MCFM results are corrected for MPI, non-perturbative QCD effects and QED radiation effects. The statistical uncertainty is quoted first in each case. The second uncertainty is either the total systematic uncertainty (data), the sum in quadrature of all theory uncertainties (MCFM), or the scale uncertainty (aMC@NLO).

Figure 7 shows $\sigma(Zb) \times N_{b\text{-jet}}$, as a function of the b -jet p_T and $|y|$. The theoretical predictions generally provide a good description of the shape of the data. The 4FNS prediction from aMC@NLO underestimates the data most significantly at central rapidities. Figure 8 shows $\sigma(Zb)$, as a function of the Z boson p_T and $|y|$. In general, all theoretical predictions provide a reasonable description of the shape of the data within uncertainties, though there is evidence for disagreement at very high Z boson p_T , and a slope in the ratio of the MCFM prediction to data for the Z boson rapidity.

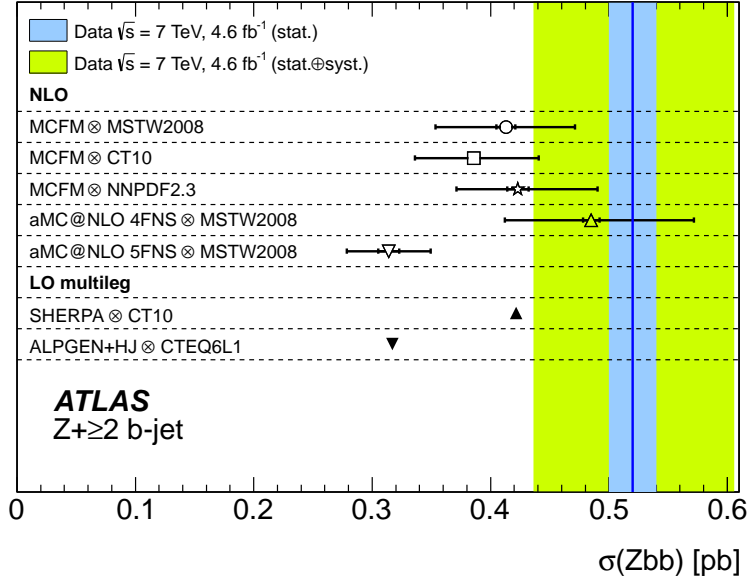
In general, good agreement with the data can be seen for $\Delta y(Z, b)$ and $y_{\text{boost}}(Z, b)$ in Figure 9, though with some evidence for a slope in the ratio of aMC@NLO 4FNS relative to the data for $y_{\text{boost}}(Z, b)$. In $\Delta\phi(Z, b)$ (Figure 10) the fixed-order pQCD prediction from MCFM has significant discrepancy at $\Delta\phi(Z, b) = \pi$, which also distorts the $\Delta R(Z, b)$ prediction. This is due to the fixed-order calculation containing at most one or two outgoing partons in association with the Z boson. In the case of one parton, $\Delta\phi(Z, b) = \pi$ by construction, leading to the distorted distribution. The inclusion of higher multiplicity matrix elements in ALPGEN and SHERPA, and matching to parton shower models in ALPGEN, SHERPA and aMC@NLO helps to populate the $\Delta\phi(Z, b)$ distribution in a way which yields a much better agreement with data. This emphasises the importance of higher order effects when considering such distributions. The region of low $\Delta\phi(Z, b)$, which is most sensitive to additional QCD radiation as well as soft corrections, is also poorly modelled by MCFM; these effects are not fully captured in the non-perturbative corrections applied to that prediction.

For the $Z + \geq 2$ b -jets differential cross-sections shown in Figures 11 and 12, all predictions provide reasonable descriptions of the data within the large experimental uncertainties. There is some evidence for disagreements between predictions and data at low $m(b, b)$ and low $\Delta R(b, b)$.

Finally, Figure 13 compares the MCFM predictions obtained using different PDFs to the data for the Z boson rapidity distribution, which is the distribution found to have the largest dependence on the PDF set used. It can be seen that, while the different PDF sets do yield different results, they all show a similar trend relative to the data, and the differences are small compared to the theoretical scale uncertainty.

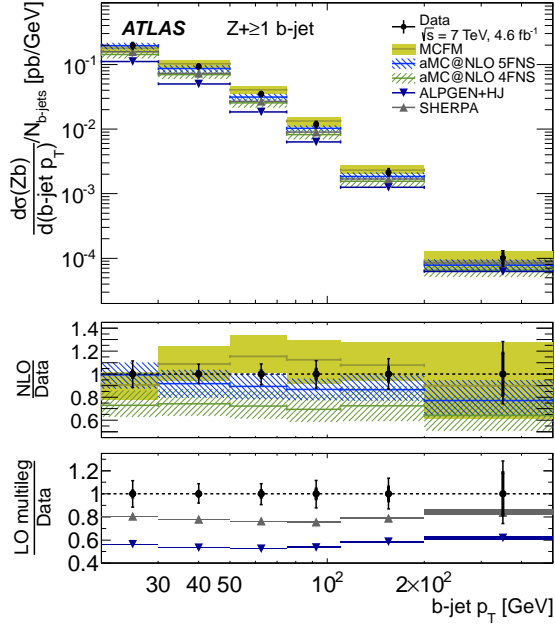


(a)

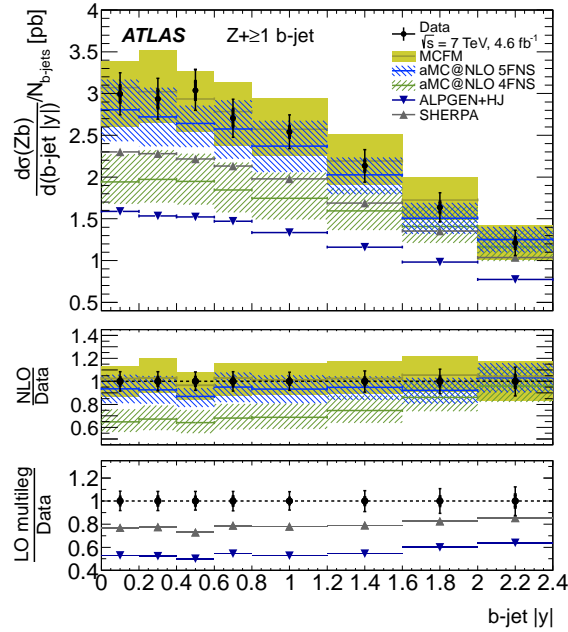


(b)

Figure 6. Cross-sections for (a) $Z+\geq 1$ b-jet, and (b) $Z+\geq 2$ b-jets. The measurement is shown as a vertical blue line with the inner blue shaded band showing the corresponding statistical uncertainty and the outer green shaded band showing the sum in quadrature of statistical and systematic uncertainties. Comparison is made to NLO predictions from MCFM interfaced to different PDF sets and aMC@NLO interfaced to the same PDF set in both the 4FNS and 5FNS. The statistical (inner bar) and total (outer bar) uncertainties are shown for these predictions, which are dominated by the theoretical scale uncertainty calculated as described in the text. Comparisons are also made to LO multi-legged predictions from ALPGEN+HERWIG+JIMMY and SHERPA; in this case the uncertainty bars are statistical only, and smaller than the marker.

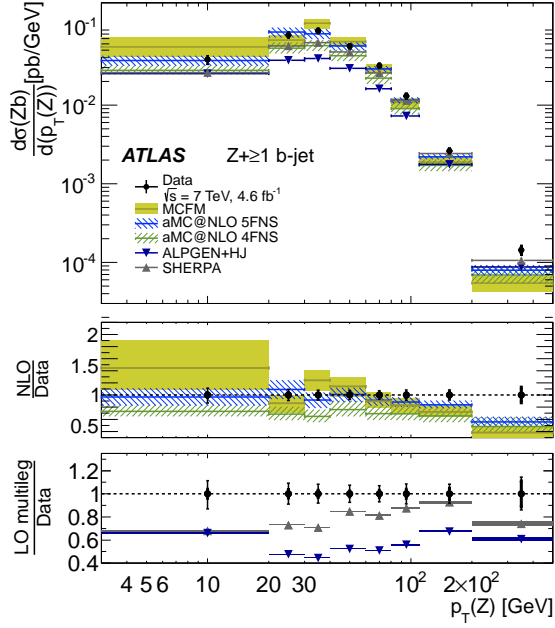


(a)

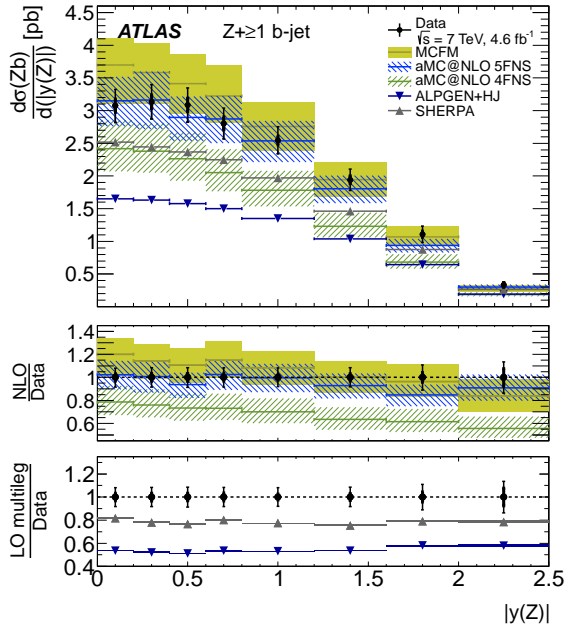


(b)

Figure 7. The inclusive b -jet cross-section $\sigma(Zb) \times N_{b\text{-jet}}$ as a function of b -jet p_T (a) and $|y|$ (b). The top panels show measured differential cross-sections as filled circles with statistical (inner) and total (outer bar) uncertainties. Overlaid for comparison are the NLO predictions from MCFM and aMC@NLO both using the MSTW2008 PDF set. The shaded bands represents the total theoretical uncertainty for MCFM and the uncertainty bands on aMC@NLO points represent the dominant theoretical scale uncertainty only. Also overlaid are LO multi-legged predictions for ALPGEN+HERWIG+JIMMY and SHERPA. The middle panels show the ratio of NLO predictions to data, and the lower panels show the ratio of LO predictions to data.

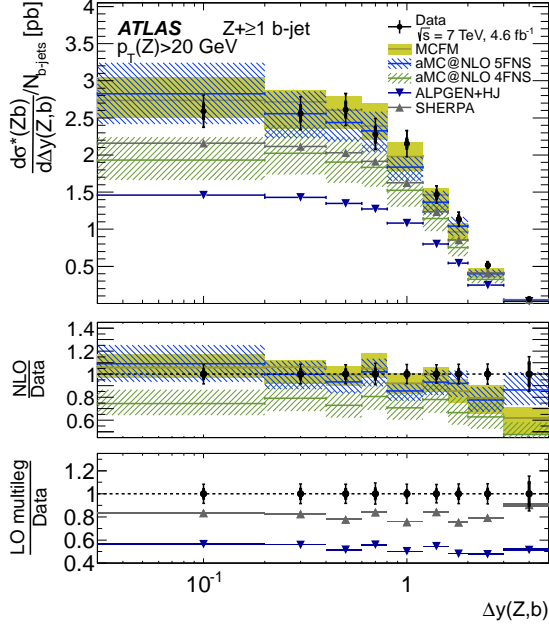


(a)

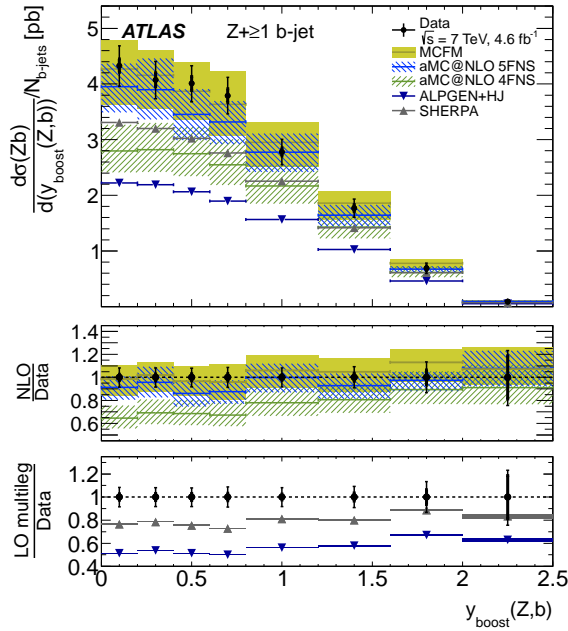


(b)

Figure 8. The cross-section $\sigma(Zb)$ as a function of Z boson p_T (a) and $|y|$ (b). The top panels show measured differential cross-sections as filled circles with statistical (inner) and total (outer bar) uncertainties. Overlaid for comparison are the NLO predictions from MCFM and aMC@NLO both using the MSTW2008 PDF set. The shaded bands represents the total theoretical uncertainty for MCFM and the uncertainty bands on aMC@NLO points represent the dominant theoretical scale uncertainty only. Also overlaid are LO multi-legged predictions for ALPGEN+HERWIG+JIMMY and SHERPA. The middle panels show the ratio of NLO predictions to data, and the lower panels show the ratio of LO predictions to data.

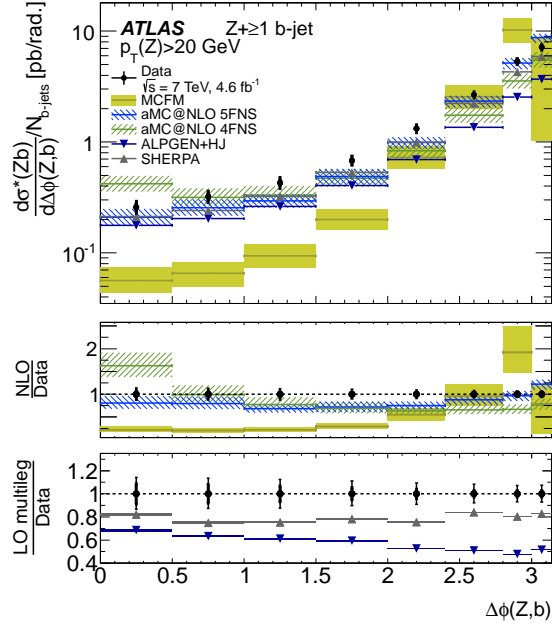


(a)

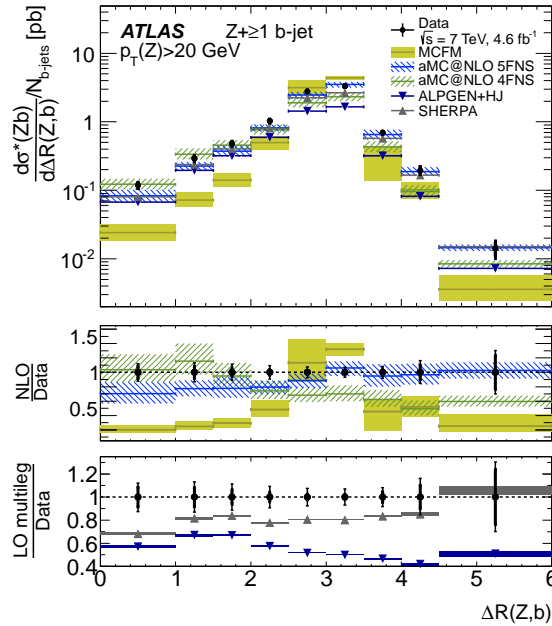


(b)

Figure 9. The inclusive b -jet cross-sections $\sigma^*(Zb) \times N_{b\text{-jet}}$ as a function of $\Delta y(Z,b)$ (a) and $\sigma(Zb) \times N_{b\text{-jet}}$ as a function of $y_{\text{boost}}(Z,b)$ (b). The former inclusive cross-section requires that the Z boson p_T be at least 20 GeV. The top panels show measured differential cross-sections as filled circles with statistical (inner) and total (outer bar) uncertainties. Overlaid for comparison are the NLO predictions from MCFM and aMC@NLO both using the MSTW2008 PDF set. The shaded bands represents the total theoretical uncertainty for MCFM and the uncertainty bands on aMC@NLO points represent the dominant theoretical scale uncertainty only. Also overlaid are LO multi-legged predictions for ALPGEN+HERWIG+JIMMY and SHERPA. The middle panels show the ratio of NLO predictions to data, and the lower panels show the ratio of LO predictions to data.

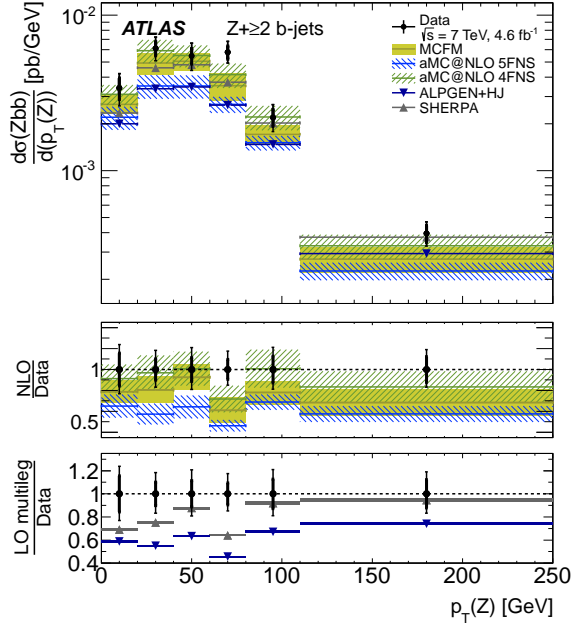


(a)

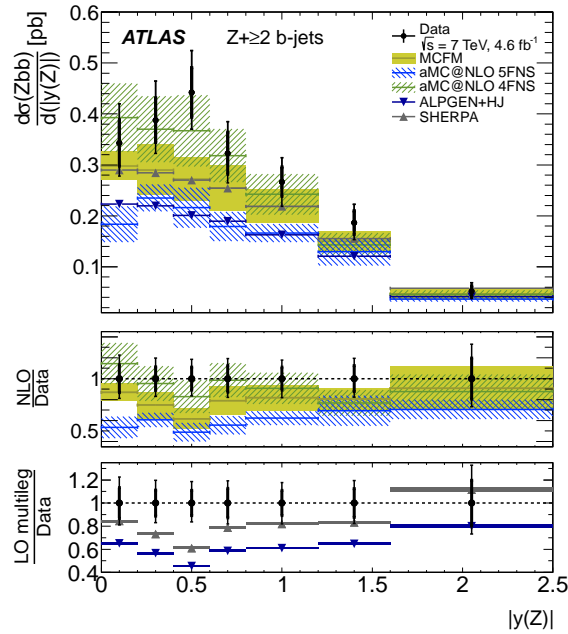


(b)

Figure 10. The inclusive b -jet cross-section $\sigma^*(Zb) \times N_{b\text{-jet}}$ as a function of $\Delta\phi(Z,b)$ (a) and $\Delta R(Z,b)$ (b). The inclusive cross-section requires that the Z boson p_T be at least 20 GeV. The top panels show measured differential cross-sections as filled circles with statistical (inner) and total (outer bar) uncertainties. Overlaid for comparison are the NLO predictions from MCFM and aMC@NLO both using the MSTW2008 PDF set. The shaded bands represents the total theoretical uncertainty for MCFM and the uncertainty bands on aMC@NLO points represent the dominant theoretical scale uncertainty only. Also overlaid are LO multi-legged predictions for ALPGEN+HERWIG+JIMMY and SHERPA. The middle panels show the ratio of NLO predictions to data, and the lower panels show the ratio of LO predictions to data.

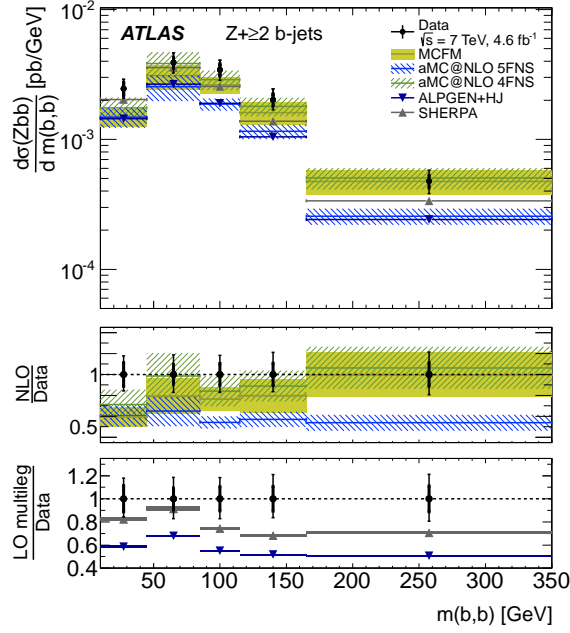


(a)

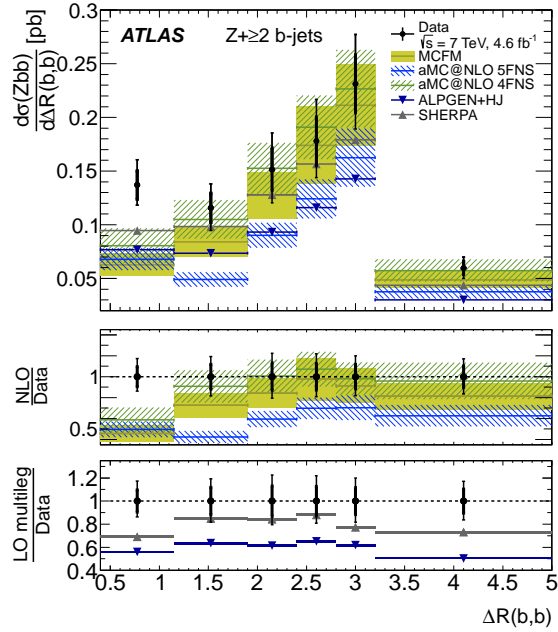


(b)

Figure 11. The cross-section $\sigma(Zbb)$ as a function of Z boson p_T (a), and $|y|$ (b). The top panels show measured differential cross-sections as filled circles with statistical (inner) and total (outer bar) uncertainties. Overlaid for comparison are the NLO predictions from MCFM and aMC@NLO both using the MSTW2008 PDF set. The shaded bands represents the total theoretical uncertainty for MCFM and the uncertainty bands on aMC@NLO points represent the dominant theoretical scale uncertainty only. Also overlaid are LO multi-legged predictions for ALPGEN+HERWIG+JIMMY and SHERPA. The middle panels show the ratio of NLO predictions to data, and the lower panels show the ratio of LO predictions to data.

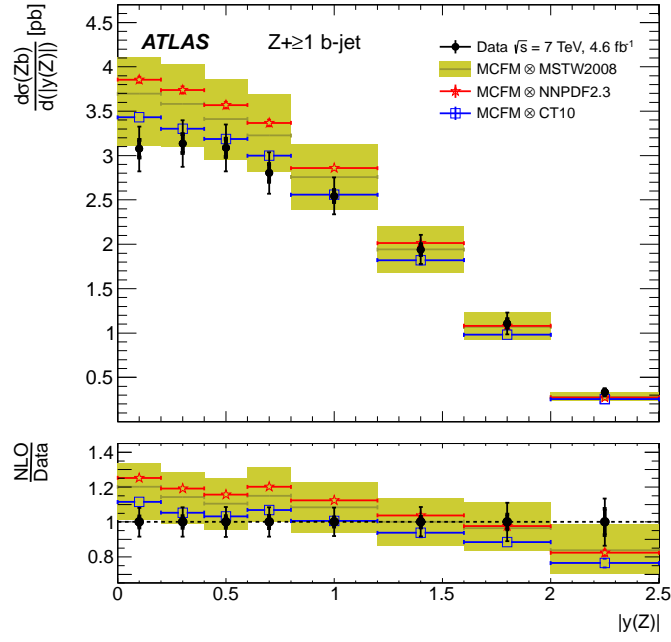


(a)

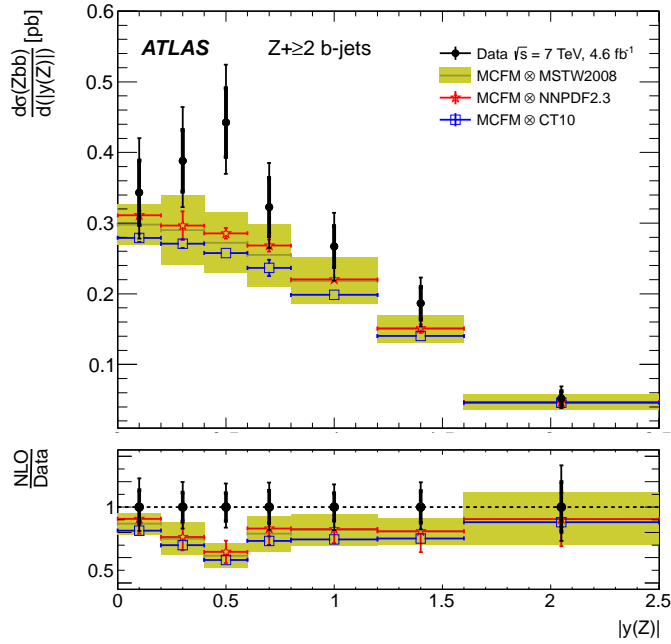


(b)

Figure 12. The cross-section $\sigma(Zbb)$ as a function of $m(b,b)$ (a) and $\Delta R(b,b)$ (b). The top panels show measured differential cross-sections as filled circles with statistical (inner) and total (outer bar) uncertainties. Overlaid for comparison are the NLO predictions from MCFM and aMC@NLO both using the MSTW2008 PDF set. The shaded bands represents the total theoretical uncertainty for MCFM and the uncertainty bands on aMC@NLO points represent the dominant theoretical scale uncertainty only. Also overlaid are LO multi-legged predictions for ALPGEN+HERWIG+JIMMY and SHERPA. The middle panels show the ratio of NLO predictions to data, and the lower panels show the ratio of LO predictions to data.



(a)



(b)

Figure 13. The MCFM prediction using different PDF sets for the cross-sections $\sigma(Zb)$ (a) and $\sigma(Zbb)$ (b) as a function of the Z boson $|y|$. The top panels show measured differential cross-sections as filled circles with statistical (inner) and total (outer bar) uncertainties. The shaded band represents the total theoretical uncertainty for MCFM interfaced to the MSTW2008 PDF set. Uncertainties on MCFM predictions with alternative PDF sets are statistical only. The lower panel shows the ratio of each prediction to data.

11 Conclusions

Differential $Z+b$ -jets cross-section measurements from the LHC have been presented using 4.6 fb^{-1} of $\sqrt{s}=7 \text{ TeV}$ pp collision data recorded by the ATLAS detector in 2011. In total, 12 distributions for $Z+\geq 1$ b -jet and $Z+\geq 2$ b -jets topologies have been investigated and compared to theoretical pQCD calculations. Next-to-leading-order predictions from MCFM and aMC@NLO generally provide the best overall description of the data. The agreement of the aMC@NLO cross-section prediction with data differs in the $Z+\geq 1$ b -jet and $Z+\geq 2$ b -jets cases, with the former better described by the 5FNS prediction and the latter better described by the 4FNS prediction. Even at NLO, scale uncertainties dominate and currently limit any sensitivity to different PDF sets. Descriptions of the shapes of the differential cross-sections are generally good within uncertainties for both LO and NLO predictions. For angular distributions in the $Z+\geq 1$ b -jet selection, where the fixed-order NLO prediction is observed to break down, the differential shapes in data are well modelled by LO multi-legged predictions.

12 Acknowledgements

We thank CERN for the very successful operation of the LHC, as well as the support staff from our institutions without whom ATLAS could not be operated efficiently.

We acknowledge the support of ANPCyT, Argentina; YerPhI, Armenia; ARC, Australia; BMWFW and FWF, Austria; ANAS, Azerbaijan; SSTC, Belarus; CNPq and FAPESP, Brazil; NSERC, NRC and CFI, Canada; CERN; CONICYT, Chile; CAS, MOST and NSFC, China; COLCIENCIAS, Colombia; MSMT CR, MPO CR and VSC CR, Czech Republic; DNRF, DNSRC and Lundbeck Foundation, Denmark; EPLANET, ERC and NSRF, European Union; IN2P3-CNRS, CEA-DSM/IRFU, France; GNSF, Georgia; BMBF, DFG, HGF, MPG and AvH Foundation, Germany; GSRT and NSRF, Greece; ISF, MINERVA, GIF, I-CORE and Benozziyo Center, Israel; INFN, Italy; MEXT and JSPS, Japan; CNRST, Morocco; FOM and NWO, Netherlands; BRF and RCN, Norway; MNiSW and NCN, Poland; GRICES and FCT, Portugal; MNE/IFA, Romania; MES of Russia and ROSATOM, Russian Federation; JINR; MSTD, Serbia; MSSR, Slovakia; ARRS and MIZŠ, Slovenia; DST/NRF, South Africa; MINECO, Spain; SRC and Wallenberg Foundation, Sweden; SER, SNSF and Cantons of Bern and Geneva, Switzerland; NSC, Taiwan; TAEK, Turkey; STFC, the Royal Society and Leverhulme Trust, United Kingdom; DOE and NSF, United States of America.

The crucial computing support from all WLCG partners is acknowledged gratefully, in particular from CERN and the ATLAS Tier-1 facilities at TRIUMF (Canada), NDGF (Denmark, Norway, Sweden), CC-IN2P3 (France), KIT/GridKA (Germany), INFN-CNAF (Italy), NL-T1 (Netherlands), PIC (Spain), ASGC (Taiwan), RAL (UK) and BNL (USA) and in the Tier-2 facilities worldwide.

References

- [1] F. Maltoni, G. Ridolfi, and M. Ubiali, *b-initiated processes at the LHC: a reappraisal*, JHEP **1207** (2012) 022, [arXiv:1203.6393 \[hep-ph\]](#).
- [2] J. M. Campbell, R. Ellis, F. Maltoni, and S. Willenbrock, *Associated production of a Z Boson and a single heavy quark jet*, Phys. Rev. **D 69** (2004) 074021, [arXiv:hep-ph/0312024](#).
- [3] J. M. Campbell, R. Ellis, F. Maltoni, and S. Willenbrock, *Production of a Z boson and two jets with one heavy quark tag*, Phys. Rev. **D 73** (2006) 054007, [arXiv:hep-ph/0510362](#).
- [4] F. Cordero, L. Reina, and D. Wackerroth, *W- and Z-boson production with a massive bottom-quark pair at the Large Hadron Collider*, Phys. Rev. **D 80** (2009) 034015, [arXiv:0906.1923 \[hep-ph\]](#).
- [5] M. L. Mangano et al., *ALPGEN, a generator for hard multiparton processes in hadronic collisions*, JHEP **0307** (2003) 001, [arXiv:hep-ph/0206293](#).
- [6] B. P. Kersevan and E. Richter-Was, *The Monte Carlo event generator AcerMC versions 2.0 to 3.8 with interfaces to PYTHIA 6.4, HERWIG 6.5 and ARIADNE 4.1*, Comput. Phys. Commun. **184** (2013) 919, [arXiv:hep-ph/0405247](#).
- [7] T. Gleisberg et al., *Event generation with SHERPA 1.1*, JHEP **0902** (2009) 007, [arXiv:0811.4622 \[hep-ph\]](#).
- [8] J. Alwall, M. Herquet, F. Maltoni, O. Mattelaer, and T. Stelzer, *MadGraph 5: Going Beyond*, JHEP **1106** (2011) 128, [arXiv:1106.0522 \[hep-ph\]](#).
- [9] R. Frederix, S. Frixione, V. Hirschi, F. Maltoni, R. Pittau, and P. Torrielli, *W and Z/ γ^* boson production in association with a bottom-antibottom pair*, JHEP **09** (2011) 061, [arXiv:1106.6019 \[hep-ph\]](#).
- [10] J. Alwall et al., *The automated computation of tree-level and next-to-leading order differential cross sections, and their matching to parton shower simulations*, JHEP **07** (2014) 079, [arXiv:1405.0301 \[hep-ph\]](#).
- [11] CDF Collaboration, T. Aaltonen et al., *Measurement of cross sections for b Jet production in events with a Z boson in $p\bar{p}$ collisions at $\sqrt{s}=1.96$ TeV*, Phys. Rev. **D 79** (2009) 052008, [arXiv:0812.4458 \[hep-ex\]](#).
- [12] D0 Collaboration, V. Abazov et al., *Measurement of the ratio of differential cross sections $\sigma(p\bar{p} \rightarrow Z + b \text{ jet})/\sigma(p\bar{p} \rightarrow Z + \text{jet})$ in $p\bar{p}$ collisions at $\sqrt{s}=1.96$ TeV*, Phys. Rev. **D 87** (2013) 092010, [arXiv:1301.2233 \[hep-ex\]](#).
- [13] ATLAS Collaboration, *Measurement of the cross-section for b-jets produced in association with a Z boson at $\sqrt{s}=7$ TeV with the ATLAS detector*, Phys. Lett. **B 706** (2012) 295, [arXiv:1109.1403 \[hep-ex\]](#).
- [14] CMS Collaboration, *Measurement of the production cross sections for a Z boson and one or more b jets in pp collisions at $\sqrt{s}=7$ TeV*, submitted to JHEP, [arXiv:1402.1521 \[hep-ex\]](#).

- [15] CMS Collaboration, *Measurement of the cross section and angular correlations for associated production of a Z boson with b hadrons in pp collisions at $\sqrt{s}=7$ TeV*, JHEP **12** (2013) 039, [arXiv:1310.1349 \[hep-ex\]](#).
- [16] ATLAS Collaboration, *The ATLAS Experiment at the CERN Large Hadron Collider*, JINST **3** (2008) S08003. <https://cds.cern.ch/record/1129811>.
- [17] G. Corcella et al., *HERWIG 6: An Event generator for hadron emission reactions with interfering gluons (including supersymmetric processes)*, JHEP **0101** (2001) 010, [arXiv:hep-ph/0011363](#).
- [18] J. M. Butterworth, J. R. Forshaw, and M. H. Seymour, *Multiparton interactions in photoproduction at HERA*, Z. Phys. **C 72** (1996) 637, [arXiv:hep-ph/9601371](#).
- [19] J. Alwall et al., *Comparative study of various algorithms for the merging of parton showers and matrix elements in hadronic collisions*, Eur. Phys. J. **C53** (2008) 473, [arXiv:0706.2569 \[hep-ph\]](#).
- [20] J. Pumplin et al., *New generation of parton distributions with uncertainties from global QCD analysis*, JHEP **0207** (2002) 012, [arXiv:hep-ph/0201195](#).
- [21] ATLAS Collaboration, *New ATLAS event generator tunes to 2010 data*, ATL-PHYS-PUB-2011-008. <http://cds.cern.ch/record/1345343>.
- [22] D. J. Lange, *The EvtGen particle decay simulation package*, Nucl. Instrum. Meth. **A 462** (2001) 152–155.
- [23] H. L. Lai et al., *New parton distributions for collider physics*, Phys. Rev. **D 82** (2010) 074024, [arXiv:1007.2241 \[hep-ph\]](#).
- [24] S. Catani, F. Krauss, R. Kuhn, and B. Webber, *QCD Matrix elements + parton showers*, JHEP **11** (2011) 063, [arXiv:hep-ph/0109231](#).
- [25] S. Frixione and B. Webber, *Matching NLO QCD computations and parton shower simulations*, JHEP **0206** (2002) 029, [arXiv:hep-ph/0204244](#).
- [26] T. Sjostrand, S. Mrenna, and P. Z. Skands, *PYTHIA 6.4 Physics and Manual*, JHEP **0605** (2006) 026, [arXiv:hep-ph/0603175](#).
- [27] S. Frixione, P. Nason, and C. Oleari, *Matching NLO QCD computations with Parton Shower simulations: the POWHEG method*, JHEP **0711** (2007) 070, [arXiv:0709.2092 \[hep-ph\]](#).
- [28] C. Anastasiou, L. Dixon, K. Melnikov, and F. Petriello, *High-precision QCD at hadron colliders: electroweak gauge boson rapidity distributions at NNLO*, Phys. Rev. **D 69** (2004) 094008, [arXiv:hep-ph/0312266](#).
- [29] M. Aliev, H. Lacker, U. Langenfeld, S. Moch, P. Uwer, and M. Wiedermann, *HATHOR: HAdronic Top and Heavy quarks crOss section calculatoR*, Comput. Phys. Commun. **182** (2011) 1034, [arXiv:1007.1327 \[hep-ph\]](#).
- [30] J. M. Campbell, R. K. Ellis, and C. Williams, *Vector boson pair production at the LHC*, JHEP **1107** (2011) 018, [arXiv:1105.0020 \[hep-ph\]](#).

- [31] J. M. Campbell, R. K. Ellis, and F. Tramontano, *Single top production and decay at next-to-leading order*, Phys. Rev. D **70** (2004) 094012, [arXiv:hep-ph/0408158](#).
- [32] ATLAS Collaboration, *ATLAS tunes of Pythia6 and Pythia8 for MC11*, ATLAS-PHYS-PUB-2011-009. <http://cds.cern.ch/record/1363300>.
- [33] S. Agostinelli et al., *GEANT4: A Simulation Toolkit*, Nucl. Instrum. Meth. **A 506** (2003) 250.
- [34] ATLAS Collaboration, *The ATLAS simulation infrastructure*, Eur. Phys. J. **C 70** (2010) 823, [arXiv:1005.4568 \[hep-ex\]](#).
- [35] ATLAS Collaboration, *Improved luminosity determination in pp collisions at $\sqrt{s}=7$ TeV using the ATLAS detector at the LHC*, submitted to Eur. Phys. J. **C**, [arXiv:1302.4393 \[hep-ex\]](#).
- [36] ATLAS Collaboration, *Electron reconstruction and identification efficiency measurements with the ATLAS detector using the 2011 LHC proton-proton collision data*, Eur. Phys. J. **C 74** (2014) 2941, [arXiv:1404.2240 \[hep-ex\]](#).
- [37] ATLAS Collaboration, *Measurement of the $W \rightarrow l\nu$ and $Z/\gamma^* \rightarrow ll$ production cross sections in proton-proton collisions at $\sqrt{s}=7$ TeV with the ATLAS detector*, JHEP **1012** (2010) 060, [arXiv:1010.2130 \[hep-ex\]](#).
- [38] ATLAS Collaboration, *Calorimeter Clustering Algorithms : Description and Performance*, ATLAS-LARG-PUB-2008-002. <http://cds.cern.ch/record/1099735>.
- [39] M. Cacciari, G. P. Salam, and G. Soyez, *The anti- k_t jet clustering algorithm*, JHEP **0804** (2008) 063, [arXiv:0802.1189 \[hep-ph\]](#).
- [40] M. Cacciari and G. P. Salam, *Dispelling the N^3 myth for the kt jet-finder*, Phys. Lett. **B641** (2006) 57, [arXiv:hep-ph/0512210](#).
- [41] ATLAS Collaboration, *Jet energy measurement and its systematic uncertainty in proton-proton collisions at $\sqrt{s} = 7$ TeV with the ATLAS detector*, [arXiv:1406.0076 \[hep-ex\]](#).
- [42] ATLAS Collaboration, *Measuring the b -tag efficiency in a $t\bar{t}$ sample with 4.7 fb^{-1} of data from the ATLAS detector*, ATLAS-CONF-2012-097. <https://cds.cern.ch/record/1460443>.
- [43] ATLAS Collaboration, *b -jet tagging calibration on c -jets containing D^* mesons*, ATLAS-CONF-2012-039. <https://cds.cern.ch/record/1435193>.
- [44] ATLAS Collaboration, *Measurement of the Mistag Rate of b -tagging algorithms with 5 fb^{-1} of Data Collected by the ATLAS Detector*, ATLAS-CONF-2012-040. <https://cds.cern.ch/record/1435194>.
- [45] ATLAS Collaboration, *Performance of missing transverse momentum reconstruction in proton-proton collisions at 7 TeV with ATLAS*, Eur. Phys. J. **C 72** (2012) 1844, [arXiv:1108.5602 \[hep-ex\]](#).

- [46] G. Piacquadio and C. Weiser, *A new inclusive secondary vertex algorithm for b-jet tagging in ATLAS*, J. Phys.: Conf. Ser. **119** (2008) 032032.
- [47] ATLAS Collaboration, *Commissioning of the ATLAS high-performance b-tagging algorithms in the 7 TeV collision data*, ATLAS-CONF-2011-102.
<https://cds.cern.ch/record/1369219>.
- [48] S. D'Agostini, *A Multidimensional unfolding method based on Bayes' theorem*, Nucl. Instrum. Meth. **A362** (1995) 487–498.
- [49] ATLAS Collaboration, *Jet energy resolution in proton-proton collisions at $s = 7$ TeV recorded in 2010 with the ATLAS detector*, Eur. Phys. J. C **73** (2013) 2603,
[arXiv:1210.6201](https://arxiv.org/abs/1210.6201) [hep-ex].
- [50] ATLAS Collaboration, *A measurement of the inclusive W^\pm and Z/γ^* cross sections in the e and μ decay channels in pp collisions at $\sqrt{s}=7$ TeV with the ATLAS detector*, Phys. Rev. D **85** (2012) 072004, [arXiv:1109.5141](https://arxiv.org/abs/1109.5141) [hep-ex].
- [51] ATLAS Collaboration, *Measurement of the inclusive and dijet cross-sections of b-jets in pp collisions at $\sqrt{s} = 7$ TeV with the ATLAS detector*, Eur. Phys. J. C **71** (2011) 1846,
[arXiv:1109.6833](https://arxiv.org/abs/1109.6833) [hep-ex].
- [52] ATLAS Collaboration, *Measurement of hard double-parton interactions in $W(\rightarrow l\nu) + 2$ jet events at $\sqrt{s} = 7$ TeV with the ATLAS detector*, New J. Phys. **15** (2013) 033038,
[arXiv:1301.6872](https://arxiv.org/abs/1301.6872) [hep-ex].
- [53] J. M. Campbell and R. Ellis, *MCFM for the Tevatron and the LHC*, Nucl. Phys. Proc. Suppl. **205-206** (2010) 10, [arXiv:1007.3492](https://arxiv.org/abs/1007.3492) [hep-ph].
- [54] R. D. Ball et al., *Parton distributions with LHC data*, Nucl.Phys. **B867** (2013) 244–289,
[arXiv:1207.1303](https://arxiv.org/abs/1207.1303) [hep-ph].
- [55] A. Martin, W. Stirling, R. Thorne, and G. Watt, *Parton distributions for the LHC*, Eur.Phys.J. **C63** (2009) 189–285, [arXiv:0901.0002](https://arxiv.org/abs/0901.0002) [hep-ph].

The ATLAS Collaboration

G. Aad⁸⁴, B. Abbott¹¹², J. Abdallah¹⁵², S. Abdel Khalek¹¹⁶, O. Abdinov¹¹, R. Aben¹⁰⁶, B. Abi¹¹³, M. Abolins⁸⁹, O.S. AbouZeid¹⁵⁹, H. Abramowicz¹⁵⁴, H. Abreu¹⁵³, R. Abreu³⁰, Y. Abulaiti^{147a,147b}, B.S. Acharya^{165a,165b,a}, L. Adamczyk^{38a}, D.L. Adams²⁵, J. Adelman¹⁷⁷, S. Adomeit⁹⁹, T. Adye¹³⁰, T. Agatonovic-Jovin^{13a}, J.A. Aguilar-Saavedra^{125a,125f}, M. Agustoni¹⁷, S.P. Ahlen²², F. Ahmadov^{64,b}, G. Aielli^{134a,134b}, H. Akerstedt^{147a,147b}, T.P.A. Åkesson⁸⁰, G. Akimoto¹⁵⁶, A.V. Akimov⁹⁵, G.L. Alberghi^{20a,20b}, J. Albert¹⁷⁰, S. Albrand⁵⁵, M.J. Alconada Verzini⁷⁰, M. Aleksa³⁰, I.N. Aleksandrov⁶⁴, C. Alexa^{26a}, G. Alexander¹⁵⁴, G. Alexandre⁴⁹, T. Alexopoulos¹⁰, M. Alhroob^{165a,165c}, G. Alimonti^{90a}, L. Alio⁸⁴, J. Alison³¹, B.M.M. Allbrooke¹⁸, L.J. Allison⁷¹, P.P. Allport⁷³, J. Almond⁸³, A. Aloisio^{103a,103b}, A. Alonso³⁶, F. Alonso⁷⁰, C. Alpigiani⁷⁵, A. Altheimer³⁵, B. Alvarez Gonzalez⁸⁹, M.G. Alviggi^{103a,103b}, K. Amako⁶⁵, Y. Amaral Coutinho^{24a}, C. Amelung²³, D. Amidei⁸⁸, S.P. Amor Dos Santos^{125a,125c}, A. Amorim^{125a,125b}, S. Amoroso⁴⁸, N. Amram¹⁵⁴, G. Amundsen²³, C. Anastopoulos¹⁴⁰, L.S. Ancu⁴⁹, N. Andari³⁰, T. Andeen³⁵, C.F. Anders^{58b}, G. Anders³⁰, K.J. Anderson³¹, A. Andreazza^{90a,90b}, V. Andrei^{58a}, X.S. Anduaga⁷⁰, S. Angelidakis⁹, I. Angelozzi¹⁰⁶, P. Anger⁴⁴, A. Angerami³⁵, F. Anghinolfi³⁰, A.V. Anisenkov¹⁰⁸, N. Anjos^{125a}, A. Annovi⁴⁷, A. Antonaki⁹, M. Antonelli⁴⁷, A. Antonov⁹⁷, J. Antos^{145b}, F. Anulli^{133a}, M. Aoki⁶⁵, L. Aperio Bella¹⁸, R. Apolle^{119,c}, G. Arabidze⁸⁹, I. Aracena¹⁴⁴, Y. Arai⁶⁵, J.P. Araque^{125a}, A.T.H. Arce⁴⁵, J-F. Arguin⁹⁴, S. Argyropoulos⁴², M. Arik^{19a}, A.J. Armbruster³⁰, O. Arnaez³⁰, V. Arnal⁸¹, H. Arnold⁴⁸, M. Arratia²⁸, O. Arslan²¹, A. Artamonov⁹⁶, G. Artoni²³, S. Asai¹⁵⁶, N. Asbah⁴², A. Ashkenazi¹⁵⁴, B. Åsman^{147a,147b}, L. Asquith⁶, K. Assamagan²⁵, R. Astalos^{145a}, M. Atkinson¹⁶⁶, N.B. Atlay¹⁴², B. Auerbach⁶, K. Augsten¹²⁷, M. Auresseau^{146b}, G. Avolio³⁰, G. Azuelos^{94,d}, Y. Azuma¹⁵⁶, M.A. Baak³⁰, A. Baas^{58a}, C. Bacci^{135a,135b}, H. Bachacou¹³⁷, K. Bachas¹⁵⁵, M. Backes³⁰, M. Backhaus³⁰, J. Backus Mayes¹⁴⁴, E. Badescu^{26a}, P. Bagiacchi^{133a,133b}, P. Bagnaia^{133a,133b}, Y. Bai^{33a}, T. Bain³⁵, J.T. Baines¹³⁰, O.K. Baker¹⁷⁷, P. Balek¹²⁸, F. Balli¹³⁷, E. Banas³⁹, Sw. Banerjee¹⁷⁴, A.A.E. Bannoura¹⁷⁶, V. Bansal¹⁷⁰, H.S. Bansil¹⁸, L. Barak¹⁷³, S.P. Baranov⁹⁵, E.L. Barberio⁸⁷, D. Barberis^{50a,50b}, M. Barbero⁸⁴, T. Barillari¹⁰⁰, M. Barisonzi¹⁷⁶, T. Barklow¹⁴⁴, N. Barlow²⁸, B.M. Barnett¹³⁰, R.M. Barnett¹⁵, Z. Barnovska⁵, A. Baroncelli^{135a}, G. Barone⁴⁹, A.J. Barr¹¹⁹, F. Barreiro⁸¹, J. Barreiro Guimarães da Costa⁵⁷, R. Bartoldus¹⁴⁴, A.E. Barton⁷¹, P. Bartos^{145a}, V. Bartsch¹⁵⁰, A. Bassalat¹¹⁶, A. Basye¹⁶⁶, R.L. Bates⁵³, J.R. Batley²⁸, M. Battaglia¹³⁸, M. Battistin³⁰, F. Bauer¹³⁷, H.S. Bawa^{144,e}, M.D. Beattie⁷¹, T. Beau⁷⁹, P.H. Beauchemin¹⁶², R. Beccherle^{123a,123b}, P. Bechtel²¹, H.P. Beck¹⁷, K. Becker¹⁷⁶, S. Becker⁹⁹, M. Beckingham¹⁷¹, C. Becot¹¹⁶, A.J. Beddall^{19c}, A. Beddall^{19c}, S. Bedikian¹⁷⁷, V.A. Bednyakov⁶⁴, C.P. Bee¹⁴⁹, L.J. Beemster¹⁰⁶, T.A. Beermann¹⁷⁶, M. Begel²⁵, K. Behr¹¹⁹, C. Belanger-Champagne⁸⁶, P.J. Bell⁴⁹, W.H. Bell⁴⁹, G. Bella¹⁵⁴, L. Bellagamba^{20a}, A. Bellerive²⁹, M. Bellomo⁸⁵, K. Belotskiy⁹⁷, O. Beltramello³⁰, O. Benary¹⁵⁴, D. Bencheikroun^{136a}, K. Bendtz^{147a,147b}, N. Benekos¹⁶⁶, Y. Benhammou¹⁵⁴, E. Benhar Nocchioli⁴⁹, J.A. Benitez Garcia^{160b}, D.P. Benjamin⁴⁵, J.R. Bensinger²³, K. Benslama¹³¹, S. Bentvelsen¹⁰⁶, D. Berge¹⁰⁶, E. Bergeaas Kuutmann¹⁶, N. Berger⁵,

F. Berghaus¹⁷⁰, J. Beringer¹⁵, C. Bernard²², P. Bernat⁷⁷, C. Bernius⁷⁸,
 F.U. Bernlochner¹⁷⁰, T. Berry⁷⁶, P. Berta¹²⁸, C. Bertella⁸⁴, G. Bertoli^{147a,147b},
 F. Bertolucci^{123a,123b}, C. Bertsche¹¹², D. Bertsche¹¹², M.I. Besana^{90a}, G.J. Besjes¹⁰⁵,
 O. Bessidskaia^{147a,147b}, M.F. Bessner⁴², N. Besson¹³⁷, C. Betancourt⁴⁸, S. Bethke¹⁰⁰,
 W. Bhimji⁴⁶, R.M. Bianchi¹²⁴, L. Bianchini²³, M. Bianco³⁰, O. Biebel⁹⁹, S.P. Bieniek⁷⁷,
 K. Bierwagen⁵⁴, J. Biesiada¹⁵, M. Biglietti^{135a}, J. Bilbao De Mendizabal⁴⁹, H. Bilokon⁴⁷,
 M. Bindi⁵⁴, S. Binet¹¹⁶, A. Bingul^{19c}, C. Bini^{133a,133b}, C.W. Black¹⁵¹, J.E. Black¹⁴⁴,
 K.M. Black²², D. Blackburn¹³⁹, R.E. Blair⁶, J.-B. Blanchard¹³⁷, T. Blazek^{145a}, I. Bloch⁴²,
 C. Blocker²³, W. Blum^{82,*}, U. Blumenschein⁵⁴, G.J. Bobbink¹⁰⁶, V.S. Bobrovnikov¹⁰⁸,
 S.S. Bocchetta⁸⁰, A. Bocci⁴⁵, C. Bock⁹⁹, C.R. Boddy¹¹⁹, M. Boehler⁴⁸, T.T. Boek¹⁷⁶,
 J.A. Bogaerts³⁰, A.G. Bogdanchikov¹⁰⁸, A. Bogouch^{91,*}, C. Boehm^{147a}, J. Boehm¹²⁶,
 V. Boisvert⁷⁶, T. Bold^{38a}, V. Boldea^{26a}, A.S. Boldyrev⁹⁸, M. Bomben⁷⁹, M. Bona⁷⁵,
 M. Boonekamp¹³⁷, A. Borisov¹²⁹, G. Borissov⁷¹, M. Borri⁸³, S. Borroni⁴², J. Bortfeldt⁹⁹,
 V. Bortolotto^{135a,135b}, K. Bos¹⁰⁶, D. Boscherini^{20a}, M. Bosman¹², H. Boterenbrood¹⁰⁶,
 J. Boudreau¹²⁴, J. Bouffard², E.V. Bouhova-Thacker⁷¹, D. Boumediene³⁴,
 C. Bourdarios¹¹⁶, N. Bousson¹¹³, S. Boutouil^{136d}, A. Boveia³¹, J. Boyd³⁰, I.R. Boyko⁶⁴,
 J. Bracinik¹⁸, A. Brandt⁸, G. Brandt¹⁵, O. Brandt^{58a}, U. Bratzler¹⁵⁷, B. Brau⁸⁵,
 J.E. Brau¹¹⁵, H.M. Braun^{176,*}, S.F. Brazzale^{165a,165c}, B. Brelier¹⁵⁹, K. Brendlinger¹²¹,
 A.J. Brennan⁸⁷, R. Brenner¹⁶⁷, S. Bressler¹⁷³, K. Bristow^{146c}, T.M. Bristow⁴⁶,
 D. Britton⁵³, F.M. Brochu²⁸, I. Brock²¹, R. Brock⁸⁹, C. Bromberg⁸⁹, J. Bronner¹⁰⁰,
 G. Brooijmans³⁵, T. Brooks⁷⁶, W.K. Brooks^{32b}, J. Brosamer¹⁵, E. Brost¹¹⁵, J. Brown⁵⁵,
 P.A. Bruckman de Renstrom³⁹, D. Bruncko^{145b}, R. Bruneliere⁴⁸, S. Brunet⁶⁰, A. Bruni^{20a},
 G. Bruni^{20a}, M. Bruschi^{20a}, L. Bryngemark⁸⁰, T. Buanes¹⁴, Q. Buat¹⁴³, F. Bucci⁴⁹,
 P. Buchholz¹⁴², R.M. Buckingham¹¹⁹, A.G. Buckley⁵³, S.I. Buda^{26a}, I.A. Budagov⁶⁴,
 F. Buehrer⁴⁸, L. Bugge¹¹⁸, M.K. Bugge¹¹⁸, O. Bulekov⁹⁷, A.C. Bundock⁷³,
 H. Burckhart³⁰, S. Burdin⁷³, B. Burghgrave¹⁰⁷, S. Burke¹³⁰, I. Burmeister⁴³, E. Busato³⁴,
 D. B"uscher⁴⁸, V. B"uscher⁸², P. Bussey⁵³, C.P. Buszello¹⁶⁷, B. Butler⁵⁷, J.M. Butler²²,
 A.I. Butt³, C.M. Buttar⁵³, J.M. Butterworth⁷⁷, P. Butti¹⁰⁶, W. Buttinger²⁸, A. Buzatu⁵³,
 M. Byszewski¹⁰, S. Cabrera Urb"an¹⁶⁸, D. Caforio^{20a,20b}, O. Cakir^{4a}, P. Calafiura¹⁵,
 A. Calandri¹³⁷, G. Calderini⁷⁹, P. Calfayan⁹⁹, R. Calkins¹⁰⁷, L.P. Caloba^{24a}, D. Calvet³⁴,
 S. Calvet³⁴, R. Camacho Toro⁴⁹, S. Camarda⁴², D. Cameron¹¹⁸, L.M. Caminada¹⁵,
 R. Caminal Armadans¹², S. Campana³⁰, M. Campanelli⁷⁷, A. Campoverde¹⁴⁹,
 V. Canale^{103a,103b}, A. Canepa^{160a}, M. Cano Bret⁷⁵, J. Cantero⁸¹, R. Cantrill^{125a},
 T. Cao⁴⁰, M.D.M. Capeans Garrido³⁰, I. Caprini^{26a}, M. Caprini^{26a}, M. Capua^{37a,37b},
 R. Caputo⁸², R. Cardarelli^{134a}, T. Carli³⁰, G. Carlino^{103a}, L. Carminati^{90a,90b},
 S. Caron¹⁰⁵, E. Carquin^{32a}, G.D. Carrillo-Montoya^{146c}, J.R. Carter²⁸, J. Carvalho^{125a,125c},
 D. Casadei⁷⁷, M.P. Casado¹², M. Casolino¹², E. Castaneda-Miranda^{146b}, A. Castelli¹⁰⁶,
 V. Castillo Gimenez¹⁶⁸, N.F. Castro^{125a}, P. Catastini⁵⁷, A. Catinaccio³⁰,
 J.R. Catmore¹¹⁸, A. Cattai³⁰, G. Cattani^{134a,134b}, S. Caughron⁸⁹, V. Cavaliere¹⁶⁶,
 D. Cavalli^{90a}, M. Cavalli-Sforza¹², V. Cavasinni^{123a,123b}, F. Ceradini^{135a,135b}, B. Cerio⁴⁵,
 K. Cerny¹²⁸, A.S. Cerqueira^{24b}, A. Cerri¹⁵⁰, L. Cerrito⁷⁵, F. Cerutti¹⁵, M. Cerv³⁰,
 A. Cervelli¹⁷, S.A. Cetin^{19b}, A. Chafaq^{136a}, D. Chakraborty¹⁰⁷, I. Chalupkova¹²⁸,
 P. Chang¹⁶⁶, B. Chapleau⁸⁶, J.D. Chapman²⁸, D. Charfeddine¹¹⁶, D.G. Charlton¹⁸,

C.C. Chau¹⁵⁹, C.A. Chavez Barajas¹⁵⁰, S. Cheatham⁸⁶, A. Chegwiddden⁸⁹, S. Chekanov⁶,
 S.V. Chekulaev^{160a}, G.A. Chelkov^{64,f}, M.A. Chelstowska⁸⁸, C. Chen⁶³, H. Chen²⁵,
 K. Chen¹⁴⁹, L. Chen^{33d,g}, S. Chen^{33c}, X. Chen^{146c}, Y. Chen⁶⁶, Y. Chen³⁵, H.C. Cheng⁸⁸,
 Y. Cheng³¹, A. Cheplakov⁶⁴, R. Cherkaoui El Moursli^{136e}, V. Chernyatin^{25,*}, E. Cheu⁷,
 L. Chevalier¹³⁷, V. Chiarella⁴⁷, G. Chiefari^{103a,103b}, J.T. Childers⁶, A. Chilingarov⁷¹,
 G. Chiodini^{72a}, A.S. Chisholm¹⁸, R.T. Chislett⁷⁷, A. Chitan^{26a}, M.V. Chizhov⁶⁴,
 S. Chouridou⁹, B.K.B. Chow⁹⁹, D. Chromek-Burckhart³⁰, M.L. Chu¹⁵², J. Chudoba¹²⁶,
 J.J. Chwastowski³⁹, L. Chytka¹¹⁴, G. Ciapetti^{133a,133b}, A.K. Ciftci^{4a}, R. Ciftci^{4a},
 D. Cinca⁵³, V. Cindro⁷⁴, A. Ciocio¹⁵, P. Cirkovic^{13b}, Z.H. Citron¹⁷³, M. Citterio^{90a},
 M. Ciubancan^{26a}, A. Clark⁴⁹, P.J. Clark⁴⁶, R.N. Clarke¹⁵, W. Cleland¹²⁴, J.C. Clemens⁸⁴,
 C. Clement^{147a,147b}, Y. Coadou⁸⁴, M. Cobal^{165a,165c}, A. Coccaro¹³⁹, J. Cochran⁶³,
 L. Coffey²³, J.G. Cogan¹⁴⁴, J. Coggeshall¹⁶⁶, B. Cole³⁵, S. Cole¹⁰⁷, A.P. Colijn¹⁰⁶,
 J. Collot⁵⁵, T. Colombo^{58c}, G. Colon⁸⁵, G. Compostella¹⁰⁰, P. Conde Muiño^{125a,125b},
 E. Coniavitis⁴⁸, M.C. Conidi¹², S.H. Connell^{146b}, I.A. Connelly⁷⁶, S.M. Consonni^{90a,90b},
 V. Consorti⁴⁸, S. Constantinescu^{26a}, C. Conta^{120a,120b}, G. Conti⁵⁷, F. Conventi^{103a,h},
 M. Cooke¹⁵, B.D. Cooper⁷⁷, A.M. Cooper-Sarkar¹¹⁹, N.J. Cooper-Smith⁷⁶, K. Copic¹⁵,
 T. Cornelissen¹⁷⁶, M. Corradi^{20a}, F. Corriveau^{86,i}, A. Corso-Radu¹⁶⁴,
 A. Cortes-Gonzalez¹², G. Cortiana¹⁰⁰, G. Costa^{90a}, M.J. Costa¹⁶⁸, D. Costanzo¹⁴⁰,
 D. Côté⁸, G. Cottin²⁸, G. Cowan⁷⁶, B.E. Cox⁸³, K. Cranmer¹⁰⁹, G. Cree²⁹,
 S. Crépe-Renaudin⁵⁵, F. Crescioli⁷⁹, W.A. Cribbs^{147a,147b}, M. Crispin Ortuzar¹¹⁹,
 M. Cristinziani²¹, V. Croft¹⁰⁵, G. Crosetti^{37a,37b}, C.-M. Cuciuc^{26a},
 T. Cuhadar Donszelmann¹⁴⁰, J. Cummings¹⁷⁷, M. Curatolo⁴⁷, C. Cuthbert¹⁵¹,
 H. Cziri¹⁴², P. Czodrowski³, Z. Czyczula¹⁷⁷, S. D'Auria⁵³, M. D'Onofrio⁷³,
 M.J. Da Cunha Sargedas De Sousa^{125a,125b}, C. Da Via⁸³, W. Dabrowski^{38a}, A. Dafinca¹¹⁹,
 T. Dai⁸⁸, O. Dale¹⁴, F. Dallaire⁹⁴, C. Dallapiccola⁸⁵, M. Dam³⁶, A.C. Daniells¹⁸,
 M. Dano Hoffmann¹³⁷, V. Dao⁴⁸, G. Darbo^{50a}, S. Darmora⁸, J.A. Dassoulas⁴²,
 A. Dattagupta⁶⁰, W. Davey²¹, C. David¹⁷⁰, T. Davidek¹²⁸, E. Davies^{119,c}, M. Davies¹⁵⁴,
 O. Davignon⁷⁹, A.R. Davison⁷⁷, P. Davison⁷⁷, Y. Davygora^{58a}, E. Dawe¹⁴³, I. Dawson¹⁴⁰,
 R.K. Daya-Ishmukhametova⁸⁵, K. De⁸, R. de Asmundis^{103a}, S. De Castro^{20a,20b},
 S. De Cecco⁷⁹, N. De Groot¹⁰⁵, P. de Jong¹⁰⁶, H. De la Torre⁸¹, F. De Lorenzi⁶³,
 L. De Nooij¹⁰⁶, D. De Pedis^{133a}, A. De Salvo^{133a}, U. De Sanctis^{165a,165b}, A. De Santo¹⁵⁰,
 J.B. De Vivie De Regie¹¹⁶, W.J. Dearnaley⁷¹, R. Debbé²⁵, C. Debenedetti¹³⁸,
 B. Dechenaux⁵⁵, D.V. Dedovich⁶⁴, I. Deigaard¹⁰⁶, J. Del Peso⁸¹, T. Del Prete^{123a,123b},
 F. Deliot¹³⁷, C.M. Delitzsch⁴⁹, M. Deliyergiyev⁷⁴, A. Dell'Acqua³⁰, L. Dell'Asta²²,
 M. Dell'Orso^{123a,123b}, M. Della Pietra^{103a,h}, D. della Volpe⁴⁹, M. Delmastro⁵,
 P.A. Delsart⁵⁵, C. Deluca¹⁰⁶, S. Demers¹⁷⁷, M. Demichev⁶⁴, A. Demilly⁷⁹, S.P. Denisov¹²⁹,
 D. Derendarz³⁹, J.E. Derkaoui^{136d}, F. Derue⁷⁹, P. Dervan⁷³, K. Desch²¹, C. Deterre⁴²,
 P.O. Deviveiros¹⁰⁶, A. Dewhurst¹³⁰, S. Dhaliwal¹⁰⁶, A. Di Ciaccio^{134a,134b}, L. Di Ciaccio⁵,
 A. Di Domenico^{133a,133b}, C. Di Donato^{103a,103b}, A. Di Girolamo³⁰, B. Di Girolamo³⁰,
 A. Di Mattia¹⁵³, B. Di Micco^{135a,135b}, R. Di Nardo⁴⁷, A. Di Simone⁴⁸, R. Di Sipio^{20a,20b},
 D. Di Valentino²⁹, F.A. Dias⁴⁶, M.A. Diaz^{32a}, E.B. Diehl⁸⁸, J. Dietrich⁴²,
 T.A. Dietzsch^{58a}, S. Diglio⁸⁴, A. Dimitrievska^{13a}, J. Dingfelder²¹, C. Dionisi^{133a,133b},
 P. Dita^{26a}, S. Dita^{26a}, F. Dittus³⁰, F. Djama⁸⁴, T. Djobava^{51b}, M.A.B. do Vale^{24c},

A. Do Valle Wemans^{125a,125g}, T.K.O. Doan⁵, D. Dobos³⁰, C. Doglioni⁴⁹, T. Doherty⁵³,
 T. Dohmae¹⁵⁶, J. Dolejsi¹²⁸, Z. Dolezal¹²⁸, B.A. Dolgoshein^{97,*}, M. Donadelli^{24d},
 S. Donati^{123a,123b}, P. Dondero^{120a,120b}, J. Donini³⁴, J. Dopke¹³⁰, A. Doria^{103a},
 M.T. Dova⁷⁰, A.T. Doyle⁵³, M. Dris¹⁰, J. Dubbert⁸⁸, S. Dube¹⁵, E. Dubreuil³⁴,
 E. Duchovni¹⁷³, G. Duckeck⁹⁹, O.A. Ducu^{26a}, D. Duda¹⁷⁶, A. Dudarev³⁰, F. Dudziak⁶³,
 L. Duflot¹¹⁶, L. Duguid⁷⁶, M. Dührssen³⁰, M. Dunford^{58a}, H. Duran Yildiz^{4a}, M. Düren⁵²,
 A. Durglishvili^{51b}, M. Dwuznik^{38a}, M. Dyndal^{38a}, J. Ebke⁹⁹, W. Edson², N.C. Edwards⁴⁶,
 W. Ehrenfeld²¹, T. Eifert¹⁴⁴, G. Eigen¹⁴, K. Einsweiler¹⁵, T. Ekelof¹⁶⁷, M. El Kacimi^{136c},
 M. Ellert¹⁶⁷, S. Elles⁵, F. Ellinghaus⁸², N. Ellis³⁰, J. Elmsheuser⁹⁹, M. Elsing³⁰,
 D. Emelianov¹³⁰, Y. Enari¹⁵⁶, O.C. Endner⁸², M. Endo¹¹⁷, R. Engelmann¹⁴⁹,
 J. Erdmann¹⁷⁷, A. Ereditato¹⁷, D. Eriksson^{147a}, G. Ernis¹⁷⁶, J. Ernst², M. Ernst²⁵,
 J. Ernwein¹³⁷, D. Errede¹⁶⁶, S. Errede¹⁶⁶, E. Ertel⁸², M. Escalier¹¹⁶, H. Esch⁴³,
 C. Escobar¹²⁴, B. Esposito⁴⁷, A.I. Etienvre¹³⁷, E. Etzion¹⁵⁴, H. Evans⁶⁰, A. Ezhilov¹²²,
 L. Fabbri^{20a,20b}, G. Facini³¹, R.M. Fakhruddinov¹²⁹, S. Falciano^{133a}, R.J. Falla⁷⁷,
 J. Faltova¹²⁸, Y. Fang^{33a}, M. Fanti^{90a,90b}, A. Farbin⁸, A. Farilla^{135a}, T. Farooque¹²,
 S. Farrell¹⁵, S.M. Farrington¹⁷¹, P. Farthouat³⁰, F. Fassi^{136e}, P. Fassnacht³⁰,
 D. Fassouliotis⁹, A. Favareto^{50a,50b}, L. Fayard¹¹⁶, P. Federic^{145a}, O.L. Fedin^{122,j},
 W. Fedorko¹⁶⁹, M. Fehling-Kaschek⁴⁸, S. Feigl³⁰, L. Feligioni⁸⁴, C. Feng^{33d}, E.J. Feng⁶,
 H. Feng⁸⁸, A.B. Fenyuk¹²⁹, S. Fernandez Perez³⁰, S. Ferrag⁵³, J. Ferrando⁵³,
 A. Ferrari¹⁶⁷, P. Ferrari¹⁰⁶, R. Ferrari^{120a}, D.E. Ferreira de Lima⁵³, A. Ferrer¹⁶⁸,
 D. Ferrere⁴⁹, C. Ferretti⁸⁸, A. Ferretto Parodi^{50a,50b}, M. Fiascaris³¹, F. Fiedler⁸²,
 A. Filipčič⁷⁴, M. Filipuzzi⁴², F. Filthaut¹⁰⁵, M. Fincke-Keeler¹⁷⁰, K.D. Finelli¹⁵¹,
 M.C.N. Fiolhais^{125a,125c}, L. Fiorini¹⁶⁸, A. Firan⁴⁰, A. Fischer², J. Fischer¹⁷⁶,
 W.C. Fisher⁸⁹, E.A. Fitzgerald²³, M. Flechl⁴⁸, I. Fleck¹⁴², P. Fleischmann⁸⁸,
 S. Fleischmann¹⁷⁶, G.T. Fletcher¹⁴⁰, G. Fletcher⁷⁵, T. Flick¹⁷⁶, A. Floderus⁸⁰,
 L.R. Flores Castillo^{174,k}, A.C. Florez Bustos^{160b}, M.J. Flowerdew¹⁰⁰, A. Formica¹³⁷,
 A. Forti⁸³, D. Fortin^{160a}, D. Fournier¹¹⁶, H. Fox⁷¹, S. Fracchia¹², P. Francavilla⁷⁹,
 M. Franchini^{20a,20b}, S. Franchino³⁰, D. Francis³⁰, L. Franconi¹¹⁸, M. Franklin⁵⁷,
 S. Franz⁶¹, M. Fraternali^{120a,120b}, S.T. French²⁸, C. Friedrich⁴², F. Friedrich⁴⁴,
 D. Froidevaux³⁰, J.A. Frost²⁸, C. Fukunaga¹⁵⁷, E. Fullana Torregrosa⁸², B.G. Fulson¹⁴⁴,
 J. Fuster¹⁶⁸, C. Gabaldon⁵⁵, O. Gabizon¹⁷³, A. Gabrielli^{20a,20b}, A. Gabrielli^{133a,133b},
 S. Gadatsch¹⁰⁶, S. Gadomski⁴⁹, G. Gagliardi^{50a,50b}, P. Gagnon⁶⁰, C. Galea¹⁰⁵,
 B. Galhardo^{125a,125c}, E.J. Gallas¹¹⁹, V. Gallo¹⁷, B.J. Gallop¹³⁰, P. Gallus¹²⁷, G. Galster³⁶,
 K.K. Gan¹¹⁰, R.P. Gandrajula⁶², J. Gao^{33b,g}, Y.S. Gao^{144,e}, F.M. Garay Walls⁴⁶,
 F. Garbersson¹⁷⁷, C. García¹⁶⁸, J.E. García Navarro¹⁶⁸, M. Garcia-Sciveres¹⁵,
 R.W. Gardner³¹, N. Garelli¹⁴⁴, V. Garonne³⁰, C. Gatti⁴⁷, G. Gaudio^{120a}, B. Gaur¹⁴²,
 L. Gauthier⁹⁴, P. Gauzzi^{133a,133b}, I.L. Gavrilenko⁹⁵, C. Gay¹⁶⁹, G. Gaycken²¹,
 E.N. Gazis¹⁰, P. Ge^{33d}, Z. Gecse¹⁶⁹, C.N.P. Gee¹³⁰, D.A.A. Geerts¹⁰⁶,
 Ch. Geich-Gimbel²¹, K. Gellerstedt^{147a,147b}, C. Gemme^{50a}, A. Gemmel⁵³, M.H. Genest⁵⁵,
 S. Gentile^{133a,133b}, M. George⁵⁴, S. George⁷⁶, D. Gerbaudo¹⁶⁴, A. Gershon¹⁵⁴,
 H. Ghazlane^{136b}, N. Ghodbane³⁴, B. Giacobbe^{20a}, S. Giagu^{133a,133b}, V. Giangiobbe¹²,
 P. Giannetti^{123a,123b}, F. Gianotti³⁰, B. Gibbard²⁵, S.M. Gibson⁷⁶, M. Gilchriese¹⁵,
 T.P.S. Gillam²⁸, D. Gillberg³⁰, G. Gilles³⁴, D.M. Gingrich^{3,d}, N. Giokaris⁹,

M.P. Giordani^{165a,165c}, R. Giordano^{103a,103b}, F.M. Giorgi^{20a}, F.M. Giorgi¹⁶,
P.F. Giraud¹³⁷, D. Giugni^{90a}, C. Giuliani⁴⁸, M. Giulini^{58b}, B.K. Gjelsten¹¹⁸,
S. Gkaitatzis¹⁵⁵, I. Gkialas^{155,l}, L.K. Gladilin⁹⁸, C. Glasman⁸¹, J. Glatzer³⁰,
P.C.F. Glaysher⁴⁶, A. Glazov⁴², G.L. Glonti⁶⁴, M. Goblirsch-Kolb¹⁰⁰, J.R. Goddard⁷⁵,
J. Godfrey¹⁴³, J. Godlewski³⁰, C. Goeringer⁸², S. Goldfarb⁸⁸, T. Golling¹⁷⁷,
D. Golubkov¹²⁹, A. Gomes^{125a,125b,125d}, L.S. Gomez Fajardo⁴², R. Gonalo^{125a},
J. Goncalves Pinto Firmino Da Costa¹³⁷, L. Gonella²¹, S. Gonzalez de la Hoz¹⁶⁸,
G. Gonzalez Parra¹², S. Gonzalez-Sevilla⁴⁹, L. Goossens³⁰, P.A. Gorbounov⁹⁶,
H.A. Gordon²⁵, I. Gorelov¹⁰⁴, B. Gorini³⁰, E. Gorini^{72a,72b}, A. Gorišek⁷⁴, E. Gornicki³⁹,
A.T. Goshaw⁶, C. Gossling⁴³, M.I. Gostkin⁶⁴, M. Gouighri^{136a}, D. Goujdami^{136c},
M.P. Goulette⁴⁹, A.G. Goussiou¹³⁹, C. Goy⁵, S. Gozpinar²³, H.M.X. Grabas¹³⁷,
L. Graber⁵⁴, I. Grabowska-Bold^{38a}, P. Grafstrom^{20a,20b}, K.-J. Grahn⁴², J. Gramling⁴⁹,
E. Gramstad¹¹⁸, S. Grancagnolo¹⁶, V. Grassi¹⁴⁹, V. Gratchev¹²², H.M. Gray³⁰,
E. Graziani^{135a}, O.G. Grebenyuk¹²², Z.D. Greenwood^{78,m}, K. Gregersen⁷⁷, I.M. Gregor⁴²,
P. Grenier¹⁴⁴, J. Griffiths⁸, A.A. Grillo¹³⁸, K. Grimm⁷¹, S. Grinstein^{12,n}, Ph. Gris³⁴,
Y.V. Grishkevich⁹⁸, J.-F. Grivaz¹¹⁶, J.P. Grohs⁴⁴, A. Grohsjean⁴², E. Gross¹⁷³,
J. Grosse-Knetter⁵⁴, G.C. Grossi^{134a,134b}, J. Groth-Jensen¹⁷³, Z.J. Grout¹⁵⁰, L. Guan^{33b},
F. Guescini⁴⁹, D. Guest¹⁷⁷, O. Gueta¹⁵⁴, C. Guicheney³⁴, E. Guido^{50a,50b},
T. Guillemin¹¹⁶, S. Guindon², U. Gul⁵³, C. Gumpert⁴⁴, J. Gunther¹²⁷, J. Guo³⁵,
S. Gupta¹¹⁹, P. Gutierrez¹¹², N.G. Gutierrez Ortiz⁵³, C. Gutschew⁷⁷, N. Guttman¹⁵⁴,
C. Guyot¹³⁷, C. Gwenlan¹¹⁹, C.B. Gwilliam⁷³, A. Haas¹⁰⁹, C. Haber¹⁵, H.K. Hadavand⁸,
N. Haddad^{136e}, P. Haefner²¹, S. Hagebock²¹, Z. Hajduk³⁹, H. Hakobyan¹⁷⁸, M. Haleem⁴²,
D. Hall¹¹⁹, G. Halladjian⁸⁹, K. Hamacher¹⁷⁶, P. Hamal¹¹⁴, K. Hamano¹⁷⁰, M. Hamer⁵⁴,
A. Hamilton^{146a}, S. Hamilton¹⁶², G.N. Hamity^{146c}, P.G. Hamnett⁴², L. Han^{33b},
K. Hanagaki¹¹⁷, K. Hanawa¹⁵⁶, M. Hance¹⁵, P. Hanke^{58a}, R. Hanna¹³⁷, J.B. Hansen³⁶,
J.D. Hansen³⁶, P.H. Hansen³⁶, K. Hara¹⁶¹, A.S. Hard¹⁷⁴, T. Harenberg¹⁷⁶, F. Hariri¹¹⁶,
S. Harkusha⁹¹, D. Harper⁸⁸, R.D. Harrington⁴⁶, O.M. Harris¹³⁹, P.F. Harrison¹⁷¹,
F. Hartjes¹⁰⁶, M. Hasegawa⁶⁶, S. Hasegawa¹⁰², Y. Hasegawa¹⁴¹, A. Hasib¹¹²,
S. Hassani¹³⁷, S. Haug¹⁷, M. Hauschild³⁰, R. Hauser⁸⁹, M. Havranek¹²⁶, C.M. Hawkes¹⁸,
R.J. Hawkings³⁰, A.D. Hawkins⁸⁰, T. Hayashi¹⁶¹, D. Hayden⁸⁹, C.P. Hays¹¹⁹,
H.S. Hayward⁷³, S.J. Haywood¹³⁰, S.J. Head¹⁸, T. Heck⁸², V. Hedberg⁸⁰, L. Heelan⁸,
S. Heim¹²¹, T. Heim¹⁷⁶, B. Heinemann¹⁵, L. Heinrich¹⁰⁹, J. Hejbal¹²⁶, L. Helary²²,
C. Heller⁹⁹, M. Heller³⁰, S. Hellman^{147a,147b}, D. Hellmich²¹, C. Helsens³⁰,
J. Henderson¹¹⁹, R.C.W. Henderson⁷¹, Y. Heng¹⁷⁴, C. Hengler⁴², A. Henrichs¹⁷⁷,
A.M. Henriques Correia³⁰, S. Henrot-Versille¹¹⁶, C. Hensel⁵⁴, G.H. Herbert¹⁶,
Y. Hernandez Jimenez¹⁶⁸, R. Herrberg-Schubert¹⁶, G. Herten⁴⁸, R. Hertenberger⁹⁹,
L. Hervas³⁰, G.G. Hesketh⁷⁷, N.P. Hessey¹⁰⁶, R. Hickling⁷⁵, E. Higon-Rodriguez¹⁶⁸,
E. Hill¹⁷⁰, J.C. Hill²⁸, K.H. Hiller⁴², S. Hillert²¹, S.J. Hillier¹⁸, I. Hinchliffe¹⁵, E. Hines¹²¹,
M. Hirose¹⁵⁸, D. Hirschbuehl¹⁷⁶, J. Hobbs¹⁴⁹, N. Hod¹⁰⁶, M.C. Hodgkinson¹⁴⁰,
P. Hodgson¹⁴⁰, A. Hoecker³⁰, M.R. Hoferkamp¹⁰⁴, F. Hoenig⁹⁹, J. Hoffman⁴⁰,
D. Hoffmann⁸⁴, J.I. Hofmann^{58a}, M. Hohlfeld⁸², T.R. Holmes¹⁵, T.M. Hong¹²¹,
L. Hooft van Huysduynen¹⁰⁹, J.-Y. Hostachy⁵⁵, S. Hou¹⁵², A. Hoummada^{136a},
J. Howard¹¹⁹, J. Howarth⁴², M. Hrabovsky¹¹⁴, I. Hristova¹⁶, J. Hrivnac¹¹⁶, T. Hryn'ova⁵,

C. Hsu^{146c}, P.J. Hsu⁸², S.-C. Hsu¹³⁹, D. Hu³⁵, X. Hu²⁵, Y. Huang⁴², Z. Hubacek³⁰,
 F. Hubaut⁸⁴, F. Huegging²¹, T.B. Huffman¹¹⁹, E.W. Hughes³⁵, G. Hughes⁷¹,
 M. Huhtinen³⁰, T.A. Hülsing⁸², M. Hurwitz¹⁵, N. Huseynov^{64,b}, J. Huston⁸⁹, J. Huth⁵⁷,
 G. Iacobucci⁴⁹, G. Iakovidis¹⁰, I. Ibragimov¹⁴², L. Iconomidou-Fayard¹¹⁶, E. Ideal¹⁷⁷,
 P. Iengo^{103a}, O. Igonkina¹⁰⁶, T. Iizawa¹⁷², Y. Ikegami⁶⁵, K. Ikematsu¹⁴², M. Ikeno⁶⁵,
 Y. Ilchenko^{31,o}, D. Iliadis¹⁵⁵, N. Ilic¹⁵⁹, Y. Inamaru⁶⁶, T. Ince¹⁰⁰, P. Ioannou⁹,
 M. Iodice^{135a}, K. Iordanidou⁹, V. Ippolito⁵⁷, A. Irlles Quiles¹⁶⁸, C. Isaksson¹⁶⁷,
 M. Ishino⁶⁷, M. Ishitsuka¹⁵⁸, R. Ishmukhametov¹¹⁰, C. Issever¹¹⁹, S. Istin^{19a},
 J.M. Iturbe Ponce⁸³, R. Iuppa^{134a,134b}, J. Ivarsson⁸⁰, W. Iwanski³⁹, H. Iwasaki⁶⁵,
 J.M. Izen⁴¹, V. Izzo^{103a}, B. Jackson¹²¹, M. Jackson⁷³, P. Jackson¹, M.R. Jaekel³⁰,
 V. Jain², K. Jakobs⁴⁸, S. Jakobsen³⁰, T. Jakoubek¹²⁶, J. Jakubek¹²⁷, D.O. Jamin¹⁵²,
 D.K. Jana⁷⁸, E. Jansen⁷⁷, H. Jansen³⁰, J. Janssen²¹, M. Janus¹⁷¹, G. Jarlskog⁸⁰,
 N. Javadov^{64,b}, T. Javůrek⁴⁸, L. Jeanty¹⁵, J. Jejelava^{51a,p}, G.-Y. Jeng¹⁵¹, D. Jennens⁸⁷,
 P. Jenni^{48,q}, J. Jentzsch⁴³, C. Jeske¹⁷¹, S. Jézéquel⁵, H. Ji¹⁷⁴, J. Jia¹⁴⁹, Y. Jiang^{33b},
 M. Jimenez Belenguer⁴², S. Jin^{33a}, A. Jinaru^{26a}, O. Jinnouchi¹⁵⁸, M.D. Joergensen³⁶,
 K.E. Johansson^{147a,147b}, P. Johansson¹⁴⁰, K.A. Johns⁷, K. Jon-And^{147a,147b}, G. Jones¹⁷¹,
 R.W.L. Jones⁷¹, T.J. Jones⁷³, J. Jongmanns^{58a}, P.M. Jorge^{125a,125b}, K.D. Joshi⁸³,
 J. Jovicevic¹⁴⁸, X. Ju¹⁷⁴, C.A. Jung⁴³, R.M. Jungst³⁰, P. Jussel⁶¹, A. Juste Rozas^{12,n},
 M. Kaci¹⁶⁸, A. Kaczmarek³⁹, M. Kado¹¹⁶, H. Kagan¹¹⁰, M. Kagan¹⁴⁴, E. Kajomovitz⁴⁵,
 C.W. Kalderon¹¹⁹, S. Kama⁴⁰, A. Kamenshchikov¹²⁹, N. Kanaya¹⁵⁶, M. Kaneda³⁰,
 S. Kaneti²⁸, V.A. Kantserov⁹⁷, J. Kanzaki⁶⁵, B. Kaplan¹⁰⁹, A. Kapliy³¹, D. Kar⁵³,
 K. Karakostas¹⁰, N. Karastathis¹⁰, M. Karnevskiy⁸², S.N. Karpov⁶⁴, Z.M. Karpova⁶⁴,
 K. Karthik¹⁰⁹, V. Kartvelishvili⁷¹, A.N. Karyukhin¹²⁹, L. Kashif¹⁷⁴, G. Kasieczka^{58b},
 R.D. Kass¹¹⁰, A. Kastanas¹⁴, Y. Kataoka¹⁵⁶, A. Katre⁴⁹, J. Katzy⁴², V. Kaushik⁷,
 K. Kawagoe⁶⁹, T. Kawamoto¹⁵⁶, G. Kawamura⁵⁴, S. Kazama¹⁵⁶, V.F. Kazanin¹⁰⁸,
 M.Y. Kazarinov⁶⁴, R. Keeler¹⁷⁰, R. Kehoe⁴⁰, M. Keil⁵⁴, J.S. Keller⁴², J.J. Kempster⁷⁶,
 H. Keoshkerian⁵, O. Kepka¹²⁶, B.P. Kerševan⁷⁴, S. Kersten¹⁷⁶, K. Kessoku¹⁵⁶,
 J. Keung¹⁵⁹, F. Khalil-zada¹¹, H. Khandanyan^{147a,147b}, A. Khanov¹¹³, A. Khodinov⁹⁷,
 A. Khomich^{58a}, T.J. Khoo²⁸, G. Khoriali²¹, A. Khoroshilov¹⁷⁶, V. Khovanskiy⁹⁶,
 E. Khramov⁶⁴, J. Khubua^{51b}, H.Y. Kim⁸, H. Kim^{147a,147b}, S.H. Kim¹⁶¹, N. Kimura¹⁷²,
 O. Kind¹⁶, B.T. King⁷³, M. King¹⁶⁸, R.S.B. King¹¹⁹, S.B. King¹⁶⁹, J. Kirk¹³⁰,
 A.E. Kiryunin¹⁰⁰, T. Kishimoto⁶⁶, D. Kisielewska^{38a}, F. Kiss⁴⁸, T. Kittelmann¹²⁴,
 K. Kiuchi¹⁶¹, E. Kladiva^{145b}, M. Klein⁷³, U. Klein⁷³, K. Kleinknecht⁸², P. Klimek^{147a,147b},
 A. Klimentov²⁵, R. Klingenberg⁴³, J.A. Klinger⁸³, T. Klioutchnikova³⁰, P.F. Klok¹⁰⁵,
 E.-E. Kluge^{58a}, P. Kluit¹⁰⁶, S. Kluth¹⁰⁰, E. Kneringer⁶¹, E.B.F.G. Knoops⁸⁴, A. Knue⁵³,
 D. Kobayashi¹⁵⁸, T. Kobayashi¹⁵⁶, M. Kobel⁴⁴, M. Kocian¹⁴⁴, P. Kodys¹²⁸,
 P. Koevesarki²¹, T. Koffas²⁹, E. Koffeman¹⁰⁶, L.A. Kogan¹¹⁹, S. Kohlmann¹⁷⁶,
 Z. Kohout¹²⁷, T. Kohriki⁶⁵, T. Koi¹⁴⁴, H. Kolanoski¹⁶, I. Koletsou⁵, J. Koll⁸⁹,
 A.A. Komar^{95,*}, Y. Komori¹⁵⁶, T. Kondo⁶⁵, N. Kondrashova⁴², K. Köneke⁴⁸,
 A.C. König¹⁰⁵, S. König⁸², T. Kono^{65,r}, R. Konoplich^{109,s}, N. Konstantinidis⁷⁷,
 R. Kopeliansky¹⁵³, S. Koperny^{38a}, L. Köpke⁸², A.K. Kopp⁴⁸, K. Korcyl³⁹, K. Kordas¹⁵⁵,
 A. Korn⁷⁷, A.A. Korol^{108,t}, I. Korolkov¹², E.V. Korolkova¹⁴⁰, V.A. Korotkov¹²⁹,
 O. Kortner¹⁰⁰, S. Kortner¹⁰⁰, V.V. Kostyukhin²¹, V.M. Kotov⁶⁴, A. Kotwal⁴⁵,

C. Kourkouvelis⁹, V. Kouskoura¹⁵⁵, A. Koutsman^{160a}, R. Kowalewski¹⁷⁰,
 T.Z. Kowalski^{38a}, W. Kozanecki¹³⁷, A.S. Kozhin¹²⁹, V. Kral¹²⁷, V.A. Kramarenko⁹⁸,
 G. Kramberger⁷⁴, D. Krasnopevtsev⁹⁷, M.W. Krasny⁷⁹, A. Krasznahorkay³⁰,
 J.K. Kraus²¹, A. Kravchenko²⁵, S. Kreiss¹⁰⁹, M. Kretz^{58c}, J. Kretzschmar⁷³,
 K. Kreutzfeldt⁵², P. Krieger¹⁵⁹, K. Kroeninger⁵⁴, H. Kroha¹⁰⁰, J. Kroll¹²¹, J. Kroseberg²¹,
 J. Krstic^{13a}, U. Kruchonak⁶⁴, H. Krüger²¹, T. Kruker¹⁷, N. Krumnack⁶³,
 Z.V. Krumshteyn⁶⁴, A. Kruse¹⁷⁴, M.C. Kruse⁴⁵, M. Kruskal²², T. Kubota⁸⁷, S. Kuday^{4a},
 S. Kuehn⁴⁸, A. Kugel^{58c}, A. Kuhl¹³⁸, T. Kuhl⁴², V. Kukhtin⁶⁴, Y. Kulchitsky⁹¹,
 S. Kuleshov^{32b}, M. Kuna^{133a,133b}, J. Kunkle¹²¹, A. Kupco¹²⁶, H. Kurashige⁶⁶,
 Y.A. Kurochkin⁹¹, R. Kurumida⁶⁶, V. Kus¹²⁶, E.S. Kuwertz¹⁴⁸, M. Kuze¹⁵⁸, J. Kvita¹¹⁴,
 A. La Rosa⁴⁹, L. La Rotonda^{37a,37b}, C. Lacasta¹⁶⁸, F. Lacava^{133a,133b}, J. Lacey²⁹,
 H. Lacker¹⁶, D. Lacour⁷⁹, V.R. Lacuesta¹⁶⁸, E. Ladygin⁶⁴, R. Lafaye⁵, B. Laforge⁷⁹,
 T. Lagouri¹⁷⁷, S. Lai⁴⁸, H. Laier^{58a}, L. Lambourne⁷⁷, S. Lammers⁶⁰, C.L. Lampen⁷,
 W. Lampl⁷, E. Lançon¹³⁷, U. Landgraf⁴⁸, M.P.J. Landon⁷⁵, V.S. Lang^{58a},
 A.J. Lankford¹⁶⁴, F. Lanni²⁵, K. Lantzschi³⁰, S. Laplace⁷⁹, C. Lapoire²¹, J.F. Laporte¹³⁷,
 T. Lari^{90a}, M. Lassnig³⁰, P. Laurelli⁴⁷, W. Lavrijsen¹⁵, A.T. Law¹³⁸, P. Laycock⁷³,
 O. Le Dortz⁷⁹, E. Le Guirriec⁸⁴, E. Le Menedeu¹², T. LeCompte⁶, F. Ledroit-Guillon⁵⁵,
 C.A. Lee¹⁵², H. Lee¹⁰⁶, J.S.H. Lee¹¹⁷, S.C. Lee¹⁵², L. Lee¹⁷⁷, G. Lefebvre⁷⁹,
 M. Lefebvre¹⁷⁰, F. Legger⁹⁹, C. Leggett¹⁵, A. Lehan⁷³, M. Lehmacher²¹,
 G. Lehmann Miotto³⁰, X. Lei⁷, W.A. Leight²⁹, A. Leisos¹⁵⁵, A.G. Leister¹⁷⁷,
 M.A.L. Leite^{24d}, R. Leitner¹²⁸, D. Lellouch¹⁷³, B. Lemmer⁵⁴, K.J.C. Leney⁷⁷, T. Lenz²¹,
 G. Lenzen¹⁷⁶, B. Lenzi³⁰, R. Leone⁷, S. Leone^{123a,123b}, K. Leonhardt⁴⁴,
 C. Leonidopoulos⁴⁶, S. Leontsinis¹⁰, C. Leroy⁹⁴, C.G. Lester²⁸, C.M. Lester¹²¹,
 M. Levchenko¹²², J. Levêque⁵, D. Levin⁸⁸, L.J. Levinson¹⁷³, M. Levy¹⁸, A. Lewis¹¹⁹,
 G.H. Lewis¹⁰⁹, A.M. Leyko²¹, M. Leyton⁴¹, B. Li^{33b,u}, B. Li⁸⁴, H. Li¹⁴⁹, H.L. Li³¹,
 L. Li⁴⁵, L. Li^{33e}, S. Li⁴⁵, Y. Li^{33c,v}, Z. Liang¹³⁸, H. Liao³⁴, B. Liberti^{134a}, P. Lichard³⁰,
 K. Lie¹⁶⁶, J. Liebal²¹, W. Liebig¹⁴, C. Limbach²¹, A. Limosani⁸⁷, S.C. Lin^{152,w},
 T.H. Lin⁸², F. Linde¹⁰⁶, B.E. Lindquist¹⁴⁹, J.T. Linnemann⁸⁹, E. Lipeles¹²¹,
 A. Lipniacka¹⁴, M. Lisovyi⁴², T.M. Liss¹⁶⁶, D. Lissauer²⁵, A. Lister¹⁶⁹, A.M. Litke¹³⁸,
 B. Liu¹⁵², D. Liu¹⁵², J.B. Liu^{33b}, K. Liu^{33b,x}, L. Liu⁸⁸, M. Liu⁴⁵, M. Liu^{33b}, Y. Liu^{33b},
 M. Livan^{120a,120b}, S.S.A. Livermore¹¹⁹, A. Lleres⁵⁵, J. Llorente Merino⁸¹, S.L. Lloyd⁷⁵,
 F. Lo Sterzo¹⁵², E. Lobodzinska⁴², P. Loch⁷, W.S. Lockman¹³⁸, T. Loddenkoetter²¹,
 F.K. Loebinger⁸³, A.E. Loevschall-Jensen³⁶, A. Loginov¹⁷⁷, T. Lohse¹⁶, K. Lohwasser⁴²,
 M. Lokajicek¹²⁶, V.P. Lombardo⁵, B.A. Long²², J.D. Long⁸⁸, R.E. Long⁷¹, L. Lopes^{125a},
 D. Lopez Mateos⁵⁷, B. Lopez Paredes¹⁴⁰, I. Lopez Paz¹², J. Lorenz⁹⁹,
 N. Lorenzo Martinez⁶⁰, M. Losada¹⁶³, P. Loscutoff¹⁵, X. Lou⁴¹, A. Lounis¹¹⁶, J. Love⁶,
 P.A. Love⁷¹, A.J. Lowe^{144,e}, F. Lu^{33a}, N. Lu⁸⁸, H.J. Lubatti¹³⁹, C. Luci^{133a,133b},
 A. Lucotte⁵⁵, F. Luehring⁶⁰, W. Lukas⁶¹, L. Luminari^{133a}, O. Lundberg^{147a,147b},
 B. Lund-Jensen¹⁴⁸, M. Lungwitz⁸², D. Lynn²⁵, R. Lysak¹²⁶, E. Lytken⁸⁰, H. Ma²⁵,
 L.L. Ma^{33d}, G. Maccarrone⁴⁷, A. Macchiolo¹⁰⁰, J. Machado Miguens^{125a,125b}, D. Macina³⁰,
 D. Madaffari⁸⁴, R. Madar⁴⁸, H.J. Maddocks⁷¹, W.F. Mader⁴⁴, A. Madsen¹⁶⁷, M. Maeno⁸,
 T. Maeno²⁵, E. Magradze⁵⁴, K. Mahboubi⁴⁸, J. Mahlstedt¹⁰⁶, S. Mahmoud⁷³,
 C. Maiani¹³⁷, C. Maidantchik^{24a}, A.A. Maier¹⁰⁰, A. Maio^{125a,125b,125d}, S. Majewski¹¹⁵,

Y. Makida⁶⁵, N. Makovec¹¹⁶, P. Mal^{137,y}, B. Malaescu⁷⁹, Pa. Malecki³⁹, V.P. Maleev¹²²,
 F. Malek⁵⁵, U. Mallik⁶², D. Malon⁶, C. Malone¹⁴⁴, S. Maltezos¹⁰, V.M. Malyshev¹⁰⁸,
 S. Malyukov³⁰, J. Mamuzic^{13b}, B. Mandelli³⁰, L. Mandelli^{90a}, I. Mandić⁷⁴,
 R. Mandrysch⁶², J. Maneira^{125a,125b}, A. Manfredini¹⁰⁰, L. Manhaes de Andrade Filho^{24b},
 J.A. Manjarres Ramos^{160b}, A. Mann⁹⁹, P.M. Manning¹³⁸, A. Manousakis-Katsikakis⁹,
 B. Mansoulie¹³⁷, R. Mantifel⁸⁶, L. Mapelli³⁰, L. March¹⁶⁸, J.F. Marchand²⁹,
 G. Marchiori⁷⁹, M. Marcisovsky¹²⁶, C.P. Marino¹⁷⁰, M. Marjanovic^{13a}, C.N. Marques^{125a},
 F. Marroquin^{24a}, S.P. Marsden⁸³, Z. Marshall¹⁵, L.F. Marti¹⁷, S. Marti-Garcia¹⁶⁸,
 B. Martin³⁰, B. Martin⁸⁹, T.A. Martin¹⁷¹, V.J. Martin⁴⁶, B. Martin dit Latour¹⁴,
 H. Martinez¹³⁷, M. Martinez^{12,n}, S. Martin-Haugh¹³⁰, A.C. Martyniuk⁷⁷, M. Marx¹³⁹,
 F. Marzano^{133a}, A. Marzin³⁰, L. Masetti⁸², T. Mashimo¹⁵⁶, R. Mashinistov⁹⁵, J. Masik⁸³,
 A.L. Maslennikov¹⁰⁸, I. Massa^{20a,20b}, L. Massa^{20a,20b}, N. Massol⁵, P. Mastrandrea¹⁴⁹,
 A. Mastroberardino^{37a,37b}, T. Masubuchi¹⁵⁶, P. Mättig¹⁷⁶, J. Mattmann⁸², J. Maurer^{26a},
 S.J. Maxfield⁷³, D.A. Maximov^{108,t}, R. Mazini¹⁵², L. Mazzaferro^{134a,134b},
 G. Mc Goldrick¹⁵⁹, S.P. Mc Kee⁸⁸, A. McCarn⁸⁸, R.L. McCarthy¹⁴⁹, T.G. McCarthy²⁹,
 N.A. McCubbin¹³⁰, K.W. McFarlane^{56,*}, J.A. Mcfayden⁷⁷, G. Mchedlidze⁵⁴,
 S.J. McMahon¹³⁰, R.A. McPherson^{170,i}, A. Meade⁸⁵, J. Mechnich¹⁰⁶, M. Medinnis⁴²,
 S. Meehan³¹, S. Mehlhase⁹⁹, A. Mehta⁷³, K. Meier^{58a}, C. Meineck⁹⁹, B. Meirose⁸⁰,
 C. Melachrinou³¹, B.R. Mellado Garcia^{146c}, F. Meloni¹⁷, A. Mengarelli^{20a,20b},
 S. Menke¹⁰⁰, E. Meoni¹⁶², K.M. Mercurio⁵⁷, S. Mergelmeyer²¹, N. Meric¹³⁷, P. Mermod⁴⁹,
 L. Merola^{103a,103b}, C. Meroni^{90a}, F.S. Merritt³¹, H. Merritt¹¹⁰, A. Messina^{30,z},
 J. Metcalfe²⁵, A.S. Mete¹⁶⁴, C. Meyer⁸², C. Meyer¹²¹, J-P. Meyer¹³⁷, J. Meyer³⁰,
 R.P. Middleton¹³⁰, S. Migas⁷³, L. Mijović²¹, G. Mikenberg¹⁷³, M. Mikestikova¹²⁶,
 M. Mikuž⁷⁴, A. Milic³⁰, D.W. Miller³¹, C. Mills⁴⁶, A. Milov¹⁷³, D.A. Milstead^{147a,147b},
 D. Milstein¹⁷³, A.A. Minaenko¹²⁹, I.A. Minashvili⁶⁴, A.I. Mincer¹⁰⁹, B. Mindur^{38a},
 M. Mineev⁶⁴, Y. Ming¹⁷⁴, L.M. Mir¹², G. Mirabelli^{133a}, T. Mitani¹⁷², J. Mitrevski⁹⁹,
 V.A. Mitsou¹⁶⁸, S. Mitsui⁶⁵, A. Miucci⁴⁹, P.S. Miyagawa¹⁴⁰, J.U. Mjörnmark⁸⁰,
 T. Moa^{147a,147b}, K. Mochizuki⁸⁴, S. Mohapatra³⁵, W. Mohr⁴⁸, S. Molander^{147a,147b},
 R. Moles-Valls¹⁶⁸, K. Mönig⁴², C. Monini⁵⁵, J. Monk³⁶, E. Monnier⁸⁴,
 J. Montejo Berlingen¹², F. Monticelli⁷⁰, S. Monzani^{133a,133b}, R.W. Moore³, A. Moraes⁵³,
 N. Morange⁶², D. Moreno⁸², M. Moreno Llácer⁵⁴, P. Morettini^{50a}, M. Morgenstern⁴⁴,
 M. Morii⁵⁷, S. Moritz⁸², A.K. Morley¹⁴⁸, G. Mornacchi³⁰, J.D. Morris⁷⁵, L. Morvaj¹⁰²,
 H.G. Moser¹⁰⁰, M. Mosidze^{51b}, J. Moss¹¹⁰, K. Motohashi¹⁵⁸, R. Mount¹⁴⁴,
 E. Mountricha²⁵, S.V. Mouraviev^{95,*}, E.J.W. Moyse⁸⁵, S. Muanza⁸⁴, R.D. Mudd¹⁸,
 F. Mueller^{58a}, J. Mueller¹²⁴, K. Mueller²¹, T. Mueller²⁸, T. Mueller⁸²,
 D. Muenstermann⁴⁹, Y. Munwes¹⁵⁴, J.A. Murillo Quijada¹⁸, W.J. Murray^{171,130},
 H. Musheghyan⁵⁴, E. Musto¹⁵³, A.G. Myagkov^{129,aa}, M. Myska¹²⁷, O. Nackenhorst⁵⁴,
 J. Nadal⁵⁴, K. Nagai⁶¹, R. Nagai¹⁵⁸, Y. Nagai⁸⁴, K. Nagano⁶⁵, A. Nagarkar¹¹⁰,
 Y. Nagasaka⁵⁹, M. Nagel¹⁰⁰, A.M. Nairz³⁰, Y. Nakahama³⁰, K. Nakamura⁶⁵,
 T. Nakamura¹⁵⁶, I. Nakano¹¹¹, H. Namasivayam⁴¹, G. Nanava²¹, R. Narayan^{58b},
 T. Nattermann²¹, T. Naumann⁴², G. Navarro¹⁶³, R. Nayyar⁷, H.A. Neal⁸⁸,
 P.Yu. Nechaeva⁹⁵, T.J. Neep⁸³, P.D. Nef¹⁴⁴, A. Negri^{120a,120b}, G. Negri³⁰, M. Negrini^{20a},
 S. Nektarijevic⁴⁹, A. Nelson¹⁶⁴, T.K. Nelson¹⁴⁴, S. Nemecek¹²⁶, P. Nemethy¹⁰⁹,

A.A. Nepomuceno^{24a}, M. Nessi^{30,ab}, M.S. Neubauer¹⁶⁶, M. Neumann¹⁷⁶, R.M. Neves¹⁰⁹,
 P. Nevski²⁵, P.R. Newman¹⁸, D.H. Nguyen⁶, R.B. Nickerson¹¹⁹, R. Nicolaidou¹³⁷,
 B. Nicquevert³⁰, J. Nielsen¹³⁸, N. Nikiforou³⁵, A. Nikiforov¹⁶, V. Nikolaenko^{129,aa},
 I. Nikolic-Audit⁷⁹, K. Nikolics⁴⁹, K. Nikolopoulos¹⁸, P. Nilsson⁸, Y. Ninomiya¹⁵⁶,
 A. Nisati^{133a}, R. Nisius¹⁰⁰, T. Nobe¹⁵⁸, L. Nodulman⁶, M. Nomachi¹¹⁷, I. Nomidis²⁹,
 S. Norberg¹¹², M. Nordberg³⁰, O. Novgorodova⁴⁴, S. Nowak¹⁰⁰, M. Nozaki⁶⁵, L. Nozka¹¹⁴,
 K. Ntekas¹⁰, G. Nunes Hanninger⁸⁷, T. Nunnemann⁹⁹, E. Nurse⁷⁷, F. Nuti⁸⁷,
 B.J. O'Brien⁴⁶, F. O'grady⁷, D.C. O'Neil¹⁴³, V. O'Shea⁵³, F.G. Oakham^{29,d},
 H. Oberlack¹⁰⁰, T. Obermann²¹, J. Ocariz⁷⁹, A. Ochi⁶⁶, M.I. Ochoa⁷⁷, S. Oda⁶⁹,
 S. Odaka⁶⁵, H. Ogren⁶⁰, A. Oh⁸³, S.H. Oh⁴⁵, C.C. Ohm¹⁵, H. Ohman¹⁶⁷, W. Okamura¹¹⁷,
 H. Okawa²⁵, Y. Okumura³¹, T. Okuyama¹⁵⁶, A. Olariu^{26a}, A.G. Olchevski⁶⁴,
 S.A. Olivares Pino⁴⁶, D. Oliveira Damazio²⁵, E. Oliver Garcia¹⁶⁸, A. Olszewski³⁹,
 J. Olszowska³⁹, A. Onofre^{125a,125e}, P.U.E. Onyisi^{31,o}, C.J. Oram^{160a}, M.J. Oreglia³¹,
 Y. Oren¹⁵⁴, D. Orestano^{135a,135b}, N. Orlando^{72a,72b}, C. Oropeza Barrera⁵³, R.S. Orr¹⁵⁹,
 B. Osculati^{50a,50b}, R. Ospanov¹²¹, G. Otero y Garzon²⁷, H. Otono⁶⁹, M. Ouchrif^{136d},
 E.A. Ouellette¹⁷⁰, F. Ould-Saada¹¹⁸, A. Ouraou¹³⁷, K.P. Oussoren¹⁰⁶, Q. Ouyang^{33a},
 A. Ovcharova¹⁵, M. Owen⁸³, V.E. Ozcan^{19a}, N. Ozturk⁸, K. Pachal¹¹⁹,
 A. Pacheco Pages¹², C. Padilla Aranda¹², M. Pagáčová⁴⁸, S. Pagan Griso¹⁵,
 E. Paganis¹⁴⁰, C. Pahl¹⁰⁰, F. Paige²⁵, P. Pais⁸⁵, K. Pajchel¹¹⁸, G. Palacino^{160b},
 S. Palestini³⁰, M. Palka^{38b}, D. Pallin³⁴, A. Palma^{125a,125b}, J.D. Palmer¹⁸, Y.B. Pan¹⁷⁴,
 E. Panagiotopoulou¹⁰, J.G. Panduro Vazquez⁷⁶, P. Pani¹⁰⁶, N. Panikashvili⁸⁸,
 S. Panitkin²⁵, D. Pantea^{26a}, L. Paolozzi^{134a,134b}, Th.D. Papadopoulou¹⁰,
 K. Papageorgiou^{155,l}, A. Paramonov⁶, D. Paredes Hernandez³⁴, M.A. Parker²⁸,
 F. Parodi^{50a,50b}, J.A. Parsons³⁵, U. Parzefall⁴⁸, E. Pasqualucci^{133a}, S. Passaggio^{50a},
 A. Passeri^{135a}, F. Pastore^{135a,135b,*}, Fr. Pastore⁷⁶, G. Pásztor²⁹, S. Patariaia¹⁷⁶,
 N.D. Patel¹⁵¹, J.R. Pater⁸³, S. Patricelli^{103a,103b}, T. Pauly³⁰, J. Pearce¹⁷⁰, M. Pedersen¹¹⁸,
 S. Pedraza Lopez¹⁶⁸, R. Pedro^{125a,125b}, S.V. Peleganchuk¹⁰⁸, D. Pelikan¹⁶⁷, H. Peng^{33b},
 B. Penning³¹, J. Penwell⁶⁰, D.V. Perepelitsa²⁵, E. Perez Codina^{160a},
 M.T. Pérez García-Estañ¹⁶⁸, V. Perez Reale³⁵, L. Perini^{90a,90b}, H. Pernegger³⁰,
 R. Perrino^{72a}, R. Peschke⁴², V.D. Peshekhonov⁶⁴, K. Peters³⁰, R.F.Y. Peters⁸³,
 B.A. Petersen³⁰, T.C. Petersen³⁶, E. Petit⁴², A. Petridis^{147a,147b}, C. Petridou¹⁵⁵,
 E. Petrolu^{133a}, F. Petrucci^{135a,135b}, N.E. Pettersson¹⁵⁸, R. Pezoa^{32b}, P.W. Phillips¹³⁰,
 G. Piacquadio¹⁴⁴, E. Pianori¹⁷¹, A. Picazio⁴⁹, E. Piccaro⁷⁵, M. Piccinini^{20a,20b},
 R. Piegai²⁷, D.T. Pignotti¹¹⁰, J.E. Pilcher³¹, A.D. Pilkington⁷⁷, J. Pina^{125a,125b,125d},
 M. Pinamonti^{165a,165c,ac}, A. Pinder¹¹⁹, J.L. Pinfold³, A. Pingel³⁶, B. Pinto^{125a}, S. Pires⁷⁹,
 M. Pitt¹⁷³, C. Pizio^{90a,90b}, L. Plazak^{145a}, M.-A. Pleier²⁵, V. Pleskot¹²⁸, E. Plotnikova⁶⁴,
 P. Plucinski^{147a,147b}, S. Poddar^{58a}, F. Podlyski³⁴, R. Poettgen⁸², L. Poggioli¹¹⁶,
 D. Pohl²¹, M. Pohl⁴⁹, G. Polesello^{120a}, A. Policicchio^{37a,37b}, R. Polifka¹⁵⁹, A. Polini^{20a},
 C.S. Pollard⁴⁵, V. Polychronakos²⁵, K. Pommès³⁰, L. Pontecorvo^{133a}, B.G. Pope⁸⁹,
 G.A. Popeneciu^{26b}, D.S. Popovic^{13a}, A. Poppleton³⁰, X. Portell Bueso¹², S. Pospisil¹²⁷,
 K. Potamianos¹⁵, I.N. Potrap⁶⁴, C.J. Potter¹⁵⁰, C.T. Potter¹¹⁵, G. Poulard³⁰,
 J. Poveda⁶⁰, V. Pozdnyakov⁶⁴, P. Pralavorio⁸⁴, A. Pranko¹⁵, S. Prasad³⁰, R. Pravahan⁸,
 S. Prell⁶³, D. Price⁸³, J. Price⁷³, L.E. Price⁶, D. Prieur¹²⁴, M. Primavera^{72a}, M. Proissl⁴⁶,

K. Prokofiev⁴⁷, F. Prokoshin^{32b}, E. Protopapadaki¹³⁷, S. Protopopescu²⁵, J. Proudfoot⁶,
 M. Przybycien^{38a}, H. Przysieszniak⁵, E. Ptacek¹¹⁵, D. Puddu^{135a,135b}, E. Pueschel⁸⁵,
 D. Puldon¹⁴⁹, M. Purohit^{25,ad}, P. Puzo¹¹⁶, J. Qian⁸⁸, G. Qin⁵³, Y. Qin⁸³, A. Quadt⁵⁴,
 D.R. Quarrie¹⁵, W.B. Quayle^{165a,165b}, M. Queitsch-Maitland⁸³, D. Quilty⁵³,
 A. Qureshi^{160b}, V. Radeka²⁵, V. Radescu⁴², S.K. Radhakrishnan¹⁴⁹, P. Radloff¹¹⁵,
 P. Rados⁸⁷, F. Ragusa^{90a,90b}, G. Rahal¹⁷⁹, S. Rajagopalan²⁵, M. Rammensee³⁰,
 A.S. Randle-Conde⁴⁰, C. Rangel-Smith¹⁶⁷, K. Rao¹⁶⁴, F. Rauscher⁹⁹, T.C. Rave⁴⁸,
 T. Ravenscroft⁵³, M. Raymond³⁰, A.L. Read¹¹⁸, N.P. Readioff⁷³, D.M. Rebuzzi^{120a,120b},
 A. Redelbach¹⁷⁵, G. Redlinger²⁵, R. Reece¹³⁸, K. Reeves⁴¹, L. Rehnisch¹⁶, H. Reisin²⁷,
 M. Relich¹⁶⁴, C. Rembser³⁰, H. Ren^{33a}, Z.L. Ren¹⁵², A. Renaud¹¹⁶, M. Rescigno^{133a},
 S. Resconi^{90a}, O.L. Rezanova^{108,t}, P. Reznicek¹²⁸, R. Rezvani⁹⁴, R. Richter¹⁰⁰,
 M. Ridel⁷⁹, P. Rieck¹⁶, J. Rieger⁵⁴, M. Rijssenbeek¹⁴⁹, A. Rimoldi^{120a,120b}, L. Rinaldi^{20a},
 E. Ritsch⁶¹, I. Riu¹², F. Rizatdinova¹¹³, E. Rizvi⁷⁵, S.H. Robertson^{86,i},
 A. Robichaud-Veronneau⁸⁶, D. Robinson²⁸, J.E.M. Robinson⁸³, A. Robson⁵³,
 C. Roda^{123a,123b}, L. Rodrigues³⁰, S. Roe³⁰, O. Røhne¹¹⁸, S. Rolli¹⁶², A. Romaniouk⁹⁷,
 M. Romano^{20a,20b}, E. Romero Adam¹⁶⁸, N. Rompotis¹³⁹, M. Ronzani⁴⁸, L. Roos⁷⁹,
 E. Ros¹⁶⁸, S. Rosati^{133a}, K. Rosbach⁴⁹, M. Rose⁷⁶, P. Rose¹³⁸, P.L. Rosendahl¹⁴,
 O. Rosenthal¹⁴², V. Rossetti^{147a,147b}, E. Rossi^{103a,103b}, L.P. Rossi^{50a}, R. Rosten¹³⁹,
 M. Rotaru^{26a}, I. Roth¹⁷³, J. Rothberg¹³⁹, D. Rousseau¹¹⁶, C.R. Royon¹³⁷, A. Rozanov⁸⁴,
 Y. Rozen¹⁵³, X. Ruan^{146c}, F. Rubbo¹², I. Rubinskiy⁴², V.I. Rud⁹⁸, C. Rudolph⁴⁴,
 M.S. Rudolph¹⁵⁹, F. Rühr⁴⁸, A. Ruiz-Martinez³⁰, Z. Rurikova⁴⁸, N.A. Rusakovich⁶⁴,
 A. Ruschke⁹⁹, J.P. Rutherford⁷, N. Ruthmann⁴⁸, Y.F. Ryabov¹²², M. Rybar¹²⁸,
 G. Rybkin¹¹⁶, N.C. Ryder¹¹⁹, A.F. Saavedra¹⁵¹, S. Sacerdoti²⁷, A. Saddique³, I. Sadeh¹⁵⁴,
 H.F.W. Sadrozinski¹³⁸, R. Sadykov⁶⁴, F. Safai Tehrani^{133a}, H. Sakamoto¹⁵⁶,
 Y. Sakurai¹⁷², G. Salamanna^{135a,135b}, A. Salamon^{134a}, M. Saleem¹¹², D. Salek¹⁰⁶,
 P.H. Sales De Bruin¹³⁹, D. Salihagic¹⁰⁰, A. Salnikov¹⁴⁴, J. Salt¹⁶⁸, D. Salvatore^{37a,37b},
 F. Salvatore¹⁵⁰, A. Salvucci¹⁰⁵, A. Salzburger³⁰, D. Sampsonidis¹⁵⁵, A. Sanchez^{103a,103b},
 J. Sánchez¹⁶⁸, V. Sanchez Martinez¹⁶⁸, H. Sandaker¹⁴, R.L. Sandbach⁷⁵, H.G. Sander⁸²,
 M.P. Sanders⁹⁹, M. Sandhoff¹⁷⁶, T. Sandoval²⁸, C. Sandoval¹⁶³, R. Sandstroem¹⁰⁰,
 D.P.C. Sankey¹³⁰, A. Sansoni⁴⁷, C. Santoni³⁴, R. Santonico^{134a,134b}, H. Santos^{125a},
 I. Santoyo Castillo¹⁵⁰, K. Sapp¹²⁴, A. Saponov⁶⁴, J.G. Saraiva^{125a,125d}, B. Sarrazin²¹,
 G. Sartisohn¹⁷⁶, O. Sasaki⁶⁵, Y. Sasaki¹⁵⁶, G. Sauvage^{5,*}, E. Sauvan⁵, P. Savard^{159,d},
 D.O. Savu³⁰, C. Sawyer¹¹⁹, L. Sawyer^{78,m}, D.H. Saxon⁵³, J. Saxon¹²¹, C. Sbarra^{20a},
 A. Sbrizzi³, T. Scanlon⁷⁷, D.A. Scannicchio¹⁶⁴, M. Scarcella¹⁵¹, V. Scarfone^{37a,37b},
 J. Schaarschmidt¹⁷³, P. Schacht¹⁰⁰, D. Schaefer¹²¹, R. Schaefer⁴², S. Schaepe²¹,
 S. Schaetzel^{58b}, U. Schäfer⁸², A.C. Schaffer¹¹⁶, D. Schaile⁹⁹, R.D. Schamberger¹⁴⁹,
 V. Scharf^{58a}, V.A. Schegelsky¹²², D. Scheirich¹²⁸, M. Schernau¹⁶⁴, M.I. Scherzer³⁵,
 C. Schiavi^{50a,50b}, J. Schieck⁹⁹, C. Schillo⁴⁸, M. Schioppa^{37a,37b}, S. Schlenker³⁰,
 E. Schmidt⁴⁸, K. Schmieden³⁰, C. Schmitt⁸², C. Schmitt⁹⁹, S. Schmitt^{58b}, B. Schneider¹⁷,
 Y.J. Schnellbach⁷³, U. Schnoor⁴⁴, L. Schoeffel¹³⁷, A. Schoening^{58b}, B.D. Schoenrock⁸⁹,
 A.L.S. Schorlemmer⁵⁴, M. Schott⁸², D. Schouten^{160a}, J. Schovancova²⁵, S. Schramm¹⁵⁹,
 M. Schreyer¹⁷⁵, C. Schroeder⁸², N. Schuh⁸², M.J. Schultens²¹, H.-C. Schultz-Coulon^{58a},
 H. Schulz¹⁶, M. Schumacher⁴⁸, B.A. Schumm¹³⁸, Ph. Schune¹³⁷, C. Schwanenberger⁸³,

A. Schwartzman¹⁴⁴, Ph. Schwegler¹⁰⁰, Ph. Schwemling¹³⁷, R. Schwienhorst⁸⁹,
 J. Schwindling¹³⁷, T. Schwindt²¹, M. Schwoerer⁵, F.G. Sciacca¹⁷, E. Scifo¹¹⁶, G. Sciolla²³,
 W.G. Scott¹³⁰, F. Scuri^{123a,123b}, F. Scutti²¹, J. Searcy⁸⁸, G. Sedov⁴², E. Sedykh¹²²,
 S.C. Seidel¹⁰⁴, A. Seiden¹³⁸, F. Seifert¹²⁷, J.M. Seixas^{24a}, G. Sekhniaidze^{103a},
 S.J. Sekula⁴⁰, K.E. Selbach⁴⁶, D.M. Seliverstov^{122,*}, G. Sellers⁷³,
 N. Semprini-Cesari^{20a,20b}, C. Serfon³⁰, L. Serin¹¹⁶, L. Serkin⁵⁴, T. Serre⁸⁴, R. Seuster^{160a},
 H. Severini¹¹², T. Sfiligoj⁷⁴, F. Sforza¹⁰⁰, A. Sfyrlla³⁰, E. Shabalina⁵⁴, M. Shamim¹¹⁵,
 L.Y. Shan^{33a}, R. Shang¹⁶⁶, J.T. Shank²², M. Shapiro¹⁵, P.B. Shatalov⁹⁶, K. Shaw^{165a,165b},
 C.Y. Shehu¹⁵⁰, P. Sherwood⁷⁷, L. Shi^{152,ae}, S. Shimizu⁶⁶, C.O. Shimmin¹⁶⁴,
 M. Shimojima¹⁰¹, M. Shiyakova⁶⁴, A. Shmeleva⁹⁵, M.J. Shochet³¹, D. Short¹¹⁹,
 S. Shrestha⁶³, E. Shulga⁹⁷, M.A. Shupe⁷, S. Shushkevich⁴², P. Sicho¹²⁶,
 O. Sidiropoulou¹⁵⁵, D. Sidorov¹¹³, A. Sidoti^{133a}, F. Siegert⁴⁴, Dj. Sijacki^{13a},
 J. Silva^{125a,125d}, Y. Silver¹⁵⁴, D. Silverstein¹⁴⁴, S.B. Silverstein^{147a}, V. Simak¹²⁷,
 O. Simard⁵, Lj. Simic^{13a}, S. Simion¹¹⁶, E. Simioni⁸², B. Simmons⁷⁷, R. Simoniello^{90a,90b},
 M. Simonyan³⁶, P. Sinervo¹⁵⁹, N.B. Sinev¹¹⁵, V. Sipica¹⁴², G. Siragusa¹⁷⁵, A. Sircar⁷⁸,
 A.N. Sisakyan^{64,*}, S.Yu. Sivoklov⁹⁸, J. Sjölin^{147a,147b}, T.B. Sjursen¹⁴, H.P. Skottowe⁵⁷,
 K.Yu. Skovpen¹⁰⁸, P. Skubic¹¹², M. Slater¹⁸, T. Slavicek¹²⁷, K. Sliwa¹⁶², V. Smakhtin¹⁷³,
 B.H. Smart⁴⁶, L. Smestad¹⁴, S.Yu. Smirnov⁹⁷, Y. Smirnov⁹⁷, L.N. Smirnova^{98,af},
 O. Smirnova⁸⁰, K.M. Smith⁵³, M. Smizanska⁷¹, K. Smolek¹²⁷, A.A. Snesarev⁹⁵,
 G. Snidero⁷⁵, S. Snyder²⁵, R. Sobie^{170,i}, F. Socher⁴⁴, A. Soffer¹⁵⁴, D.A. Soh^{152,ae},
 C.A. Solans³⁰, M. Solar¹²⁷, J. Solc¹²⁷, E.Yu. Soldatov⁹⁷, U. Soldevila¹⁶⁸,
 A.A. Solodkov¹²⁹, A. Soloshenko⁶⁴, O.V. Solovyanov¹²⁹, V. Solovyev¹²², P. Sommer⁴⁸,
 H.Y. Song^{33b}, N. Soni¹, A. Sood¹⁵, A. Sopczak¹²⁷, B. Sopko¹²⁷, V. Sopko¹²⁷, V. Sorin¹²,
 M. Sosebee⁸, R. Soualah^{165a,165c}, P. Soueid⁹⁴, A.M. Soukharev¹⁰⁸, D. South⁴²,
 S. Spagnolo^{72a,72b}, F. Spanò⁷⁶, W.R. Spearman⁵⁷, F. Spettel¹⁰⁰, R. Spighi^{20a}, G. Spigo³⁰,
 M. Spousta¹²⁸, T. Spreitzer¹⁵⁹, B. Spurlock⁸, R.D. St. Denis^{53,*}, S. Staerz⁴⁴,
 J. Stahlman¹²¹, R. Stamen^{58a}, E. Stanecka³⁹, R.W. Stanek⁶, C. Stanescu^{135a},
 M. Stanescu-Bellu⁴², M.M. Stanitzki⁴², S. Stapnes¹¹⁸, E.A. Starchenko¹²⁹, J. Stark⁵⁵,
 P. Staroba¹²⁶, P. Starovoitov⁴², R. Staszewski³⁹, P. Stavina^{145a,*}, P. Steinberg²⁵,
 B. Stelzer¹⁴³, H.J. Stelzer³⁰, O. Stelzer-Chilton^{160a}, H. Stenzel⁵², S. Stern¹⁰⁰,
 G.A. Stewart⁵³, J.A. Stillings²¹, M.C. Stockton⁸⁶, M. Stoebe⁸⁶, G. Stoicea^{26a}, P. Stolte⁵⁴,
 S. Stonjek¹⁰⁰, A.R. Stradling⁸, A. Straessner⁴⁴, M.E. Stramaglia¹⁷, J. Strandberg¹⁴⁸,
 S. Strandberg^{147a,147b}, A. Strandlie¹¹⁸, E. Strauss¹⁴⁴, M. Strauss¹¹², P. Strizenecek^{145b},
 R. Ströhmer¹⁷⁵, D.M. Strom¹¹⁵, R. Stroynowski⁴⁰, S.A. Stucci¹⁷, B. Stugu¹⁴,
 N.A. Styles⁴², D. Su¹⁴⁴, J. Su¹²⁴, R. Subramaniam⁷⁸, A. Succurro¹², Y. Sugaya¹¹⁷,
 C. Suhr¹⁰⁷, M. Suk¹²⁷, V.V. Sulin⁹⁵, S. Sultansoy^{4c}, T. Sumida⁶⁷, S. Sun⁵⁷, X. Sun^{33a},
 J.E. Sundermann⁴⁸, K. Suruliz¹⁴⁰, G. Susinno^{37a,37b}, M.R. Sutton¹⁵⁰, Y. Suzuki⁶⁵,
 M. Svatos¹²⁶, S. Swedish¹⁶⁹, M. Swiatlowski¹⁴⁴, I. Sykora^{145a}, T. Sykora¹²⁸, D. Ta⁸⁹,
 C. Taccini^{135a,135b}, K. Tackmann⁴², J. Taenzer¹⁵⁹, A. Taffard¹⁶⁴, R. Tafirot^{160a},
 N. Taiblum¹⁵⁴, H. Takai²⁵, R. Takashima⁶⁸, H. Takeda⁶⁶, T. Takeshita¹⁴¹, Y. Takubo⁶⁵,
 M. Talby⁸⁴, A.A. Talyshev^{108,t}, J.Y.C. Tam¹⁷⁵, K.G. Tan⁸⁷, J. Tanaka¹⁵⁶, R. Tanaka¹¹⁶,
 S. Tanaka¹³², S. Tanaka⁶⁵, A.J. Tanasijczuk¹⁴³, B.B. Tannenwald¹¹⁰, N. Tannoury²¹,
 S. Tapprogge⁸², S. Tarem¹⁵³, F. Tarrade²⁹, G.F. Tartarelli^{90a}, P. Tas¹²⁸, M. Tasevsky¹²⁶,

T. Tashiro⁶⁷, E. Tassi^{37a,37b}, A. Tavares Delgado^{125a,125b}, Y. Tayalati^{136d}, F.E. Taylor⁹³,
 G.N. Taylor⁸⁷, W. Taylor^{160b}, F.A. Teischinger³⁰, M. Teixeira Dias Castanheira⁷⁵,
 P. Teixeira-Dias⁷⁶, K.K. Temming⁴⁸, H. Ten Kate³⁰, P.K. Teng¹⁵², J.J. Teoh¹¹⁷,
 S. Terada⁶⁵, K. Terashi¹⁵⁶, J. Terron⁸¹, S. Terzo¹⁰⁰, M. Testa⁴⁷, R.J. Teuscher^{159,i},
 J. Therhaag²¹, T. Theveneaux-Pelzer³⁴, J.P. Thomas¹⁸, J. Thomas-Wilsker⁷⁶,
 E.N. Thompson³⁵, P.D. Thompson¹⁸, P.D. Thompson¹⁵⁹, A.S. Thompson⁵³,
 L.A. Thomsen³⁶, E. Thomson¹²¹, M. Thomson²⁸, W.M. Thong⁸⁷, R.P. Thun^{88,*},
 F. Tian³⁵, M.J. Tibbetts¹⁵, V.O. Tikhomirov^{95,ag}, Yu.A. Tikhonov^{108,t}, S. Timoshenko⁹⁷,
 E. Tiouchichine⁸⁴, P. Tipton¹⁷⁷, S. Tisserant⁸⁴, T. Todorov⁵, S. Todorova-Nova¹²⁸,
 B. Toggerson⁷, J. Tojo⁶⁹, S. Tokár^{145a}, K. Tokushuku⁶⁵, K. Tollefson⁸⁹, L. Tomlinson⁸³,
 M. Tomoto¹⁰², L. Tompkins³¹, K. Toms¹⁰⁴, N.D. Topilin⁶⁴, E. Torrence¹¹⁵, H. Torres¹⁴³,
 E. Torró Pastor¹⁶⁸, J. Toth^{84,ah}, F. Touchard⁸⁴, D.R. Tovey¹⁴⁰, H.L. Tran¹¹⁶,
 T. Trefzger¹⁷⁵, L. Tremblet³⁰, A. Tricoli³⁰, I.M. Trigger^{160a}, S. Trincaz-Duvoid⁷⁹,
 M.F. Tripiana¹², W. Trischuk¹⁵⁹, B. Trocme⁵⁵, C. Troncon^{90a}, M. Trottier-McDonald¹⁴³,
 M. Trovatelli^{135a,135b}, P. True⁸⁹, M. Trzebinski³⁹, A. Trzupek³⁹, C. Tsarouchas³⁰,
 J.C-L. Tseng¹¹⁹, P.V. Tsiarashka⁹¹, D. Tsionou¹³⁷, G. Tsipolitis¹⁰, N. Tsirintanis⁹,
 S. Tsiskaridze¹², V. Tsiskaridze⁴⁸, E.G. Tskhadadze^{51a}, I.I. Tsukerman⁹⁶, V. Tsulaia¹⁵,
 S. Tsuno⁶⁵, D. Tsybychev¹⁴⁹, A. Tudorache^{26a}, V. Tudorache^{26a}, A.N. Tuna¹²¹,
 S.A. Tuppuri^{20a,20b}, S. Turchikhin^{98,af}, D. Turecek¹²⁷, I. Turk Cakir^{4d}, R. Turra^{90a,90b},
 P.M. Tuts³⁵, A. Tykhonov⁴⁹, M. Tylmad^{147a,147b}, M. Tyndel¹³⁰, K. Uchida²¹, I. Ueda¹⁵⁶,
 R. Ueno²⁹, M. Ughetto⁸⁴, M. Ugland¹⁴, M. Uhlenbrock²¹, F. Ukegawa¹⁶¹, G. Unal³⁰,
 A. Undrus²⁵, G. Unel¹⁶⁴, F.C. Ungaro⁴⁸, Y. Unno⁶⁵, D. Urbaniec³⁵, P. Urquijo⁸⁷,
 G. Usai⁸, A. Usanova⁶¹, L. Vacavant⁸⁴, V. Vacek¹²⁷, B. Vachon⁸⁶, N. Valencic¹⁰⁶,
 S. Valentinetti^{20a,20b}, A. Valero¹⁶⁸, L. Valery³⁴, S. Valkar¹²⁸, E. Valladolid Gallego¹⁶⁸,
 S. Vallecorsa⁴⁹, J.A. Valls Ferrer¹⁶⁸, W. Van Den Wollenberg¹⁰⁶, P.C. Van Der Deijl¹⁰⁶,
 R. van der Geer¹⁰⁶, H. van der Graaf¹⁰⁶, R. Van Der Leeuw¹⁰⁶, D. van der Ster³⁰,
 N. van Eldik³⁰, P. van Gemmeren⁶, J. Van Nieuwkoop¹⁴³, I. van Vulpen¹⁰⁶,
 M.C. van Woerden³⁰, M. Vanadia^{133a,133b}, W. Vandelli³⁰, R. Vanguri¹²¹, A. Vaniachine⁶,
 P. Vankov⁴², F. Vannucci⁷⁹, G. Vardanyan¹⁷⁸, R. Vari^{133a}, E.W. Varnes⁷, T. Varol⁸⁵,
 D. Varouchas⁷⁹, A. Vartapetian⁸, K.E. Varvell¹⁵¹, F. Vazeille³⁴, T. Vazquez Schroeder⁵⁴,
 J. Veatch⁷, F. Veloso^{125a,125c}, S. Veneziano^{133a}, A. Ventura^{72a,72b}, D. Ventura⁸⁵,
 M. Venturi¹⁷⁰, N. Venturi¹⁵⁹, A. Venturini²³, V. Vercesi^{120a}, M. Verducci^{133a,133b},
 W. Verkerke¹⁰⁶, J.C. Vermeulen¹⁰⁶, A. Vest⁴⁴, M.C. Vetterli^{143,d}, O. Viazlo⁸⁰,
 I. Vichou¹⁶⁶, T. Vickey^{146c,ai}, O.E. Vickey Boeriu^{146c}, G.H.A. Viehhauser¹¹⁹, S. Viel¹⁶⁹,
 R. Vigne³⁰, M. Villa^{20a,20b}, M. Villaplana Perez^{90a,90b}, E. Vilucchi⁴⁷, M.G. Vincter²⁹,
 V.B. Vinogradov⁶⁴, J. Virzi¹⁵, I. Vivarelli¹⁵⁰, F. Vives Vaque³, S. Vlachos¹⁰,
 D. Vladoiu⁹⁹, M. Vlasak¹²⁷, A. Vogel²¹, M. Vogel^{32a}, P. Vokac¹²⁷, G. Volpi^{123a,123b},
 M. Volpi⁸⁷, H. von der Schmitt¹⁰⁰, H. von Radziewski⁴⁸, E. von Toerne²¹, V. Vorobel¹²⁸,
 K. Vorobev⁹⁷, M. Vos¹⁶⁸, R. Voss³⁰, J.H. Vosseveld⁷³, N. Vranjes¹³⁷,
 M. Vranjes Milosavljevic¹⁰⁶, V. Vrba¹²⁶, M. Vreeswijk¹⁰⁶, T. Vu Anh⁴⁸, R. Vuillermet³⁰,
 I. Vukotic³¹, Z. Vykydal¹²⁷, P. Wagner²¹, W. Wagner¹⁷⁶, H. Wahlberg⁷⁰, S. Wahrmund⁴⁴,
 J. Wakabayashi¹⁰², J. Walder⁷¹, R. Walker⁹⁹, W. Walkowiak¹⁴², R. Wall¹⁷⁷, P. Waller⁷³,
 B. Walsh¹⁷⁷, C. Wang^{152,aj}, C. Wang⁴⁵, F. Wang¹⁷⁴, H. Wang¹⁵, H. Wang⁴⁰, J. Wang⁴²,

J. Wang^{33a}, K. Wang⁸⁶, R. Wang¹⁰⁴, S.M. Wang¹⁵², T. Wang²¹, X. Wang¹⁷⁷,
C. Wanotayaroj¹¹⁵, A. Warburton⁸⁶, C.P. Ward²⁸, D.R. Wardrope⁷⁷, M. Warsinsky⁴⁸,
A. Washbrook⁴⁶, C. Wasicki⁴², P.M. Watkins¹⁸, A.T. Watson¹⁸, I.J. Watson¹⁵¹,
M.F. Watson¹⁸, G. Watts¹³⁹, S. Watts⁸³, B.M. Waugh⁷⁷, S. Webb⁸³, M.S. Weber¹⁷,
S.W. Weber¹⁷⁵, J.S. Webster³¹, A.R. Weidberg¹¹⁹, P. Weigell¹⁰⁰, B. Weinert⁶⁰,
J. Weingarten⁵⁴, C. Weiser⁴⁸, H. Weits¹⁰⁶, P.S. Wells³⁰, T. Wenaus²⁵, D. Wendland¹⁶,
Z. Weng^{152,ae}, T. Wengler³⁰, S. Wenig³⁰, N. Wermes²¹, M. Werner⁴⁸, P. Werner³⁰,
M. Wessels^{58a}, J. Wetter¹⁶², K. Whalen²⁹, A. White⁸, M.J. White¹, R. White^{32b},
S. White^{123a,123b}, D. Whiteson¹⁶⁴, D. Wicke¹⁷⁶, F.J. Wickens¹³⁰, W. Wiedenmann¹⁷⁴,
M. Wielers¹³⁰, P. Wienemann²¹, C. Wiglesworth³⁶, L.A.M. Wiik-Fuchs²¹,
P.A. Wijeratne⁷⁷, A. Wildauer¹⁰⁰, M.A. Wildt^{42,ak}, H.G. Wilkens³⁰, J.Z. Will⁹⁹,
H.H. Williams¹²¹, S. Williams²⁸, C. Willis⁸⁹, S. Willocq⁸⁵, A. Wilson⁸⁸, J.A. Wilson¹⁸,
I. Wingerter-Seez⁵, F. Winklmeier¹¹⁵, B.T. Winter²¹, M. Wittgen¹⁴⁴, T. Wittig⁴³,
J. Wittkowski⁹⁹, S.J. Wollstadt⁸², M.W. Wolter³⁹, H. Wolters^{125a,125c}, B.K. Wosiek³⁹,
J. Wotschack³⁰, M.J. Woudstra⁸³, K.W. Wozniak³⁹, M. Wright⁵³, M. Wu⁵⁵, S.L. Wu¹⁷⁴,
X. Wu⁴⁹, Y. Wu⁸⁸, E. Wulf³⁵, T.R. Wyatt⁸³, B.M. Wynne⁴⁶, S. Xella³⁶, M. Xiao¹³⁷,
D. Xu^{33a}, L. Xu^{33b,al}, B. Yabsley¹⁵¹, S. Yacoob^{146b,am}, R. Yakabe⁶⁶, M. Yamada⁶⁵,
H. Yamaguchi¹⁵⁶, Y. Yamaguchi¹¹⁷, A. Yamamoto⁶⁵, K. Yamamoto⁶³, S. Yamamoto¹⁵⁶,
T. Yamamura¹⁵⁶, T. Yamanaka¹⁵⁶, K. Yamauchi¹⁰², Y. Yamazaki⁶⁶, Z. Yan²²,
H. Yang^{33e}, H. Yang¹⁷⁴, U.K. Yang⁸³, Y. Yang¹¹⁰, S. Yanush⁹², L. Yao^{33a}, W-M. Yao¹⁵,
Y. Yasu⁶⁵, E. Yatsenko⁴², K.H. Yau Wong²¹, J. Ye⁴⁰, S. Ye²⁵, A.L. Yen⁵⁷, E. Yildirim⁴²,
M. Yilmaz^{4b}, R. Yoosoofmiya¹²⁴, K. Yorita¹⁷², R. Yoshida⁶, K. Yoshihara¹⁵⁶,
C. Young¹⁴⁴, C.J.S. Young³⁰, S. Youssef²², D.R. Yu¹⁵, J. Yu⁸, J.M. Yu⁸⁸, J. Yu¹¹³,
L. Yuan⁶⁶, A. Yurkewicz¹⁰⁷, I. Yusuf^{28,an}, B. Zabinski³⁹, R. Zaidan⁶², A.M. Zaitsev^{129,aa},
A. Zaman¹⁴⁹, S. Zambito²³, L. Zanello^{133a,133b}, D. Zanzi¹⁰⁰, C. Zeitnitz¹⁷⁶, M. Zeman¹²⁷,
A. Zemla^{38a}, K. Zengel²³, O. Zenin¹²⁹, T. Ženiš^{145a}, D. Zerwas¹¹⁶, G. Zevi della Porta⁵⁷,
D. Zhang⁸⁸, F. Zhang¹⁷⁴, H. Zhang⁸⁹, J. Zhang⁶, L. Zhang¹⁵², X. Zhang^{33d}, Z. Zhang¹¹⁶,
Z. Zhao^{33b}, A. Zhemchugov⁶⁴, J. Zhong¹¹⁹, B. Zhou⁸⁸, L. Zhou³⁵, N. Zhou¹⁶⁴,
C.G. Zhu^{33d}, H. Zhu^{33a}, J. Zhu⁸⁸, Y. Zhu^{33b}, X. Zhuang^{33a}, K. Zhukov⁹⁵, A. Zibell¹⁷⁵,
D. Zieminska⁶⁰, N.I. Zimine⁶⁴, C. Zimmermann⁸², R. Zimmermann²¹, S. Zimmermann²¹,
S. Zimmermann⁴⁸, Z. Zinonos⁵⁴, M. Ziolkowski¹⁴², G. Zobernig¹⁷⁴, A. Zoccoli^{20a,20b},
M. zur Nedden¹⁶, G. Zurzolo^{103a,103b}, V. Zutshi¹⁰⁷, L. Zwalinski³⁰.

¹ Department of Physics, University of Adelaide, Adelaide, Australia

² Physics Department, SUNY Albany, Albany NY, United States of America

³ Department of Physics, University of Alberta, Edmonton AB, Canada

⁴ ^(a) Department of Physics, Ankara University, Ankara; ^(b) Department of Physics, Gazi University, Ankara; ^(c) Division of Physics, TOBB University of Economics and Technology, Ankara; ^(d) Turkish Atomic Energy Authority, Ankara, Turkey

⁵ LAPP, CNRS/IN2P3 and Université de Savoie, Annecy-le-Vieux, France

⁶ High Energy Physics Division, Argonne National Laboratory, Argonne IL, United States of America

⁷ Department of Physics, University of Arizona, Tucson AZ, United States of America

- ⁸ Department of Physics, The University of Texas at Arlington, Arlington TX, United States of America
- ⁹ Physics Department, University of Athens, Athens, Greece
- ¹⁰ Physics Department, National Technical University of Athens, Zografou, Greece
- ¹¹ Institute of Physics, Azerbaijan Academy of Sciences, Baku, Azerbaijan
- ¹² Institut de Física d'Altes Energies and Departament de Física de la Universitat Autònoma de Barcelona, Barcelona, Spain
- ¹³ ^(a) Institute of Physics, University of Belgrade, Belgrade; ^(b) Vinca Institute of Nuclear Sciences, University of Belgrade, Belgrade, Serbia
- ¹⁴ Department for Physics and Technology, University of Bergen, Bergen, Norway
- ¹⁵ Physics Division, Lawrence Berkeley National Laboratory and University of California, Berkeley CA, United States of America
- ¹⁶ Department of Physics, Humboldt University, Berlin, Germany
- ¹⁷ Albert Einstein Center for Fundamental Physics and Laboratory for High Energy Physics, University of Bern, Bern, Switzerland
- ¹⁸ School of Physics and Astronomy, University of Birmingham, Birmingham, United Kingdom
- ¹⁹ ^(a) Department of Physics, Bogazici University, Istanbul; ^(b) Department of Physics, Dogus University, Istanbul; ^(c) Department of Physics Engineering, Gaziantep University, Gaziantep, Turkey
- ²⁰ ^(a) INFN Sezione di Bologna; ^(b) Dipartimento di Fisica e Astronomia, Università di Bologna, Bologna, Italy
- ²¹ Physikalisches Institut, University of Bonn, Bonn, Germany
- ²² Department of Physics, Boston University, Boston MA, United States of America
- ²³ Department of Physics, Brandeis University, Waltham MA, United States of America
- ²⁴ ^(a) Universidade Federal do Rio De Janeiro COPPE/EE/IF, Rio de Janeiro; ^(b) Federal University of Juiz de Fora (UFJF), Juiz de Fora; ^(c) Federal University of Sao Joao del Rei (UFSJ), Sao Joao del Rei; ^(d) Instituto de Fisica, Universidade de Sao Paulo, Sao Paulo, Brazil
- ²⁵ Physics Department, Brookhaven National Laboratory, Upton NY, United States of America
- ²⁶ ^(a) National Institute of Physics and Nuclear Engineering, Bucharest; ^(b) National Institute for Research and Development of Isotopic and Molecular Technologies, Physics Department, Cluj Napoca; ^(c) University Politehnica Bucharest, Bucharest; ^(d) West University in Timisoara, Timisoara, Romania
- ²⁷ Departamento de Física, Universidad de Buenos Aires, Buenos Aires, Argentina
- ²⁸ Cavendish Laboratory, University of Cambridge, Cambridge, United Kingdom
- ²⁹ Department of Physics, Carleton University, Ottawa ON, Canada
- ³⁰ CERN, Geneva, Switzerland
- ³¹ Enrico Fermi Institute, University of Chicago, Chicago IL, United States of America
- ³² ^(a) Departamento de Física, Pontificia Universidad Católica de Chile, Santiago; ^(b) Departamento de Física, Universidad Técnica Federico Santa María, Valparaíso, Chile
- ³³ ^(a) Institute of High Energy Physics, Chinese Academy of Sciences, Beijing; ^(b)

Department of Modern Physics, University of Science and Technology of China, Anhui;
(^c) Department of Physics, Nanjing University, Jiangsu; (^d) School of Physics, Shandong
University, Shandong; (^e) Physics Department, Shanghai Jiao Tong University, Shanghai,
China

³⁴ Laboratoire de Physique Corpusculaire, Clermont Université and Université Blaise
Pascal and CNRS/IN2P3, Clermont-Ferrand, France

³⁵ Nevis Laboratory, Columbia University, Irvington NY, United States of America

³⁶ Niels Bohr Institute, University of Copenhagen, Kobenhavn, Denmark

³⁷ (^a) INFN Gruppo Collegato di Cosenza, Laboratori Nazionali di Frascati; (^b)

Dipartimento di Fisica, Università della Calabria, Rende, Italy

³⁸ (^a) AGH University of Science and Technology, Faculty of Physics and Applied
Computer Science, Krakow; (^b) Marian Smoluchowski Institute of Physics, Jagiellonian
University, Krakow, Poland

³⁹ The Henryk Niewodniczanski Institute of Nuclear Physics, Polish Academy of Sciences,
Krakow, Poland

⁴⁰ Physics Department, Southern Methodist University, Dallas TX, United States of
America

⁴¹ Physics Department, University of Texas at Dallas, Richardson TX, United States of
America

⁴² DESY, Hamburg and Zeuthen, Germany

⁴³ Institut für Experimentelle Physik IV, Technische Universität Dortmund, Dortmund,
Germany

⁴⁴ Institut für Kern- und Teilchenphysik, Technische Universität Dresden, Dresden,
Germany

⁴⁵ Department of Physics, Duke University, Durham NC, United States of America

⁴⁶ SUPA - School of Physics and Astronomy, University of Edinburgh, Edinburgh, United
Kingdom

⁴⁷ INFN Laboratori Nazionali di Frascati, Frascati, Italy

⁴⁸ Fakultät für Mathematik und Physik, Albert-Ludwigs-Universität, Freiburg, Germany

⁴⁹ Section de Physique, Université de Genève, Geneva, Switzerland

⁵⁰ (^a) INFN Sezione di Genova; (^b) Dipartimento di Fisica, Università di Genova, Genova,
Italy

⁵¹ (^a) E. Andronikashvili Institute of Physics, Iv. Javakhishvili Tbilisi State University,
Tbilisi; (^b) High Energy Physics Institute, Tbilisi State University, Tbilisi, Georgia

⁵² II Physikalisches Institut, Justus-Liebig-Universität Giessen, Giessen, Germany

⁵³ SUPA - School of Physics and Astronomy, University of Glasgow, Glasgow, United
Kingdom

⁵⁴ II Physikalisches Institut, Georg-August-Universität, Göttingen, Germany

⁵⁵ Laboratoire de Physique Subatomique et de Cosmologie, Université Grenoble-Alpes,
CNRS/IN2P3, Grenoble, France

⁵⁶ Department of Physics, Hampton University, Hampton VA, United States of America

⁵⁷ Laboratory for Particle Physics and Cosmology, Harvard University, Cambridge MA,
United States of America

- ⁵⁸ ^(a) Kirchhoff-Institut für Physik, Ruprecht-Karls-Universität Heidelberg, Heidelberg;
^(b) Physikalisches Institut, Ruprecht-Karls-Universität Heidelberg, Heidelberg; ^(c) ZITI
Institut für technische Informatik, Ruprecht-Karls-Universität Heidelberg, Mannheim,
Germany
- ⁵⁹ Faculty of Applied Information Science, Hiroshima Institute of Technology, Hiroshima,
Japan
- ⁶⁰ Department of Physics, Indiana University, Bloomington IN, United States of America
- ⁶¹ Institut für Astro- und Teilchenphysik, Leopold-Franzens-Universität, Innsbruck,
Austria
- ⁶² University of Iowa, Iowa City IA, United States of America
- ⁶³ Department of Physics and Astronomy, Iowa State University, Ames IA, United States
of America
- ⁶⁴ Joint Institute for Nuclear Research, JINR Dubna, Dubna, Russia
- ⁶⁵ KEK, High Energy Accelerator Research Organization, Tsukuba, Japan
- ⁶⁶ Graduate School of Science, Kobe University, Kobe, Japan
- ⁶⁷ Faculty of Science, Kyoto University, Kyoto, Japan
- ⁶⁸ Kyoto University of Education, Kyoto, Japan
- ⁶⁹ Department of Physics, Kyushu University, Fukuoka, Japan
- ⁷⁰ Instituto de Física La Plata, Universidad Nacional de La Plata and CONICET, La
Plata, Argentina
- ⁷¹ Physics Department, Lancaster University, Lancaster, United Kingdom
- ⁷² ^(a) INFN Sezione di Lecce; ^(b) Dipartimento di Matematica e Fisica, Università del
Salento, Lecce, Italy
- ⁷³ Oliver Lodge Laboratory, University of Liverpool, Liverpool, United Kingdom
- ⁷⁴ Department of Physics, Jožef Stefan Institute and University of Ljubljana, Ljubljana,
Slovenia
- ⁷⁵ School of Physics and Astronomy, Queen Mary University of London, London, United
Kingdom
- ⁷⁶ Department of Physics, Royal Holloway University of London, Surrey, United Kingdom
- ⁷⁷ Department of Physics and Astronomy, University College London, London, United
Kingdom
- ⁷⁸ Louisiana Tech University, Ruston LA, United States of America
- ⁷⁹ Laboratoire de Physique Nucléaire et de Hautes Energies, UPMC and Université
Paris-Diderot and CNRS/IN2P3, Paris, France
- ⁸⁰ Fysiska institutionen, Lunds universitet, Lund, Sweden
- ⁸¹ Departamento de Física Teórica C-15, Universidad Autónoma de Madrid, Madrid,
Spain
- ⁸² Institut für Physik, Universität Mainz, Mainz, Germany
- ⁸³ School of Physics and Astronomy, University of Manchester, Manchester, United
Kingdom
- ⁸⁴ CPPM, Aix-Marseille Université and CNRS/IN2P3, Marseille, France
- ⁸⁵ Department of Physics, University of Massachusetts, Amherst MA, United States of
America

- ⁸⁶ Department of Physics, McGill University, Montreal QC, Canada
- ⁸⁷ School of Physics, University of Melbourne, Victoria, Australia
- ⁸⁸ Department of Physics, The University of Michigan, Ann Arbor MI, United States of America
- ⁸⁹ Department of Physics and Astronomy, Michigan State University, East Lansing MI, United States of America
- ⁹⁰ ^(a) INFN Sezione di Milano; ^(b) Dipartimento di Fisica, Università di Milano, Milano, Italy
- ⁹¹ B.I. Stepanov Institute of Physics, National Academy of Sciences of Belarus, Minsk, Republic of Belarus
- ⁹² National Scientific and Educational Centre for Particle and High Energy Physics, Minsk, Republic of Belarus
- ⁹³ Department of Physics, Massachusetts Institute of Technology, Cambridge MA, United States of America
- ⁹⁴ Group of Particle Physics, University of Montreal, Montreal QC, Canada
- ⁹⁵ P.N. Lebedev Institute of Physics, Academy of Sciences, Moscow, Russia
- ⁹⁶ Institute for Theoretical and Experimental Physics (ITEP), Moscow, Russia
- ⁹⁷ Moscow Engineering and Physics Institute (MEPhI), Moscow, Russia
- ⁹⁸ D.V.Skobel'tsyn Institute of Nuclear Physics, M.V.Lomonosov Moscow State University, Moscow, Russia
- ⁹⁹ Fakultät für Physik, Ludwig-Maximilians-Universität München, München, Germany
- ¹⁰⁰ Max-Planck-Institut für Physik (Werner-Heisenberg-Institut), München, Germany
- ¹⁰¹ Nagasaki Institute of Applied Science, Nagasaki, Japan
- ¹⁰² Graduate School of Science and Kobayashi-Maskawa Institute, Nagoya University, Nagoya, Japan
- ¹⁰³ ^(a) INFN Sezione di Napoli; ^(b) Dipartimento di Fisica, Università di Napoli, Napoli, Italy
- ¹⁰⁴ Department of Physics and Astronomy, University of New Mexico, Albuquerque NM, United States of America
- ¹⁰⁵ Institute for Mathematics, Astrophysics and Particle Physics, Radboud University Nijmegen/Nikhef, Nijmegen, Netherlands
- ¹⁰⁶ Nikhef National Institute for Subatomic Physics and University of Amsterdam, Amsterdam, Netherlands
- ¹⁰⁷ Department of Physics, Northern Illinois University, DeKalb IL, United States of America
- ¹⁰⁸ Budker Institute of Nuclear Physics, SB RAS, Novosibirsk, Russia
- ¹⁰⁹ Department of Physics, New York University, New York NY, United States of America
- ¹¹⁰ Ohio State University, Columbus OH, United States of America
- ¹¹¹ Faculty of Science, Okayama University, Okayama, Japan
- ¹¹² Homer L. Dodge Department of Physics and Astronomy, University of Oklahoma, Norman OK, United States of America
- ¹¹³ Department of Physics, Oklahoma State University, Stillwater OK, United States of America

- 114 Palacký University, RCPTM, Olomouc, Czech Republic
- 115 Center for High Energy Physics, University of Oregon, Eugene OR, United States of America
- 116 LAL, Université Paris-Sud and CNRS/IN2P3, Orsay, France
- 117 Graduate School of Science, Osaka University, Osaka, Japan
- 118 Department of Physics, University of Oslo, Oslo, Norway
- 119 Department of Physics, Oxford University, Oxford, United Kingdom
- 120 ^(a) INFN Sezione di Pavia; ^(b) Dipartimento di Fisica, Università di Pavia, Pavia, Italy
- 121 Department of Physics, University of Pennsylvania, Philadelphia PA, United States of America
- 122 Petersburg Nuclear Physics Institute, Gatchina, Russia
- 123 ^(a) INFN Sezione di Pisa; ^(b) Dipartimento di Fisica E. Fermi, Università di Pisa, Pisa, Italy
- 124 Department of Physics and Astronomy, University of Pittsburgh, Pittsburgh PA, United States of America
- 125 ^(a) Laboratório de Instrumentação e Física Experimental de Partículas - LIP, Lisboa; ^(b) Faculdade de Ciências, Universidade de Lisboa, Lisboa; ^(c) Department of Physics, University of Coimbra, Coimbra; ^(d) Centro de Física Nuclear da Universidade de Lisboa, Lisboa; ^(e) Departamento de Física, Universidade do Minho, Braga; ^(f) Departamento de Física Teórica y del Cosmos and CAFPE, Universidad de Granada, Granada (Spain); ^(g) Dep Física and CEFITEC of Faculdade de Ciências e Tecnologia, Universidade Nova de Lisboa, Caparica, Portugal
- 126 Institute of Physics, Academy of Sciences of the Czech Republic, Praha, Czech Republic
- 127 Czech Technical University in Prague, Praha, Czech Republic
- 128 Faculty of Mathematics and Physics, Charles University in Prague, Praha, Czech Republic
- 129 State Research Center Institute for High Energy Physics, Protvino, Russia
- 130 Particle Physics Department, Rutherford Appleton Laboratory, Didcot, United Kingdom
- 131 Physics Department, University of Regina, Regina SK, Canada
- 132 Ritsumeikan University, Kusatsu, Shiga, Japan
- 133 ^(a) INFN Sezione di Roma; ^(b) Dipartimento di Fisica, Sapienza Università di Roma, Roma, Italy
- 134 ^(a) INFN Sezione di Roma Tor Vergata; ^(b) Dipartimento di Fisica, Università di Roma Tor Vergata, Roma, Italy
- 135 ^(a) INFN Sezione di Roma Tre; ^(b) Dipartimento di Matematica e Fisica, Università Roma Tre, Roma, Italy
- 136 ^(a) Faculté des Sciences Ain Chock, Réseau Universitaire de Physique des Hautes Energies - Université Hassan II, Casablanca; ^(b) Centre National de l'Énergie des Sciences Techniques Nucleaires, Rabat; ^(c) Faculté des Sciences Semlalia, Université Cadi Ayyad, LPHEA-Marrakech; ^(d) Faculté des Sciences, Université Mohamed Premier and LPTPM, Oujda; ^(e) Faculté des sciences, Université Mohammed V-Agdal, Rabat, Morocco

- ¹³⁷ DSM/IRFU (Institut de Recherches sur les Lois Fondamentales de l'Univers), CEA Saclay (Commissariat à l'Energie Atomique et aux Energies Alternatives), Gif-sur-Yvette, France
- ¹³⁸ Santa Cruz Institute for Particle Physics, University of California Santa Cruz, Santa Cruz CA, United States of America
- ¹³⁹ Department of Physics, University of Washington, Seattle WA, United States of America
- ¹⁴⁰ Department of Physics and Astronomy, University of Sheffield, Sheffield, United Kingdom
- ¹⁴¹ Department of Physics, Shinshu University, Nagano, Japan
- ¹⁴² Fachbereich Physik, Universität Siegen, Siegen, Germany
- ¹⁴³ Department of Physics, Simon Fraser University, Burnaby BC, Canada
- ¹⁴⁴ SLAC National Accelerator Laboratory, Stanford CA, United States of America
- ¹⁴⁵ ^(a) Faculty of Mathematics, Physics & Informatics, Comenius University, Bratislava; ^(b) Department of Subnuclear Physics, Institute of Experimental Physics of the Slovak Academy of Sciences, Kosice, Slovak Republic
- ¹⁴⁶ ^(a) Department of Physics, University of Cape Town, Cape Town; ^(b) Department of Physics, University of Johannesburg, Johannesburg; ^(c) School of Physics, University of the Witwatersrand, Johannesburg, South Africa
- ¹⁴⁷ ^(a) Department of Physics, Stockholm University; ^(b) The Oskar Klein Centre, Stockholm, Sweden
- ¹⁴⁸ Physics Department, Royal Institute of Technology, Stockholm, Sweden
- ¹⁴⁹ Departments of Physics & Astronomy and Chemistry, Stony Brook University, Stony Brook NY, United States of America
- ¹⁵⁰ Department of Physics and Astronomy, University of Sussex, Brighton, United Kingdom
- ¹⁵¹ School of Physics, University of Sydney, Sydney, Australia
- ¹⁵² Institute of Physics, Academia Sinica, Taipei, Taiwan
- ¹⁵³ Department of Physics, Technion: Israel Institute of Technology, Haifa, Israel
- ¹⁵⁴ Raymond and Beverly Sackler School of Physics and Astronomy, Tel Aviv University, Tel Aviv, Israel
- ¹⁵⁵ Department of Physics, Aristotle University of Thessaloniki, Thessaloniki, Greece
- ¹⁵⁶ International Center for Elementary Particle Physics and Department of Physics, The University of Tokyo, Tokyo, Japan
- ¹⁵⁷ Graduate School of Science and Technology, Tokyo Metropolitan University, Tokyo, Japan
- ¹⁵⁸ Department of Physics, Tokyo Institute of Technology, Tokyo, Japan
- ¹⁵⁹ Department of Physics, University of Toronto, Toronto ON, Canada
- ¹⁶⁰ ^(a) TRIUMF, Vancouver BC; ^(b) Department of Physics and Astronomy, York University, Toronto ON, Canada
- ¹⁶¹ Faculty of Pure and Applied Sciences, University of Tsukuba, Tsukuba, Japan
- ¹⁶² Department of Physics and Astronomy, Tufts University, Medford MA, United States of America

- ¹⁶³ Centro de Investigaciones, Universidad Antonio Narino, Bogota, Colombia
- ¹⁶⁴ Department of Physics and Astronomy, University of California Irvine, Irvine CA, United States of America
- ¹⁶⁵ ^(a) INFN Gruppo Collegato di Udine, Sezione di Trieste, Udine; ^(b) ICTP, Trieste; ^(c) Dipartimento di Chimica, Fisica e Ambiente, Università di Udine, Udine, Italy
- ¹⁶⁶ Department of Physics, University of Illinois, Urbana IL, United States of America
- ¹⁶⁷ Department of Physics and Astronomy, University of Uppsala, Uppsala, Sweden
- ¹⁶⁸ Instituto de Física Corpuscular (IFIC) and Departamento de Física Atómica, Molecular y Nuclear and Departamento de Ingeniería Electrónica and Instituto de Microelectrónica de Barcelona (IMB-CNM), University of Valencia and CSIC, Valencia, Spain
- ¹⁶⁹ Department of Physics, University of British Columbia, Vancouver BC, Canada
- ¹⁷⁰ Department of Physics and Astronomy, University of Victoria, Victoria BC, Canada
- ¹⁷¹ Department of Physics, University of Warwick, Coventry, United Kingdom
- ¹⁷² Waseda University, Tokyo, Japan
- ¹⁷³ Department of Particle Physics, The Weizmann Institute of Science, Rehovot, Israel
- ¹⁷⁴ Department of Physics, University of Wisconsin, Madison WI, United States of America
- ¹⁷⁵ Fakultät für Physik und Astronomie, Julius-Maximilians-Universität, Würzburg, Germany
- ¹⁷⁶ Fachbereich C Physik, Bergische Universität Wuppertal, Wuppertal, Germany
- ¹⁷⁷ Department of Physics, Yale University, New Haven CT, United States of America
- ¹⁷⁸ Yerevan Physics Institute, Yerevan, Armenia
- ¹⁷⁹ Centre de Calcul de l'Institut National de Physique Nucléaire et de Physique des Particules (IN2P3), Villeurbanne, France
- ^a Also at Department of Physics, King's College London, London, United Kingdom
- ^b Also at Institute of Physics, Azerbaijan Academy of Sciences, Baku, Azerbaijan
- ^c Also at Particle Physics Department, Rutherford Appleton Laboratory, Didcot, United Kingdom
- ^d Also at TRIUMF, Vancouver BC, Canada
- ^e Also at Department of Physics, California State University, Fresno CA, United States of America
- ^f Also at Tomsk State University, Tomsk, Russia
- ^g Also at CPPM, Aix-Marseille Université and CNRS/IN2P3, Marseille, France
- ^h Also at Università di Napoli Parthenope, Napoli, Italy
- ⁱ Also at Institute of Particle Physics (IPP), Canada
- ^j Also at Department of Physics, St. Petersburg State Polytechnical University, St. Petersburg, Russia
- ^k Also at Chinese University of Hong Kong, China
- ^l Also at Department of Financial and Management Engineering, University of the Aegean, Chios, Greece
- ^m Also at Louisiana Tech University, Ruston LA, United States of America
- ⁿ Also at Institutio Catalana de Recerca i Estudis Avancats, ICREA, Barcelona, Spain

- ^o Also at Department of Physics, The University of Texas at Austin, Austin TX, United States of America
- ^p Also at Institute of Theoretical Physics, Iliia State University, Tbilisi, Georgia
- ^q Also at CERN, Geneva, Switzerland
- ^r Also at Ochadai Academic Production, Ochanomizu University, Tokyo, Japan
- ^s Also at Manhattan College, New York NY, United States of America
- ^t Also at Novosibirsk State University, Novosibirsk, Russia
- ^u Also at Institute of Physics, Academia Sinica, Taipei, Taiwan
- ^v Also at LAL, Université Paris-Sud and CNRS/IN2P3, Orsay, France
- ^w Also at Academia Sinica Grid Computing, Institute of Physics, Academia Sinica, Taipei, Taiwan
- ^x Also at Laboratoire de Physique Nucléaire et de Hautes Energies, UPMC and Université Paris-Diderot and CNRS/IN2P3, Paris, France
- ^y Also at School of Physical Sciences, National Institute of Science Education and Research, Bhubaneswar, India
- ^z Also at Dipartimento di Fisica, Sapienza Università di Roma, Roma, Italy
- ^{aa} Also at Moscow Institute of Physics and Technology State University, Dolgoprudny, Russia
- ^{ab} Also at Section de Physique, Université de Genève, Geneva, Switzerland
- ^{ac} Also at International School for Advanced Studies (SISSA), Trieste, Italy
- ^{ad} Also at Department of Physics and Astronomy, University of South Carolina, Columbia SC, United States of America
- ^{ae} Also at School of Physics and Engineering, Sun Yat-sen University, Guangzhou, China
- ^{af} Also at Faculty of Physics, M.V.Lomonosov Moscow State University, Moscow, Russia
- ^{ag} Also at Moscow Engineering and Physics Institute (MEPhI), Moscow, Russia
- ^{ah} Also at Institute for Particle and Nuclear Physics, Wigner Research Centre for Physics, Budapest, Hungary
- ^{ai} Also at Department of Physics, Oxford University, Oxford, United Kingdom
- ^{aj} Also at Department of Physics, Nanjing University, Jiangsu, China
- ^{ak} Also at Institut für Experimentalphysik, Universität Hamburg, Hamburg, Germany
- ^{al} Also at Department of Physics, The University of Michigan, Ann Arbor MI, United States of America
- ^{am} Also at Discipline of Physics, University of KwaZulu-Natal, Durban, South Africa
- ^{an} Also at University of Malaya, Department of Physics, Kuala Lumpur, Malaysia
- * Deceased